STUDIES IN TIME-OF-FLIGHT MASS SPECTROMETRY: IMPROVED MASS RESOLVING POWER AND VERSATILITY, AND MASS SPECTROMETRY/ MASS SPECTROMETRY BY TIME-RESOLVED ION KINETIC ENERGY SPECTROMETRY

By

John David Pinkston

A DISSERTATION

Submitted to
Michigan State University
in partial fulfillment of the requirements
for the degree of

DOCTOR OF PHILOSOPHY

Department of Chemistry

1985

ABSTRACT

STUDIES IN TIME-OF-FLIGHT MASS SPECTROMETRY: IMPROVED MASS RESOLVING POWER AND VERSATILITY, AND MASS SPECTROMETRY/ MASS SPECTROMETRY BY TIME-RESOLVED ION KINETIC ENERGY SPECTROMETRY

By

John David Pinkston

Conventional time-of-flight (TOF) mass spectrometers employ a pulsed ion source to accelerate a burst of ions into a field-free flight tube. Ions separate into isobaric packets during their flight to a detector situated at the end of the flight tube. Ideally, all ions within any given packet should reach the detector simultaneously. However, three conditions which exist within the ion source before acceleration of the ions produce a spread in arrival times at the detector and thus limit mass resolving power. They are: a) the initial spatial spread of the ions, b) the spread in magnitude of the initial kinetic energies of the ions, and c) the angular distribution of the initial kinetic energies (source of the "turn-around time").

Deflection of a continuous beam across an aperture is another method of producing a pulse of ions. Beam deflection in TOF mass spectrometry (MS) eliminates conditions a) and c) as resolution limiting phenomena. A new TOF mass spectrometer, the BEam Deflection Energy-Resolved TOF mass spectrometer (BEDER-TOF) has been designed and constructed. The instrument combines the advantages of beam deflection for ion pulse formation with an electrostatic analyzer which reduces the

energy spread of the ions admitted to the TOF region. The instrument is able to use ion sources which cannot be pulsed on a time scale suitable for conventional TOF analysis (e.g., chemical ionization sources). Improved mass resolution is demonstrated over a wide mass range in such a manner that all the ions are in focus simultaneously. A full-width-at-half-maximum resolution of 982 is achieved for the molecular ion peak of perfluorotributylamine at m/z 614.

A preliminary investigation of a proposed technique for collecting information typically obtained by tandem mass spectrometry (MS/MS) has been conducted using the BEDER-TOF. This new method, named time-resolved ion kinetic energy spectrometry (TRIKES), combines time-of-flight (velocity) and kinetic energy analysis of undissociated "parent ions" and the ionic products of parent ion dissociations, ("daughter ions") which occur between the ion source and electrostatic analyzer of the BEDER-TOF. Unit resolution of the daughter ions produced upon metastable decomposition of the molecular ion of n-decane has been achieved in daughter scans. The realization of rapid time-of-flight data collection rates in TRIKES may yield improved data collection rates in MS/MS.

to Carol

ACKNOWLEDGMENTS

Many have led and contributed during the course of and the preparations for this work. I want to especially thank a few here.

My parents, Edwin and Greta, gave their children a wonderful Christian home in which to grow. They gave me the confidence in myself and the faith in God that carried me through many difficult times. Likewise, Carol, my wife, endured my most oppressive moods with understanding and encouragement. I'll always be grateful to her for this.

I have great admiration for the outstanding educators who, over the years, have led me down this path. Among those most gratefully remembered are Mrs. Jo-Ann Riffe, Chemistry teacher at Harrison High School in Harrison, Arkansas; Joe Nix and Joe Jeffers of Ouachita Baptist University in Arkadelphia, Arkansas; and John Allison and Jack Watson of Michigan State University. Their dedication and leadership have shaped my life.

Finally, I want to thank the friends in the Watson group, the Allison group, and the Mass Spectrometry Facility that have helped and encouraged during the course of this work. They have certainly added to the enjoyment of the past five years.

TABLE OF CONTENTS

Page

LIST OF TABLES

LIST OF FIGURES

Figure

19

20

21

22

23

24

25

26

27

LIST OF SYMBOLS

a	electrostatic analyzer radius
acc_y	transverse acceleration of ions within deflection plate region
b	distance between object slit and electrostatic analyzer
B	magnetic field strength
D	distance between deflection plates
e	charge on the electron
E_d	electrostatic analyzer field strength necessary to pass daughter ion
E_p	electrostatic analyzer field strength necessary to pass parent ion
f, g	parameters related to geometry of radial electrostatic analyzer
j	distance orthogonal to flight tube axis which must be travelled by ions exiting image slit to strike deflection plate
L	flight tube length
m	mass of ion
m_d	mass of daughter ion
m_p	mass of parent ion
Δm	width of peak in units of mass
P	maximum deflection plate length
S	width of aperture across which beam is deflected
tof	time-of-flight

tof_{crit}	time-of-flight required for ions to strike deflection plate after entering deflecting field
tof_d	time-of-flight of daughter ion
tof_p	time-of-flight of parent ion
Δ tof	width of peak in units of time
Δtof_e	width of peak due to energy spread
Δtof_p	width of peak due to beam deflection
v	velocity of ion
v_o	average velocity of ions
$v_{\mp}$	minimum and maximum velocities
v_x	velocity of ion in axial direction
v_d	velocity of daughter ion
v_p	velocity of parent ion
V_o	accelerating voltage
V'	deflection voltage
w_c	cyclotron frequency of ion
x	object slit width
y	image slit width
z	number of charges carried by ion
δ	parameter related to energy bandpass of electrostatic analyzer
θ	electrostatic analyzer sector angle
τ	time during which accelerating field is applied

CHAPTER 1

INTRODUCTION

This introduction will describe the manner in which this project originated. The introduction will also place this work with respect to the overall goal of the current "core" research of the Michigan State University/ National Institutes of Health Mass Spectrometry Facility of making the time-of-flight (TOF) mass spectrometer a better instrument (the best in certain aspects) for gas chromatography (GC) - mass spectrometry (MS). A brief introduction to tandem mass spectrometry (MS/MS) and how the instrument described in this thesis can be used for MS/MS will be reserved for a later chapter.

Chromatographic methods of separation is a field in which rapid improvements in separating power and efficiencies continue to occur. As the number of resolvable peaks per unit time increases, the peak widths necessarily decrease. This presents no particular problem for the majority of chromatographic detectors which yield an analogue response so long as the response time of the detection/recording system is sufficiently short. However, some detectors produce a discontinuous response, yielding data points representing the chromatogram separated by time periods during which the detector is "blind". As illustrated in

Figure 1, the fidelity of the representation of the chromatogram may suffer in these cases.

In particular, the case may be worse than that illustrated in Figure 1(a) and 1(b) when using a conventional scanning mass spectrometer as a detector for a high performance chromatographic method. For example, peak widths may be as narrow as 1 or 2 seconds in capillary GC while the minimum scan cycle time for scanning over a mass decade is 0.3 to 1 second for both quadrupole and magnetic instruments. In fact some investigators have been forced to purposefully degrade the chromatographic resolution in a capillary GC-MS run in order to obtain a sufficient number of points across chromatographic peaks (3 to 4 points would be an absolute minimum, 8 to 10 points per peak is desirable) (1).

A discussion group was organized in the Spring of 1981 to discuss these problems and potential solutions. The group consisted of J. T. Watson, J. Allison, C. G. Enke, J. F. Holland, J. T. Stults, B. D. Musselman, and myself. Discussions centered on identifying a mass spectrometric method with a high full-scan data collection rate, a wide dynamic range, good sensitivity, reasonable mass resolving power, and capacity to use a variety of ionization methods; in other words the ideal mass spectrometer for use as a chromatographic detector.

Figure 1.

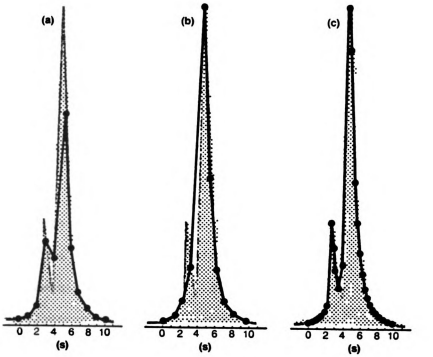

Figure 1. Comparison of the true chromatographic peaks (shaded area) with mass chromatograms reconstructed from mass spectra acquired in a repetitive fashion (area under lines connecting points). (a) Mass chromatogram prepared from mass spectra acquired at a rate of 1 scan/s. (b) Mass spectra acquired at rate of 1 scan/s, but synchrony of chromatogram and scan cycle shifted by one-third second. (c) Mass spectra acquired at rate of 3 scans/s. Reprinted from reference 29, courtesy of the American Chemical Society.

Most conventional instruments used in GC-MS today record ion current of one m/z at a time, scanning through sequential m/z values. The most promising route to the objectives listed above involves the simultaneous detection of all the ion current using an array type detection scheme which would encode m/z and intensity data for all ions simultaneously. Three potential solutions, each employing a different type of array detection, were envisioned and will be briefly discussed here. They are: use of the electro-optical ion detector (EOID) in magnetic instruments (spatial array detection), Fourier transform ion cyclotron resonance mass spectrometry (FTMS) (frequency array detection), and use of the integrating transient recorder (ITR) in TOF-MS (time array detection).

The EOID is an electronic analogue of the traditional photoplate detection scheme used in Mattauch-Herzog-Robinson geometry double focussing mass spectrometers. Ions accelerated from the source are dispersed by the magnet according to their momenta. Each ion beam of a particular m/z (related to momentum) achieves simultaneous second order angular and energy focus at a single point along a focal plane. The photoplate is placed at this focal plane. The photoplate is an excellent example of a spatial array detector, as all ions are detected simultaneously. However, the photoplate has a low dynamic range (on the order of 30:1), fairly poor sensitivity (10^2- 10^3 ions are generally required to produce a detectable image), the processing of the plate is cumbersome, and a single photoplate is designed for use with a limited number of samples. The EOID (see Figure 2) generally consists of a flat channel electron multiplier array (CEMA) which is located at the focal

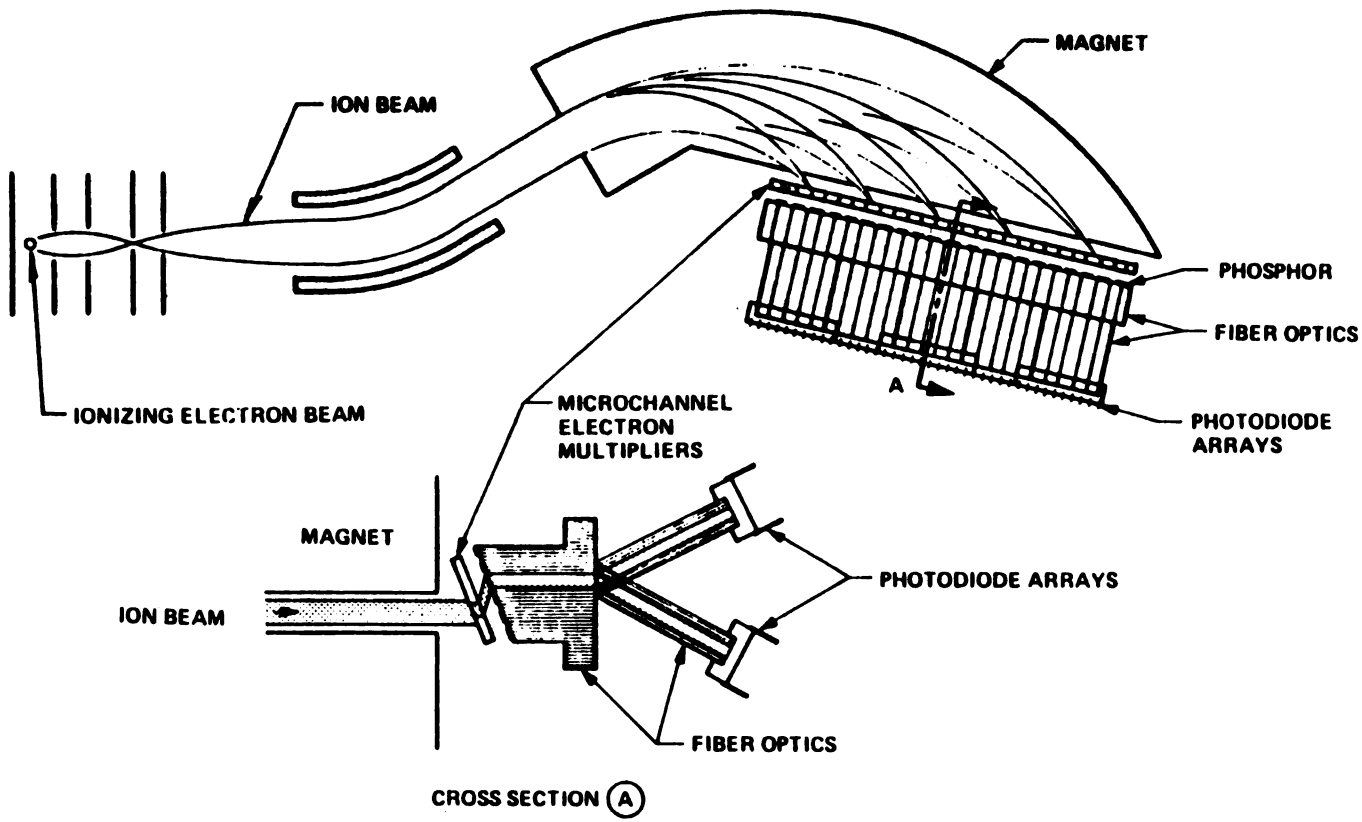

Figure 2. Schematic representation of one version of the EOID. The double focussing mass spectrometer is of the Mattauch-Herzog-Robinson geometry. Reprinted from reference 7, courtesy of the American Chemical Society.

plane of the magnet followed by a phosphor coated plate. Light is emitted from the phosphor when it is struck by the secondary electrons from the CEMA. These photons are detected using a photodiode array or a vidicon camera. Other than the brief "dead time" which occurs as each pixel is read, the EOID truly detects all ions within its mass range simultaneously.

Initial experiments involved shielding the EOID from the magnetic fringe field of the mass spectrometer (2), characterizing the EOID using single focussing magnetic instruments (3-5), and the use of quadrupole fields for additional focussing (6). A resolution of over 1,000 was achieved in Boettger, Giffin, and Norris' design with a ratio of 1.6 between the highest and lowest masses simultaneously in focus (2,7). That ratio was increased to a maximum of 4:1 in a subsequent design by Louter et al. (8) for studies in tandem MS. The EOID may be ideal for studying short-lived phenomena or for use with small permanent magnet mass spectrometers such as those employed in space exploration (7). However, the disadvantages of current versions of the EOID for GC-MS type applications are summarized in the works of Hedfjall and Ryhage (9,10) who used an EOID equipped LKB-2091 (a single focussing GC-MS instrument). Mass resolution at higher m/z values was sometimes reduced when intense peaks "blossomed" into the pixels of neighboring m/z's. The gain of individual microchannels differed significantly in magnitude and that magnitude varied randomly in time. In spite of cooling the photodiode array to -35°C, the investigators were unable to increase the dynamic range beyond 100 without varying the integration time for different pixels which entails variations in precision and accuracy over

the

syste

insu

avail

ECCD

acqui

experi

of 2.5

Tesla)

metho

the i

which

where

the i

streng

applic

plates

common

wave pu

Paralle

of larg

cyclotr

the mass spectrum. An attempt to improve the dynamic range of the system by rapidly changing the voltage on the microchannel plate was unsuccessful due to the long dead time of the detector.

In view of the complexity of the EOID and of the limitations of the available hardware for GC-MS applications, it was decided to abandon the EOID as a possible solution to the chromatographic peak width-data acquisition rate dilemma in GC-MS.

Frequency array detection using FTMS was then discussed. The FTMS experiment (see Figure 3) is conducted within a cubic cell (on the order of 2.5 cm on an edge) which is placed in a strong (generally 1 to 9 Tesla) magnetic field. Ions are formed within the cell using a pulsed method of ionization. Due to the presence of the strong magnetic field, the ions move in circular orbits at their cyclotron frequencies (w_c) which are characteristic of the ions' m/z values:

$$w_c = z\ e\ B\ /\ 2\ \pi\ m \qquad (1)$$

where m is the mass of the ion, z is the number of charges carried by the ion, e is the unit electronic charge, and B is the magnetic field strength. The ions are constrained to remain within the cell by the application of low (1 to 5 volts) trapping voltages on the two cell plates which lie perpendicular to the magnetic field lines. In the most common mode of analysis, a frequency swept "chirp" signal or a square wave pulse is applied to one of the two pairs of cell plates which lie parallel to the field. Ions absorb energy and coherently move to orbits of larger radii as the frequency of the applied signal matches their own cyclotron frequency. The excited ions of one m/z move coherently as one

ure 3

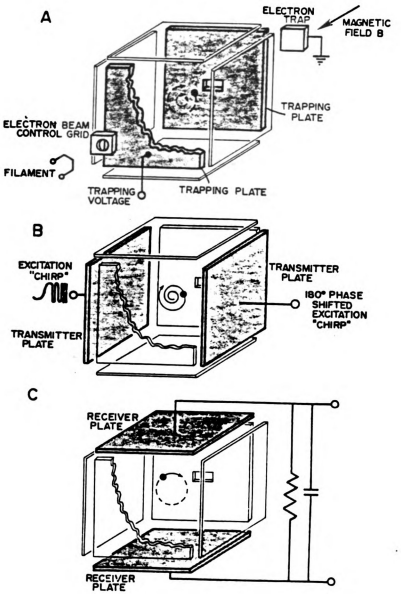

Figure 3. The FTMS "sequence of events". A, B, and C are sequential in time. In A, ions are formed and trapped within the FTMS cell by the action of the magnetic field and a small voltage applied to the trapping plates. In B, the trapped ions are excited by a signal applied to the transmitter plates. In C, the image currents transmitted by the coherently orbiting ions to the reciever plates are detected and digitized. Fourier transformation of this signal yields a frequency (mass) spectrum of the ions. See text for additional details. Reprinted from reference 29, courtesy of the American Chemical Society.

packet in their new orbit. This ion packet induces image currents in the cell plates. The second pair of plates which lies parallel to the magnetic field lines, called the "receiver" plates, is connected by an external circuit. The image currents moving through this circuit are detected, amplified and digitized. The intensity of this signal, called the "free induction decay", decreases with time as the ion motion becomes less coherent due to collisions within the cell and the radii of the ion packet's orbit decrease due to transmission of energy to the external conducting circuit of the receiver plates. The free induction decay contains frequency components of all the coherently moving ions in the cell. The excited ions are therefore all detected simultaneously in FTMS. The array here is one of cyclotron frequencies instead of locations along the focal plane of a mass spectrometer as with the EOID. Finally, the free induction decay is subjected to Fourier transformation to yield a frequency vs. intensity (or mass vs. intensity) spectrum.

FTMS has promised many advantages over conventional techniques since its conception (11,12). These advantages, both realized and expected, have been extensively reviewed (13-18). At low pressure, high magnetic field strength, and long observation times extremely high mass resolving power is available (19). Signal to noise ratios (S/N) or the time required to collect a full mass spectrum are improved over conventional ion cyclotron resonance mass spectrometry as all the ions are detected simultaneously in FTMS (the "multiplex" or Fellgett (20) advantage). The possibilities of performing exact mass measurements in the absence of calibrant have been explored (21). Due to its ability to store ions for long periods of time, sequential collisionally induced

dissociations (CIDs) for multiple tandem MS (MS/MS) experiments have been performed using FTMS (22,23). (This aspect of FTMS will be discussed in Chapter 5.)

The ability of the FTMS instrument to rapidly acquire mass spectra has been exploited in capillary GC-FTMS experiments (24). The entire process of ion formation, excitation, and detection can occur in as little as 20 ms. A number of spectra are often averaged for S/N improvement. However, 4 to 5 averaged spectra per second gives fairly accurate reconstruction of most chromatograms, excluding only the early peaks in most capillary GC-MS runs.

The fact that ion formation, excitation, and detection all occur within the same cell in FTMS is both an advantage and a disadvantage. The system is mechanically very simple and does not require extremely high tolerance machining as is the case with certain conventional mass spectrometers (in magnetic instruments, for example, the image of the entrance slit must be focussed on the exit slit). On the other hand, the available ionization methods are limited to those which can be pulsed. There are limitations in sample inlet systems due to the need to maintain high vacuum for reasonable mass resolving power. This has led to the need for special interface designs in GC-FTMS (25). However, the main limitation of FTMS, in its use as a detector for the analysis of complex mixtures by GC, is a restricted dynamic range due to space charge effects in the FTMS cell. The concentration ratios of coeluting components in certain metabolic profiling runs can be greater than one thousand to one. Indeed, the mass spectrometer used as a detector in

these runs must have a wide dynamic range. Recent improvements in the FTMS cell design (26) and hybrid quadrupole-FTMS instruments (27) have improved the situation described above but still have not solved all of the problems in GC-FTMS. For these reasons it was decided to look elsewhere for a solution to the scan speed-chromatographic peak width dilemma in GC-MS.

It was then decided to look at the potential solutions to the scan speed- chromatographic peak width dilemma offered by TOF-MS. The operational principles of TOF-MS, first published in 1946 (28), are simple (see Figure 4). Ions are formed in the ion source using a pulsed method of ionization, such as pulsed electron impact (EI) ionization or pulsed photoionization (PI). These ions are then accelerated to constant kinetic energy (all the ions are allowed to move through the entire accelerating field) or to constant momentum (the accelerating field is turned off before any ions move through the entire field gradient) into a field-free flight tube. Lighter ions reach a detector placed at the end of the flight tube before heavier ions and the resulting detector output constitutes a mass spectrum. The flight times of ions to the detector obey the following equations:

$$(tof) = L \sqrt{m / 2 z e V_o} \qquad (2)$$

in constant energy acceleration and

$$(tof) = m L / \tau z e E \qquad (3)$$

in constant momentum acceleration. L represents flight tube length, tof represents the time-of-flight, V_o represents accelerating voltage, E represents accelerating field strength, and τ represents the time during which the accelerating field is applied. The tof is proportional to the

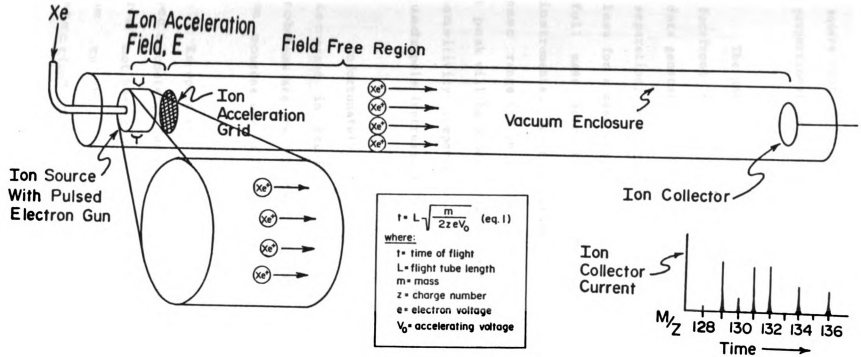

Figure 4. Schematic representation of the idealized TOF mass spectrometer. A, B, and C are sequential in time. The ions are formed in the source by a pulsed mode of ionization. These ions are then accelerated from the source into the flight tube. The tof of the ions to the detector is a function of mass. The detector output constitutes a tof (mass) spectrum.

square root of mass in constant energy acceleration while it is directly proportional to mass in constant momentum acceleration.

The one outstanding feature of TOF-MS which brought it to the forefront in our discussions is its unparalleled potential for rapid data generation. In fact, the entire ion formation, acceleration, separation, and detection scheme described above can occur in 100 μs or less for a mass spectrum encompassing a wide mass range. Ten thousand full mass spectra strike the detector each second in conventional TOF instruments. Other advantages of TOF-MS include a physically unlimited mass range (if an ion survives through the initial acceleration period, a peak will be produced in the mass spectrum representing its mass), sensitivity comparable to that of most conventional magnetic and quadrupole instruments, simple construction, and relatively low cost.

Unfortunately, there are problems in TOF-MS. These will be discussed in detail in the following chapter. Briefly, the two major problems are low mass resolving power and restrictions in the types of ion sources one may use in TOF-MS.

In spite of the great data generation rate of the TOF mass spectrometer, data acquisition rates using conventional TOF instruments have not been superior to those using other mass spectrometers. This is due to the conventional data acquisition method called "Time Slice Detection" (TSD) (see Figure 5). Using TSD, the detector output is sampled after each pulse of the ion source only during a very short "slice" or window of time. The slice is generally so narrow that it

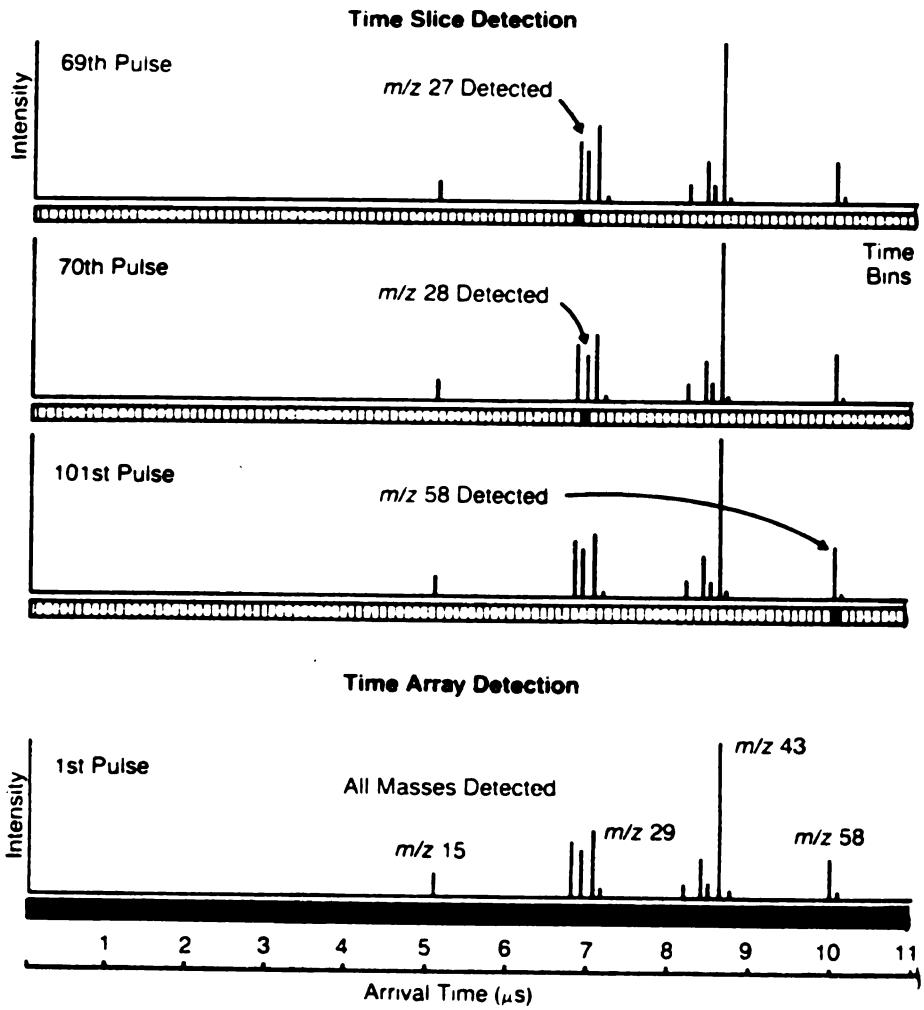

Figure 5. Comparison of time slice detection and time array detection. A simulated TOF spectrum is shown for n-butane, using a flight tube length of 100 cm and an accelerating voltage of 3,000 V. In time slice detection, only one time bin is measured for each pulse of the ion source, necessitating multiple pulses to acquire the entire spectrum. In time array detection, the entire spectrum is acquired from each pulse of the ion source. Reprinted from reference 29, courtesy of the American Chemical Society.

encompasses only a portion of the range of arrival times corresponding to ions of a single mass. The position of the sampled time slice is slowly scanned across the range of potential arrival times to record a full mass spectrum. Conventional TOF instruments using a 10 kHz source pulse rate would exhibit arrival times ranging from roughly 20 to 100 μs. If the time slice sampled after each source pulse is typically 5 ns wide, fully 99.995% of the available information is being discarded.

The discussion group concluded that order-of-magnitude improvements could be achieved in data acquisition rates and/or S/N using recent advances in electronics to achieve "Time Array Detection" (TAD) in TOF-MS (29). In TAD (see Figure 5) all the information exiting the detector is collected and used. It was proposed that 1,000 full mass spectra per second, each consisting of an average of 10 mass spectra resulting from individual ion source pulses, could be stored for later retrieval in applications where the nature of the ions produced in the source is changing rapidly (29). In other applications where 1 spectrum per second, for example, is sufficient, major improvements in S/N are to be expected as each spectrum stored will be an average of 10,000 mass spectra resulting from individual source pulses. If the noise is truly random in nature the S/N improvement should be proportional to the square root of the number of individual spectra averaged.

Thus TAD in TOF-MS presents an excellent solution to our original scan speed-chromatographic peak width dilemma in GC-MS. It also opens up exciting new areas of investigation in MS where the ion current produced in the source varies rapidly in time such as in laser desorption MS (30) and possibly in particle bombardment MS. However, to make full use of TAD, the problems alluded to earlier in TOF-MS must be dealt with successfully. This project originated with this realization.

The original goals of this project were to:

1. improve the mass resolving power of the TOF instrument to at least unit mass resolution over a 1 to 800 u mass range such that all ions are in focus simultaneously, and

2. allow for the use of ion sources not suited to pulsing on the time scale requisite in conventional TOF-MS.

The results presented in chapter 4 will demonstrate that these goals have been achieved.

During the design period it became apparent that the instrument would be suited for a preliminary investigation of time-resolved ion kinetic energy spectrometry (TRIKES), a proposed method for obtaining information generally obtained by MS/MS (31,32). Conducting this preliminary investigation became a further goal of this project.

CHAPTER 2

THEORY

This chapter will first address the reasons for the limitations in mass resolving power in TOF-MS and the relative importance of each of these causes. Limitations in methods of ionization compatible with TOF-MS will also be discussed. Notable attempts by previous investigators to compensate for and/or eliminate these problems in TOF-MS will then be investigated. Finally, the theory and equations governing the research which is the subject of this thesis will be presented.

Figure 6 illustrates the three basic problems which limit mass resolving power in TOF-MS. The first considered here is the initial spatial spread of the ions. Gas-phase samples are ionized with a pulsed EI or PI beam. Ions are created within the volume of the ionizing beam. When the extracting field is applied in the source, ions are accelerated from their various positions within this initial spatial spread. Ions accelerated from different planes of the ion source which are perpendicular to the flight tube axis experience different accelerating fields and therefore acquire different amounts of kinetic energy. This contributes to a spread in flight times to the detector among ions of

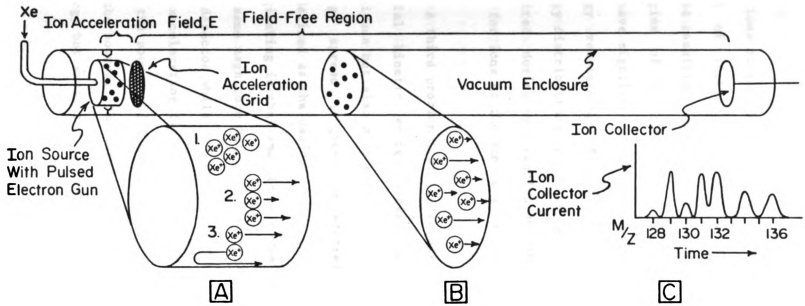

Figure 6. Basic problems limiting mass resolution in TOF-MS: 1. initial spatial spread of the ions in the ion source, 2. spread in magnitude of the initial kinetic energies, 3. angular distribution of the initial kinetic energies (the "turn-around" time). The situations depicted in A, B, and C are consecutive in time.

the same mass and therefore to lower mass resolving power.

Ions originating from the same plane of the ion source exhibit a range of initial kinetic energies. All ions possess a kinetic energy spread resulting from the initial Boltzman distribution of thermal energies of the neutral parent molecules. In addition, fragment ions may have significantly higher kinetic energy spreads due to kinetic energy release upon fragmentation of the molecular ion. These kinetic energy distributions will be superimposed upon the kinetic energy acquired during acceleration and will result in a range of flight times even for ions of the same mass originating in the same plane.

A third problem limiting resolving power in TOF-MS is that the initial kinetic energy spread is of course not only a spread in magnitude but also a spread in direction. This manifestation of the energy spread is generally referred to as the "turn-around" time which is defined as the maximum difference in flight times between two ions originating in the same plane of the ion source with kinetic energies of the same magnitude but of opposite sign (i.e., one ion is moving toward the detector while the other is moving in the opposite direction). When the accelerating field is turned on one ion is accelerated directly out of the source while the other slows, stops, and then is accelerated out of the source. The two ions exit the source with the same kinetic energy but separated by the turn-around time.

Using the CVC Products Type M2000 TOF mass spectrometer as a model, one may calculate the relative importance of each of the problems. The 2000 installed in this laboratory currently has a 2.0 m flight tube, a final accelerating voltage of 2.7 kV, and a series of electron collimating slits of 0.18 mm (0.007 in.) for the pulsed EI beam (by comparison the slits on the Bendix 12-101 are 0.020 in. wide). These values and those of the other source parameters used in the calculations (such as the ion grid spacings) are taken directly from the schematics supplied with the instrument. The ion extraction pulse is variable from approximately 70 V in magnitude to 250 V. This pulse amplitude was optimized for maximum resolution (using the "ion focus" potentiometer) over a mass range of 4 to roughly 150 u. The measured value of the extraction pulse at that optimum was 75 V and this value is used in the calculations. It is assumed that the minimum "on" time for the electron beam of approximately 1 μs is used and that the extraction pulse is turned on immediately after the ion formation pulse ends (no "time-lag" focussing). An initial energy spread of 0.09 eV is assumed and no additional translational energy from kinetic energy release upon fragmentation is assumed to be present. A value of 0.09 eV is chosen as it represents the upper limit of the thermal energy of 98 % of the ions at an effective source temperature of 230°C; this value has been used in previous works (33). It has been shown (34,35) that positive ions having thermal energies may be trapped in the potential well formed by the ionizing electron beam. It is therefore assumed that the ions occupy only the volume defined by the electron beam before they are pulsed out of the source. This minimizes the contribution of the initial spatial spread to peak broadening in the calculations.

It is instructive to first consider the case of a one grid ion source. The calculations are performed as if all but the first grid of the CVC 2000 ion source has been removed and that a 2.7 kV extraction pulse is applied on that first grid. For ions of mass 132 the arrival times cover a range of 15.264 μs yielding a resolution (peak width measured at baseline) of 4.7. The initial spatial spread accounts for 99.93 % of the peak width, 0.05 % is due to the initial energy spread, and 0.02 % is due to the turn-around time.

Now using the modified Wiley-McLaren (see reference 33 and following paragraphs) 4 grid ion source of the CVC 2000, one obtains a range of arrival times of 67.6 ns at m/z 132 which yields a resolution (peak width again measured at baseline) of 246.8. The space-focussing source performs its intended purpose with only 6.6 % of the peak width due to the spatial spread. The thermal energy spread accounts for 31.1 %, and 62.3 % is due to the turn-around time. The turn-around time is thus a major factor in reducing resolving power in TOF instruments using space-focussing sources. Space-focussing (trying to reduce the effects of the initial spatial spread) or energy-focussing (reducing the effects of the initial energy spread) using time-independent fields does not lessen the effect of the turn-around time (36).

To achieve high resolving power, conventional TOF instruments rely upon ion sources from which ions may be extracted in a narrow burst. This results in another major limitation in TOF-MS: TOF instruments are not compatible with certain methods of ionization. For example, chemical ionization (CI) sources are generally operated at high pressure (usually between 100 mtorr and 1 torr). Ion mobilities within a CI source are therefore low (37) and ions cannot be extracted from a CI source in a short, narrow pulse. Another incompatible method of ionization may be fast atom bombardment (FAB) due to the fact that it may be impossible to pulse the primary beam of fast neutral particles with the sharpness that is required for reasonable TOF analysis of the resulting secondary ions (in contrast, beam deflection has been used to pulse the primary beam in TOF-secondary ion mass spectrometry (SIMS) work (38)). In addition, the relatively high source pressure in FAB experiments may limit the mobility of the secondary ions.

Most of the work in TOF-MS instrumentation has been directed toward improving the available mass resolving power. In the first published account of a working instrument (39), the initial spatial spread and the turn-around time were eliminated as resolution-limiting phenomena. The instrument described used a continuous ion source and the ion beam was brought into line with the flight tube for a variable time period to begin the time-of-flight (tof) measurement. Unfortunately, a Faraday cup with a 1 MHz bandpass, 1.6 Megaohm input impedance pulse amplifier was used to detect the ions. The sensitivity was so low that the ion beam had to be "on" (in focus with the flight tube) for 5 μs to detect a reasonable signal. The resulting ion pulses were on the order of 20 to

30 μs long and the resulting mass resolution was of course very low. The leading edges of the peaks were used to estimate the arrival times of the ions.

In 1949, R. Keller published the next account of a functional TOF instrument (40). The instrument was pulsed by simply increasing the current flowing through a Penning discharge by two orders-of-magnitude for 0.2 μs. The final accelerating voltage was 30 kV and a Faraday cup was used as a detector. Discernible humps for ions up through O_2^+ were observed. However, the mass resolution was no greater than 2.

A third brief report appeared in 1951 (41) in which the instrument again used deflection of a continuous beam of ions to produce ion pulses for TOF. For the first time, beam deflection was used in which the beam was injected into the flight tube only during the rising and falling edges of a voltage pulse applied to a deflection plate. This is basically the same type of pulsing mechanism used in the research which is the subject of this dissertation (the advantages of this method of pulse generation will be described in a subsequent paragraph). Unfortunately, the report is less than one page long and no results are given except that "the pulse size of the oscillograph was very broad". The details given concerning the instrument and the experimental conditions are insufficient to determine what the problems were.

Wolff and Stephens published an account of a TOF mass spectrometer in which, similarly to Keller's instrument, the ionizing electron current was pulsed while all other voltages were constant (42). The mass resolution was about 10 at m/z 20. Stephens' instrument was designed such that it was able to provide the first experimental demonstration of constant momentum acceleration in TOF-MS. Ions are accelerated to constant momentum instead of constant kinetic energy if the accelerating field is turned off before the ions have traversed the entire accelerating region. The tof of ions accelerated to constant momentum is proportional to the mass of the ion (not the square root of the ion as in constant energy acceleration) as described by equation (3) of Chapter 1. A resolution of 20 at m/z 40 was obtained. The major problem limiting resolving power was the long electron pulse duration of 0.5 μs. Ions were continuously being accelerated into the flight tube during this ionization period.

In 1954 an in-depth theoretical and experimental analysis of TOF methods was published by Fishwick of the University of Edinburgh (43). Various ways of pulsing the ion beam were discussed such as pulsing the electron beam, pulsing an accelerating grid, decelerating the ions within a "holding" region and subsequently reaccelerating them into the flight tube, and deflection of a continuous beam across an aperture situated in front of the flight tube. Experimentally, pulsing the electron beam gave poor results so the instrument was modified for beam deflection. However, a voltage ramp was used to bring the beam into focus instead of the rising edge of a square pulse, and the resolution reported was no greater than 20.

In 1955, the first major breakthrough in TOF technology occurred when two teams of scientists independently published accounts of their research involving TOF mass spectrometers using pulsed EI ionization and a multigrid ion source (44,33). In both cases an ion extraction pulse of relatively low voltage followed by an accelerating grid at a higher d.c. potential was used.

The first instrument, that of Katzenstein and Friedland (44), was designed primarily for measuring appearance potentials. The electron beam entered the source from the rear, co-axial with the flight tube. Thus, ions were pulsed into the flight tube from a wide range of positions within the ion source. In spite of this, the authors demonstrated a mass resolution greater than 100 at m/z 75. They made no attempt to improve the resolving power beyond this point.

The instrument described by Wiley and McLaren (33) formed the basis for the first commercial TOF mass spectrometer. Commercially available instruments for analysis of gas-phase samples have been based on Wiley and McLaren's work until the present. For the first time, these two authors gave a step-by-step analysis of the various problems limiting resolving in TOF-MS. They concluded that the problem contributing the most to low resolving power was the initial spatial spread of the ions in the source. They therefore developed a two grid space-focussing (i.e., compensating for the effects of the initial spatial spread) ion source. The Wiley-McLaren design is shown schematically in Figure 7. By varying the relative positions of the electron beam, the first and second ion grids, and the magnitude of the ion extraction pulse applied

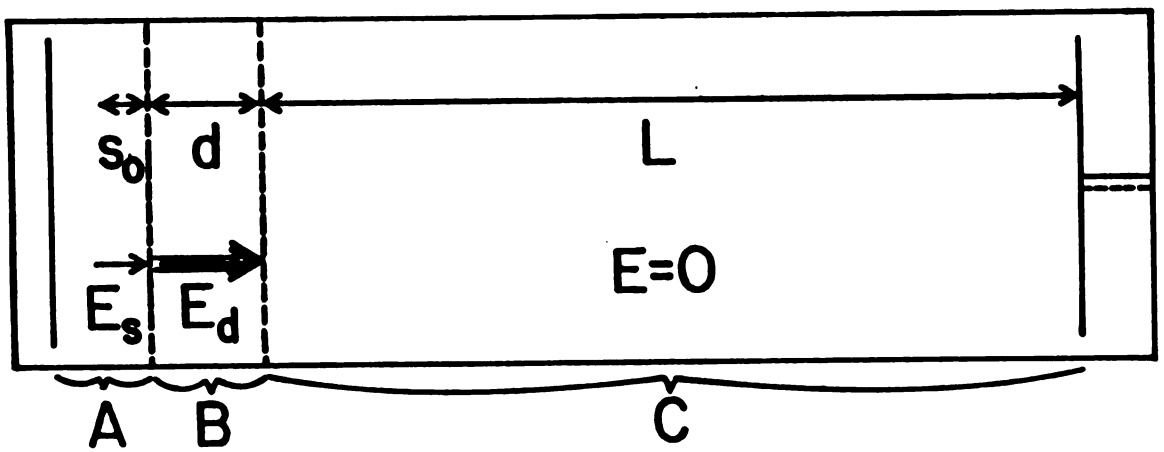

Figure 7. Schematic representation of the Wiley-McLaren space-focussing TOF instrument. A = ionization region; B = acceleration region; C = field-free flight tube and detector; average distance from electron beam to first grid = s_o; separation of grids = d; flight tube length = L; extraction field strength = E_s; accelerating field = E_d. These parameters can be arranged to produce a focal plane at the detector for ions originating from different planes of the source.

to the first ion grid, ions beginning their flight from a range of initial positions within the ion source are focussed to a plane which coincides with the active surface of the detector.

Wiley and McLaren also derived and tested a further type of focussing which compensates for the initial energy spread and the turn-around time of the ions. This method of energy-focussing is called time-lag focussing. By introducing a delay between the ionization pulse and the ion extraction pulse, ions are allowed to move away from the region of the electron beam where they were originally trapped. When accelerated out of the source from their new positions, the ions acquire the proper amount of kinetic energy to compensate for their initial energy spread and turn-around times and they are thus focussed at the detector plane. However, space-focussing and energy-focussing are mutually exclusive as the space-focussing requirement that flight time is independent of initial position is violated during the derivation of the time-lag energy-focussing equations. The greatest disadvantage of time-lag focussing is the fact that the optimum time-lag is proportional to the square root of the mass. When the time-lag focus is optimized for low mass ions, the initial energy spread effects still contribute to the spread in arrival times for higher mass ions. If the time-lag is increased to focus higher mass ions, lower mass ions may move to regions of the source from which they are actually defocussed, as the change in flight times with change in source position is linear only over a narrow range of positions. However, time-lag focussing has proven to be a useful tool in applications where the energy spread effects are significant and in which one is interested in only a short range of

masses at any one time. Wiley and McLaren do not list the maximum resolution obtained using their instrument in the publication, but the best spectrum presented yields a resolution of roughly 600 at m/z 132 of Xe^+.

The next major step in TOF technology came in the early 1970's with the introduction of the mass "reflectron" by Mamyrin and co-workers in the U.S.S.R. (45-47). A schematic diagram of one version of the reflectron is presented in Figure 8. Janes (48) independently filed for a patent describing a similar instrument in 1971. The mass reflectron uses a traditional space-focussing source to focus the ion packet at a plane very near the exit of the ion source instead of at the detector as in previous TOF instruments. The width of the ion packet at the space-focus plane is limited by the initial energy spread of the ions and is proportional to the focal length used. Since the focal length in the reflectron is short, the width of the ion packet is also much shorter than in traditional space-focussing instruments. Due to the fact that the ions must acquire different amounts of kinetic energy upon acceleration from the source to achieve space-focussing, the ion packet spreads out as it traverses the rest of the first field-free region. The flight time in the field-free region is inversely proportional to the square root of the kinetic energy. The ions are then decelerated and reflected by electrostatic fields at the end of the first field-free region. The flight time in the reflection region is proportional to the square root of the kinetic energy, thus slower ions actually spend less time in the reflecting region than do faster ions. Once the ions have traversed a second field-free region the total flight times for the fast

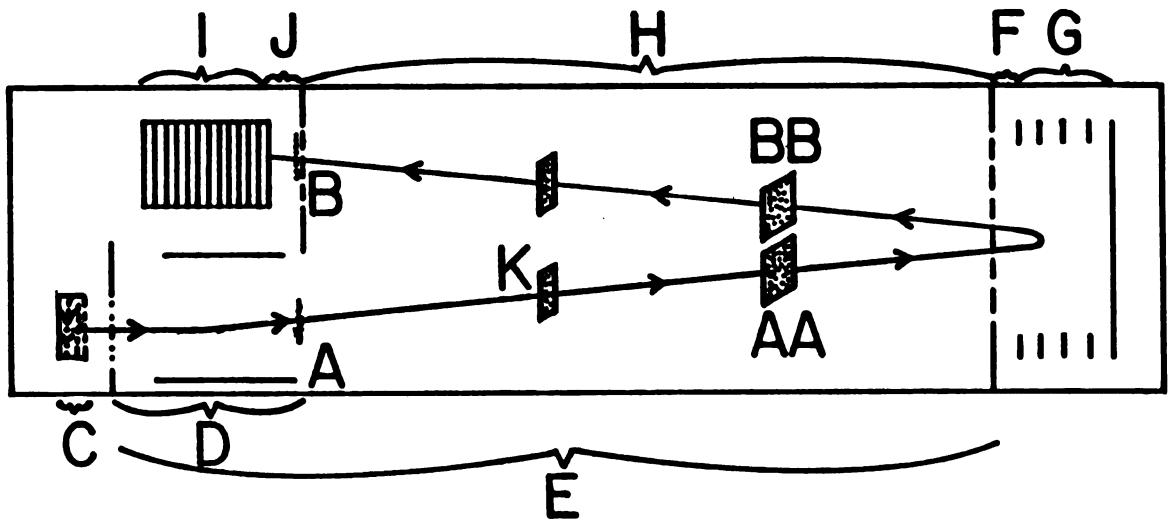

Figure 8. Schematic representation of the "mass reflectron": C = ion source; D = steering field; E = first field-free region; F, G = decelerating and reflection regions; H = second field-free region; I, J = detector; at A and B the widths of an ion packet is shown at the focal plane; at AA and BB the width of an ion packet is shown just before and just after reflection.

and slow ions are identical. The detector is situated at the end of the second field-free region at a focal plane which is the mirror image of the original space-focussing focal plane. Thus the length of the flight tube has been increased (allowing the ion packets to separate based on their m/z) without a proportional increase in the width of the ion packet at the detector. A FWHM (Full Width at Half Maximum; i.e., the width of the peak is measured at half peak height) resolution of over 3,000 was demonstrated for the trimer of rhenium bromide (46). The reflectron has been used in a number of studies, such as in laser desorption (LD) (49,50), in multiphoton ionization (MPI) experiments (51,52), and in pulsed field desorption (FD) (53). Limitations of the reflectron are a loss in sensitivity in the ion mirror and the appearance of extraneous peaks in the mass spectrum due to metastable decompositions occurring in the first field-free region. This latter effect has been used to observe both metastable (51) and photon-induced (54) daughters using the reflectron.

Gohl *et al.* (55) have recently published an account of research demonstrating improved mass resolving power using the reflectron. However, their extraction pulse widths are so short that ions above a low mass limit were accelerated with at least some constant momentum acceleration character (the experimental details such as actual voltages used and number of accelerating grids were not given, so it is impossible to determine what the low mass limit is). This would of course serve to improve mass resolving power above this low mass limit. Some focussing similar to that observed by Moorman and Bonham (56) and discussed in a following paragraph concerning time-dependent

acceleration may also be present. This supposition is supported by the observation that Gohl et al. (55) use different extraction pulse widths for different mass ranges.

Other investigators have used electric and magnetic fields in TOF instruments to compensate for the effects of the initial spatial and energy spreads. The most notable of these will now be discussed.

Moorman and Parmater (57) have obtained a patent for a TOF mass spectrometer containing a linear TOF region and a curved electrostatic sector region whose energy dispersions with time are mutually compensatory. The two-grid ion source is pulsed, but it is not clear where the space-focus plane lies. The exit of the electrostatic sector is not bounded by a narrow slit and ions having a range of energies are passed to the linear TOF region. No experimental results are presented.

An excellent series of papers was published by Poschenrieder (58-60) concerning a number of TOF designs in which linear TOF regions are combined with magnetic fields for constant momentum acceleration instruments or with electrostatic fields for constant kinetic energy acceleration instruments. The single field ion sources used are not designed to compensate for the initial spatial spread nor is any compensation for the turn-around time provided. The instruments are primarily designed for applications in which the initial energy spread ranges up to and even beyond 100 eV and thus overshadows all other resolution-limiting phenomena. Instruments built according to Poschenrieder's designs (61,62) are thus TOF atom probes in which ions

are "field evaporated" by high voltage (10 to 30 kV) pulses from surfaces. The energy spread of the desorbed ions can range up to several hundred electron volts. Experimental resolutions of up to 1,100 (FWHM) at m/z 62 ($^{186}W^{3+}$) have been obtained. Recently, an excellent mathematical analysis by Sakurai et al. (63) has enlarged upon Poschenrieder's work. Impressive designs incorporating two and four electrostatic analyzers have been proposed.

Another notable series of papers are those published by Bakker. In the "Spiratron" (64) ions follow helical paths in an electric field established between two coaxial cylinders. The principles underlying an instrument similar to those described by Poschenrieder were presented (65). The design again combines both an "active" element (electrostatic sector) and a "passive" element (a field-free flight tube) with mutually compensatory roles in correcting for the effects of the initial energy spread of the ions. This principle, called "time-focussing" by Bakker, was expanded in subsequent publications by extensive mathematical analyses (66,67). Unfortunately, the experimental results never lived up to the expectations.

Another exciting development has been the design of TOF instruments using cylindrical electrostatic mirrors (68,69). These may someday combine the advantages of Mamyrin's planar electrostatic mirror for TOF with the ability to focus ions having a wide angular divergence. A recent publication describes an instrument which incorporates both an electrostatic cylindrical mirror and an electrostatic sector analyzer and has yielded a resolution of 250 for ions of wide initial energy

spread (70).

Stein has shown (36) that simultaneous space- and energy-focussing is impossible in TOF instruments using conservative (time-independent) fields. Consequently, the development of TOF instruments using time-dependent extraction and accelerating fields to compensate for these two limitations is of great interest. Sanzone (71,72) has developed "impulse-field focussing theory". A normal space-focussing source is used but a short (30 ns) high voltage (up to 130 V) pulse is applied to the back plate of the ion source at the same time that the normal ion extraction pulse is applied to the first ion grid. The author states that this serves to reduce the turn-around time. This type of ion extraction also mixes constant energy acceleration with constant momentum acceleration. This helps spread out the masses (the tof is no longer strictly proportional to the mass nor to the square root of the mass) and provides improved resolving power, especially at higher mass. The maximum mass of perfluorokerosene which was resolved at 50% valley was mass 671 (i.e., FWHM resolution of 671 at mass 671). (This is an unusual mass for perfluorokerosene.)

This effect may be at least partially responsible for the improved resolving power observed by Studier (and termed "Studier focussing") when he used continuous ionization in TOF-MS (73). Studier applied a negative voltage pulse to the back plate of the source after the initial ion extraction pulse was applied to the first ion grid. This prevented ions which were formed after the majority of the ions had left the source from being accelerated out of the source. Studier ascribed the

resolution of over 500 he obtained at m/z 208 to trapping of the ions in the potential well of the electron beam.

Another type of time-dependent acceleration has recently been developed by Muga in his "velocity compaction" design (74,75). Ions are extracted from the conventional space-focussing source and ion packets are allowed to begin their normal separation according to velocity in a first field-free region. The ion packets are then subjected to a time-dependent acceleration voltage which imparts slightly more additional kinetic energy to ions at the rear of each ion packet than to those at the leading edge of the packet. This allows the former ions to catch up with the latter and improves mass resolving power. Velocity compaction is simply an enlargement on previous designs for "bunching" ions with a single average velocity (76).

A phenomenon similar to Muga's velocity compaction is reported by Moorman and Bonham (56). These latter two investigators were using a normal space-focussing TOF instrument and simply turned off the ion extraction voltage (on the first ion grid) before all of the ions had exited the region between the first and second ion grids. These slower ions thus experienced a stronger accelerating field within this region than did the ions that had already passed through the second ion grid. By varying the length of the extraction pulse one could optimize the focus for a narrow mass range. In Muga's design the ions have already been allowed to separate according to mass in the first field-free region when the time-dependent acceleration voltage is applied. The voltage is scanned as consecutive ion packets pass through the

acceleration region, providing optimum focussing for each m/z.

Muga reports a mass resolution of over 1,000 for $CHBr_2^+$ and suggests using a double time-dependent acceleration/deceleration instrument for still greater mass resolving power. Unfortunately, daughter ions resulting from metastable decompositions occurring within the first field-free region will produce extraneous peaks in the mass spectrum. Muga has not addressed this problem (77). It may be that this supposed limitation could be used for studying decompositions which occur within the first field-free region as has been the case with the mass reflectron.

Two of the problems which limit resolving power in TOF-MS, both the initial spatial spread and the turn-around time, are significant because conventional TOF sources attempt to pulse randomly moving ions out of the source in a narrow burst. Another way to form a pulse of ions is by simply deflecting a continuous beam across an aperture, as mentioned when discussing the work of Cameron and Eggers, Takekoshi *et al.*, and Fishwick (39,41,43). Figure 9 is a representation of a simple beam deflection system. Not only does this method of ion pulse generation eliminate the initial spatial spread and the turn-around time as resolution-limiting phenomena but it also allows for the use of continuous ion sources in TOF-MS. This is especially important for applications involving the use of ion sources from which ions cannot be extracted in a narrow pulse, such as CI sources.

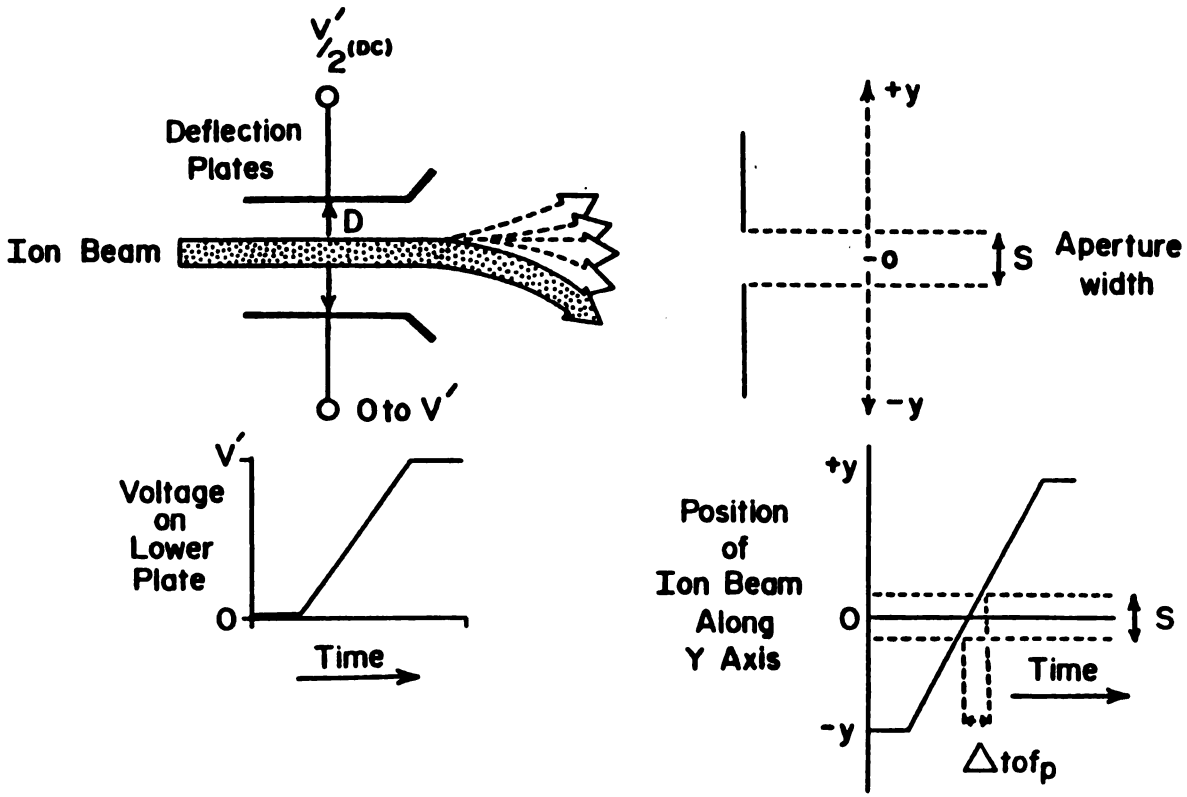

Figure 9. Ion pulse formation by deflection of a continuous beam across an aperture. D = separation between deflection plates; S = aperture width; V' = deflection voltage; Δ tof$_p$ = width in time of ion packet passing through the aperture.

A comprehensive theoretical examination of various methods of obtaining short bursts of ions from a continuous beam by beam deflection has been presented by Fowler and Good (78). They first present equations for the writing speed (i.e., speed with which the ion beam is swept across the limiting aperture) for "impulse beam deflection" where the width of the pulse applied to the deflection plate is short with respect to the transit time of the ions within the deflection plates. Equations are then developed for what they name "differential impulse sweeping" where the beam deflection is performed by sinusoidal, ramped, sawtooth, and square waves with periods longer than the transit time of the ions within the deflection plates. An analysis of the deterioration of the beam quality (i.e., maintaining a monoenergetic beam, for example) is then presented for beams in which the beam diameter is significant with respect to the separation between the deflection plates. A more generalized mathematical analysis of these particular cases is then attempted along with a discussion of the effect of "bunching" on beam quality.

Beam deflection has been used with considerable success in nuclear physics, especially in the production of pulsed proton and light ion beams (79-81). In spite of the early attempts already mentioned (39,41,43), beam deflection was not used with great success in "organic" TOF-MS until the work of Bakker (82-84). He published an excellent theoretical analysis of beam deflection applied to the production of pulses of ions of a variety of masses (83). He was able to show that any beam deflection waveform other than a square wave (some of which are enumerated earlier in discussing Fowler and Good's work) should

introduce mass discrimination. He used a simple continuous EI ion source and a Mullard cathode-ray tube deflection plate assembly (82). The deflection waveform used was a 30 V square pulse (84). A resolution of 700 was obtained at m/z 131 of Xe, while a resolution of 680 was obtained at m/z 44 of propane. These results were obtained using a 1.5 m flight tube.

These results are exciting. However, in using beam deflection in TOF-MS Bakker has eliminated only two of the problems limiting mass resolving power: the initial spatial spread and the turn-around time. Bakker assumed that the energy spread of the ions within the continuous ion beam is negligeable. This remains as a resolution-limiting phenomenon in his beam deflection instrument.

Figure 10 is a conceptual diagram of the instrument designed to combine the advantages of beam deflection in TOF with a kinetic energy filter to limit the energy spread of the ions which are pulsed into the flight tube. Ions are continuously extracted from the ion source. The energy spread of the ion beam is reduced by passing the continuous beam through a kinetic energy filter. The beam is then chopped by beam deflection and the ion packets are detected once they have separated on the basis of velocity in the flight tube. From this point forward, the instrument designed and constructed from this original concept will be referred to as the BEDER-TOF (BEam Deflection-Energy Resolved TOF mass spectrometer).

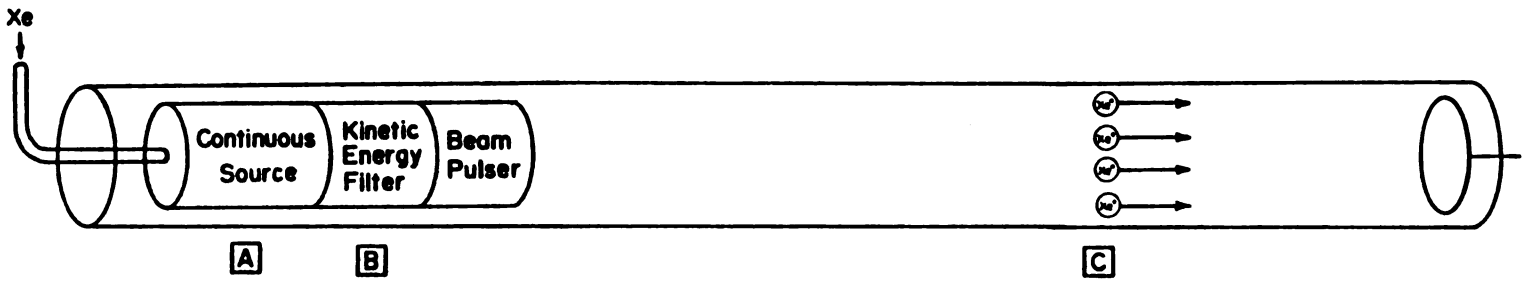

Figure 10. Conceptual diagram of an instrument combining the advantages of beam deflection with a kinetic energy filter and a continuous ion source.

Before the instrument was actually constructed, a mathematical model was developed which would evaluate the manner in which the various instrumental parameters would affect the width in time of the ion packets (and therefore the resolving power). In TOF-MS the mass resolving power, R, is related to the mass, m, at which the measurement is being performed, and the tof of that mass by the relationship:

$$R = m / \Delta m = (tof) / 2\,\Delta(tof) \qquad (4)$$

where Δm and Δtof are a measure of the width of the peak in units of mass and time, respectively. This can easily be seen by taking the derivative of equation (2a) (a variation of equation (2)):

$$m = 2\,z\,e\,V_o\,(tof)^2 / L^2 \qquad (2a)$$

with respect to tof:

$$dm = 4\,z\,e\,V_o\,(tof)\,d(tof) / L^2 \qquad (2b).$$

Substituting for m and dm in equation (4), the desired relationship is obtained.

To derive a relationship between R and the various instrumental parameters, relationships for tof and Δtof must be found. Equation (2) of Chapter 1 describes the tof. The ions extracted from the source are first energy-filtered then pulsed into the TOF region using beam deflection. The spread in arrival times at the detector, Δtof, of an isobaric packet of ions has two components:

$$\Delta tof = \Delta tof_e + \Delta tof_p \qquad (5).$$

Δtof_e is the spread in arrival times due to the energy bandpass of the energy filter. Δtof_p is the width of the ion packet introduced into the TOF region by beam deflection. This assumes that any additional energy spread imparted to the ions along the flight axis by the beam

deflection process is negligible. This assumption is good so long as the diameter of the ion beam is small with respect to the separation between the deflection plates.

First consider Δtof_e. A convenient type of kinetic energy filter is a radial electrostatic analyzer. Equation (6) describes the energy bandpass of an electrostatic analyzer (85):

$$\delta = \frac{y/2 + x/2\ (f\ /\ (b - g))}{a\ (1 + (f\ /\ (b - g)))} \qquad (6).$$

As illustrated in Figure 11, a is the sector radius; b is the distance from the object slit to the sector field; x and y are the entrance and exit slit widths, respectively; the f and g terms are related to the geometry of the sector such that:

$$f = a\ /(\sqrt{2}\sin\sqrt{2}\theta) \qquad (7)$$

and

$$g = (a\ /\sqrt{2})\cot\sqrt{2}\theta \qquad (8)$$

where θ is the sector angle; and δ is related to the energy bandpass of the electrostatic analyzer such that:

$$v_{\mp} = v_o \mp \delta v_o \qquad (9)$$

where $v_{\mp}$ represents the minimum and maximum velocities for ions of a particular mass which exit the electrostatic analyzer and v_o is the average velocity of those ions. Using equation (6) we assume first order focussing, no fringing fields, a small angular divergence from the beam axis, a much greater than the spacing between the electrostatic analyzer electrodes, and motion in the plane parallel to the electrostatic analyzer plates is negligible.

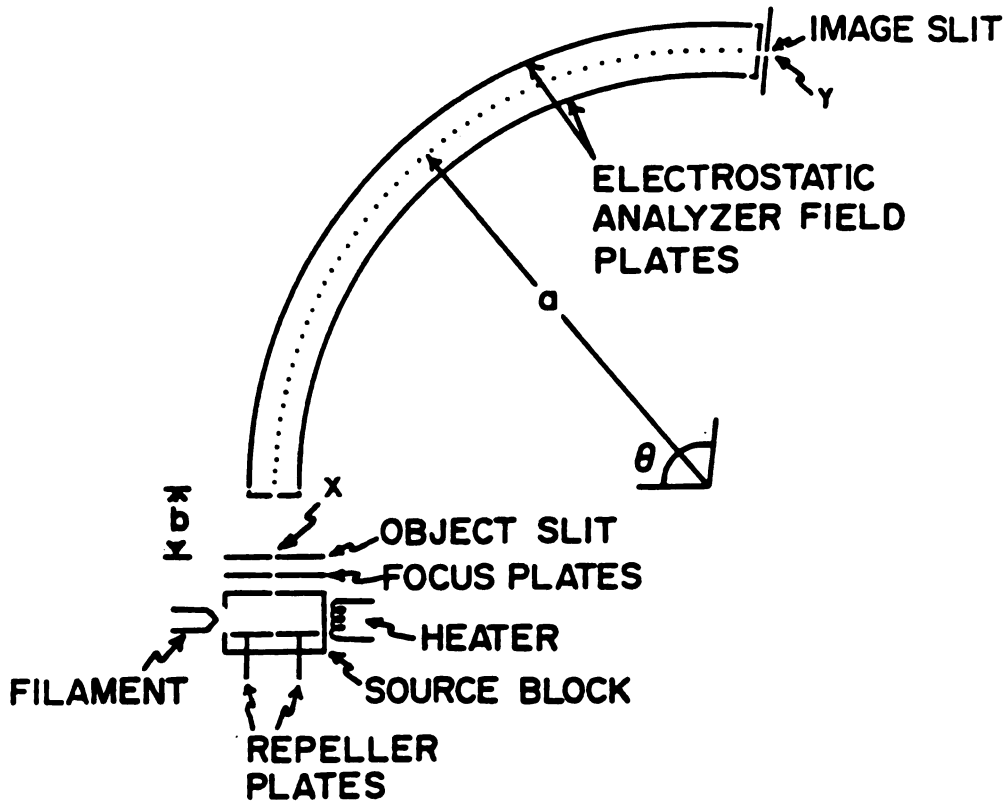

Figure 11. Schematic representation of the ion source and electrostatic analyzer of the BEDER-TOF: a = sector radius (16.3 cm), b = distance from object slit to electrostatic analyzer (7.4 cm); x = object slit width; y = image slit width; θ = 95°, typical operating voltages: ion source block = 2,800 V, repellers = 2,830 V, focus electrodes = 2,600 V, object slit = 0 V, electrostatic analyzer field plates = +/-280 V.

Δtof_e is the difference in flight times between the slowest and fastest ions exiting the electrostatic analyzer:

$$\Delta tof_e = \frac{L}{v_o (1 - \delta)} - \frac{L}{v_o (1 + \delta)} \qquad (10).$$

An equation for Δtof_p has been derived previously (78,83):

$$\Delta tof_p = S\ D \sqrt{2\ m\ V_o} \ /\ V'\ L \sqrt{e} \qquad (11).$$

As illustrated in Figure 9, S is the width of the aperture across which the beam is deflected, D is the separation between the deflection plates, and V' is the deflection voltage. The assumptions made in deriving this equation are: S is much greater than the beam diameter, the tof of the ions through the deflection plates is much greater than the risetime of V', and the total tof of the ions to the detector is much greater than the tof through the deflection plates.

Using equations (2), (4), (5), (10), and (11) a relationship between mass resolving power and instrumental parameters is obtained:

$$R = \frac{L^2\ V'(1 - \delta^2)}{4\ S\ D\ V_o(1 - \delta^2) + 4\ L^2\ V'\delta} \qquad (12).$$

If the energy spread of the ions is assumed to be negligible, (i.e., $\delta = 0$), equation (12) reduces to that obtained by Bakker (83):

$$R = \frac{L^2\ V'}{4\ S\ D\ V_o} \qquad (12a).$$

Since the energy spread of the ions is not negligible (i.e., $\delta \neq 0$) even in the BEDER-TOF, there is not a direct relationship between resolving power and the square of the flight tube length as indicated in equation (12a).

The significance of the δ term in equation (12) can be illustrated by a simple calculation. Using the energy spread of an ion beam accelerated from a typical ion source such as that of the Dupont 21-491B double focussing mass spectrometer one may calculate the resolving power obtainable using equations (12) and (12a). The distance from the repeller plates to the exit plate of the ionization volume in the Dupont source is 0.5 cm. The electron entrance aperture is 0.1 cm in diameter and is located midway between the repellers and the exit plate. A typical repeller voltage of 30 V is used and a linear field gradient is assumed between the repellers and the ionization volume exit plate. The ions are accelerated to 1,400 V after they exit the ionization volume. It is also assumed that the beam deflection TOF mass spectrometer in question uses no kinetic energy filtration. Thus equation (7) (and not equation (6)) is used to calcuate a δ factor of 1.0824×10^{-3}. For a flight tube length of 2.0 m, a deflection voltage of 40 V, an aperture diameter of 0.0254 m, and a separation between the deflection plates of 0.002 m one obtains a resolution of 562 using equation (12a). Equation (12) yields a resolution of 164 (peak widths measured at baseline). The δ factor is indeed significant in this case.

A restriction which is a function of the deflecting field exists on the length of the deflection plates (in the direction of the flight tube axis) when using beam deflection to produce ion pulses for tof measurements. Only ions which are midway along the deflection plates when the field reversal occurs experience equal and compensatory forces during their flight (Figure 28 of Chapter 4 illustrates the path taken by these and other ions within the deflection plates). Only these ions

and a narrow band of ions on either side of the central packet eventually make it through the aperture. If the deflection conditions are such that the ions strike the deflection plate before they have traversed half the length of the deflection plate, no ions will be able to exit the deflection plate region when a field reversal occurs. Thus one may derive an equation for the maximum deflection plate length which is allowed, P. The distance which must be travelled by the first ions to strike the deflection plate, j, is:

$$j = 1/2D - 1/2y \qquad (13).$$

Assuming that the deflection plate which is struck by the ions is at ground and the opposite plate is at a d.c. potential of one half the deflection pulse amplitude, V', one may calculate the transverse acceleration experienced by the ions when they enter the deflection plate region, acc_y:

$$acc_y = e\ V'\ /\ 2\ D\ m \qquad (14).$$

Assuming that there are no fringing fields and that the ions possess no velocity component in the direction in which they are being deflected before they enter the deflecting field, one may write an expression for the time elapsed between the time the ions enter the deflection plate region and the time at which they strike the deflection plate, tof_{crit}:

$$tof_{crit} = \sqrt{2\ j\ /\ acc_y} \qquad (15).$$

The velocity in the axial direction, v_x, is assumed to be unmodified by the beam deflection process. It is:

$$v_x = \sqrt{2\ e\ V_o\ /\ m} \qquad (16).$$

The distance travelled in the axial direction during tof_{crit} is simply one half the maximum plate length, P:

$$1/2\ P = tof_{crit}\ v_x \qquad (17).$$

Substituting from equations (15) and (16) into (17) one obtains:

$$1/2\ P = \sqrt{4\ j\ e\ V_o\ /\ acc_y\ m} \qquad (18).$$

Substituting from equations (13) and (14) into (18) and rearranging one obtains:

$$P = 4\ \sqrt{(D - y)\ D\ V_o\ /\ V'} \qquad (19).$$

If the length of the deflection plates exceeds $\underline{P}$, no ions will be admitted to the flight tube. These equations have been used in designing an optimized beam deflection assembly which will be described in the following chapter.

CHAPTER 3

INSTRUMENTATION AND PROCEDURES

This chapter will begin with brief descriptions of the Bendix 12-101 TOF mass spectrometer and its progeny, the CVC Products 2000. The performance of these two commercially available instruments was used as a benchmark by which to judge the performance of the BEDER-TOF. The BEDER-TOF will then be described in greater detail. Finally, the experimental procedures used to collect data will be reviewed.

A. Description of the Bendix and CVC TOF mass spectrometers

The functional descriptions of the CVC and Bendix instruments are virtually identical to that presented in the respective Operations Manuals since only small modifications have been made on the instruments. Both use modified Wiley-McLaren space-focussing ion sources. The Bendix uses a three-grid ion source in which the first two grids are pulsed. The CVC uses a four-grid source in which the first two grids are pulsed. The electronics for the CVC are new solid state electronics while the Bendix uses the original tube electronics. The main advantage of the newer electronics from the standpoint of instrumental performance is the much shorter rise times of the ion

source and detector pulses. This improves mass resolving power.

The flight tube lengths are comparable at 1.75 m for the Bendix and 2.0 m for the CVC. Both use an acceleration voltage of 2.8 kV. The source of each instrument is at ground potential such that it is not necessary to float the pulsing electronics at high positive potentials. Consequently, the last ion grid and the flight tube liner of each instrument are held at the accelerating voltage. While the Bendix was equipped with time-lag focussing capabilities in the past, only the CVC has the capacity for time-lag focussing presently. The flight tube liner and the detector used in the Bendix are those used in the BEDER-TOF and are described in subsequent paragraphs. Both the liner and detector of the CVC are virtually identical to those of the Bendix in function and performance. The original Bendix multiplier plates have been replaced by plates carrying the "herring bone" pattern of the modern CVC detector plates.

The original Hg diffusion pump of the Bendix has been replaced by a DPD-4 diffusion pump which is also described in the BEDER-TOF section. The CVC is pumped by a 4 inch and a 6 inch oil diffusion pump.

Though a comparison of sensitivities has not yet been performed, the ion grid apertures and the electron slits of the CVC are narrower than those of the Bendix by a factor of at least two. If the detectors are assumed to be equivalent, the sensitivity of the Bendix should be greater than that of the CVC. However, the short rise times of the CVC control pulses should improve this instrument's sensitivity as well as

its resolving power.

The Bendix uses the gas phase sample inlet described in the BEDER-TOF section. The CVC uses either a Hewlett-Packard capillary GC or a fixed molecular leak inlet system.

B. Description of the BEDER-TOF

Figure 12 is a schematic diagram of the BEDER-TOF. Figure 13 is a photograph of the entire instrument excluding the data system, while Figure 14 is a close-up photograph of the modification which turns the Bendix 12-101 into the BEDER-TOF. The description of the instrument will begin with the ion source region and conclude with the detector and the data collection hardware.

1. The Ion Source and Sample Inlet Systems:

The ion source of the BEDER-TOF consists of the unmodified source of a Dupont 21-491B double focussing mass spectrometer. As shown in Figure 11 of Chapter 2, the source is simple in design (for an expanded view of the source see Figure 5-4 of the 21-491B manual). The source block operates at the accelerating potential. To the source block are attached the filament, the heater (in a position opposite the filament where the electron trap of most ion sources would be located), and the thermocouple. Looking from the source toward the detector, two openings (roughly 1 mm in diameter) are located on the left side of the source. They are used for the gas inlet (or GC inlet) and for the direct probe.

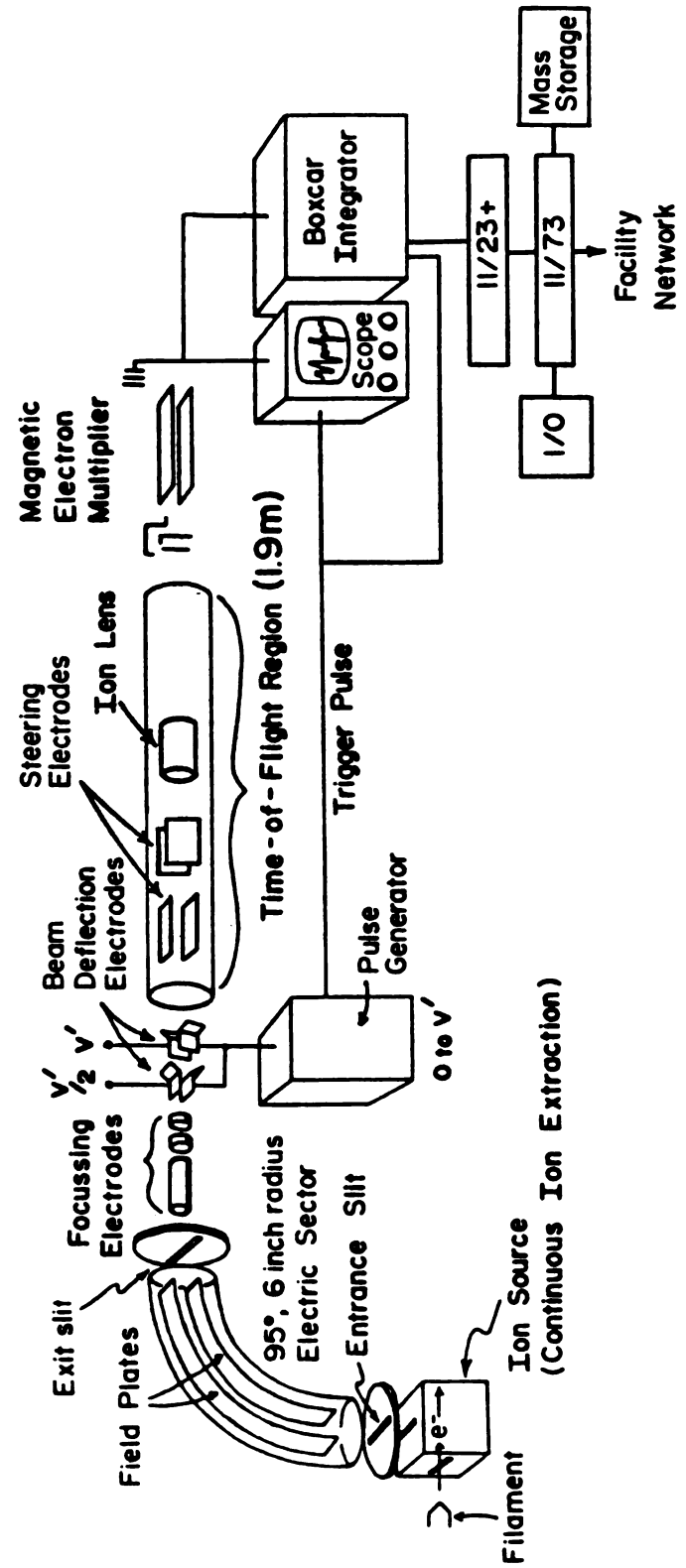

Figure 12. Schematic representation of the complete BEDER-TOF (BEam Deflection Energy-Resolved TOF mass spectrometer). The CRT beam deflection assembly is shown here.

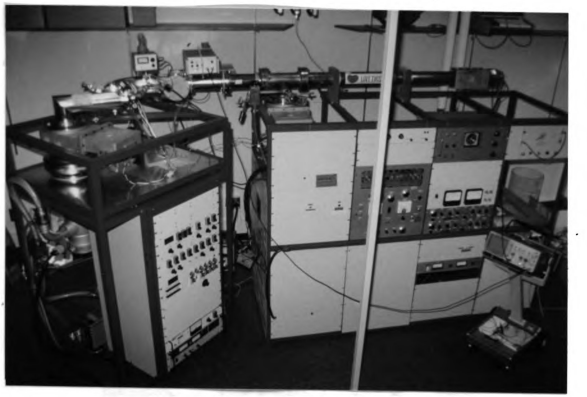

Figure 13. Photograph of the entire BEDER-TOF, excluding the data system.

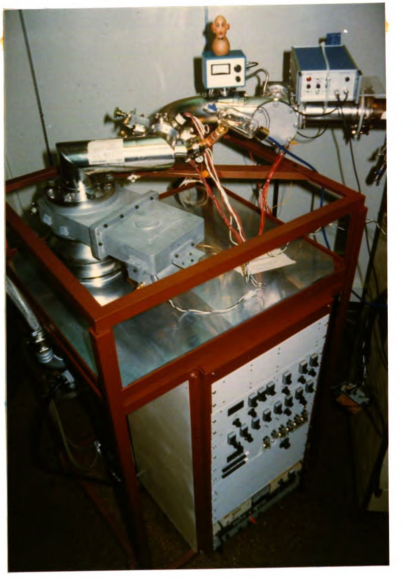

Figure 14. Close-up photograph of the modification which transforms the Bendix 12-101 into the BEDER-TOF. Pictured are the ion source, electrostatic analyzer, and beam deflection regions.

The ionization volume within the source is 1.9 cm in diameter by 0.5 cm in depth. At the rear of this volume are the two semi-circular repeller plates which operate at voltages slightly greater than that of the block. The "No. 1 slit assembly" forms the front boundary of the ionization volume and is at the block potential. The ion beam is focussed by a pair of focussing plates which operate at voltages below the accelerating potential. Finally the ion beam is defined by the object slit, which is at ground potential. The only modification from the original design is that the filament used to produce ionizing electrons is a 0.05 cm by 0.0025 cm (0.020 in. by 0.001 in.) 100 % rhenium ribbon (Scientific Instrument Services, Pennington, New Jersey).

The CI source differs from the EI source in the reduction of the electron entrance aperture in the source block from 0.127 cm (0.050 in.) in diameter to 0.036 cm (0.014 in.) in diameter and the reduction of the size of the No. 1 slit assembly from 1.07 cm (0.422 in.) by 0.046 cm (0.018 in.) to 0.079 cm (0.031 in.) by 0.025 cm (0.010 in.). Also, a gold foil molecular leak is located on the right side of the CI source.

The primary means of sample introduction is through a simple heated inlet system constructed from stainless steel Swagelok fittings and tubing. Figure 15 is a schematic diagram of the inlet system. A Nupro SS-4MGD double needle valve is used to leak vapor into the mass spectrometer and is sufficient to give reasonably good regulation of ion source housing pressures from 6×10^{-7} to 2×10^{-4} torr at inlet pressures of approximately 1 torr to above atmospheric pressure, respectively. Electrical isolation of the inlet system from the source

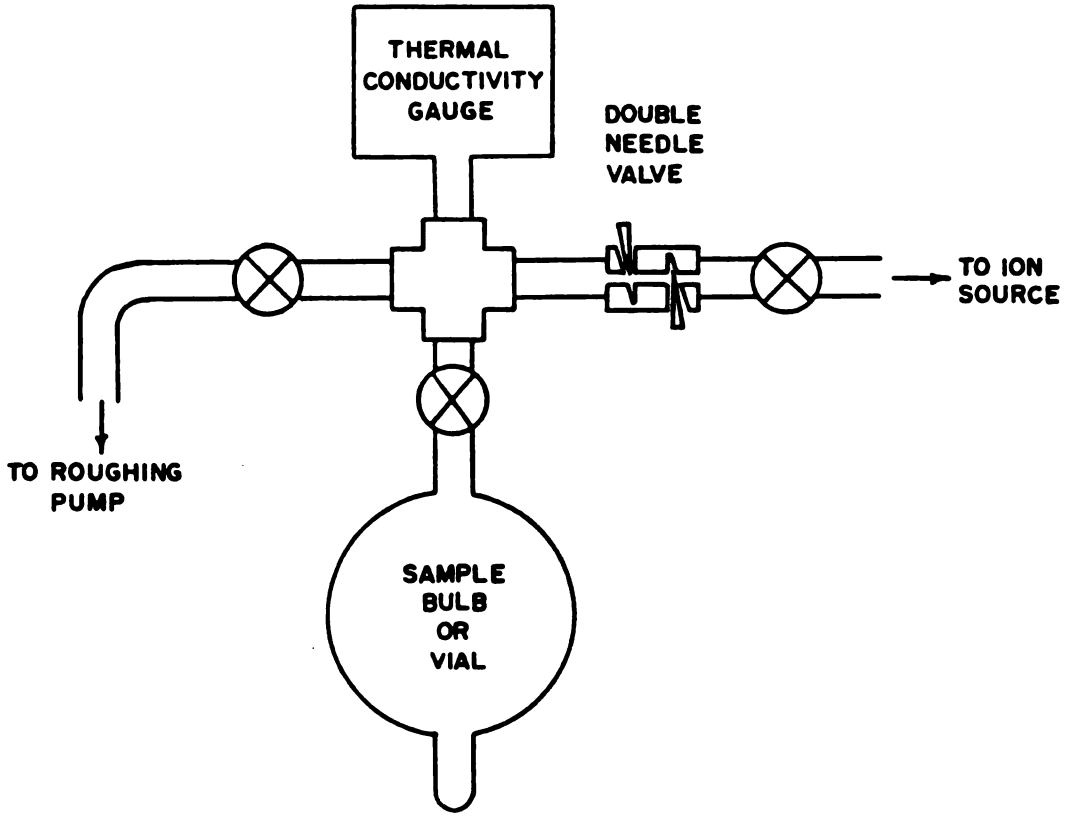

Figure 15. Schematic representation of the inlet system, excluding the heating tape.

block is provided by a 5 cm length of SP-3 Vespel polyimide tube (Dupont Chemical Company) of 0.64 cm o.d. and 0.32 cm i.d.. Heating of the inlet system is accomplished using a simple fiberglass insulated heating tape and a variable transformer.

The standard Dupont solids probe (Figure 5-6 of the Dupont manual) is also available as an inlet system. It is designed for conventional solid sample introduction and for desorption/chemical ionization (DCI) studies using a Vespel probe tip.

The electronics to power and control the source were designed and constructed with the help of Martin Rabb to allow for much greater versatility than that provided by the original Dupont electronics. The design requirements were:

1. provide d.c. voltages for the ion source elements;

2. heat the ion source and monitor the source block temperature;

3. supply current to the electron-producing filament of the ion source such that the current may be regulated for constant filament current or constant emission current; also bias the filament with respect to the ion source block.

The voltage dividers shown schematically in Figure 39 of the Appendix supply the ion source voltages. The 0 to 5 kV power supply used is the model 205A-05R from Bertan Assoc., Inc. (Syosset, NY). A DM-4105 2 V full scale digital panel meter (Datel-Intersil, Inc., Mansfield, MA) is used to monitor these voltages. Low voltages (as those shown in Figure 40 of the Appendix) are selected by a push-button switch and measured via a 10,000:1 divider. Voltages above 500 V are presented to the divider via a bank of high voltage relays.

The Dupont ion source heater and thermocouple are used to heat the ion source and monitor the source temperature. The heating coil is powered by a variable transformer through an isolation transformer. The thermocouple meter is floated on a recessed panel at the ion source "block" potential.

The circuit which controls the current supplied to the ion source filament is designed to operate in two modes of control: filament current control mode and emission current control mode. Figure 16 is a simplified circuit diagram of the former control mode.

Current through the filament, I(f), develops a feedback voltage across the 0.4 Ω "filament current sense" resistor which is compared with the voltage set by the front panel "current" control. The power transistor acts to reduce any difference by altering the current supplied to the filament. The voltage developed across the "limit current sense" resistor is used by the current limiting circuit to limit the filament current at 5 amperes.

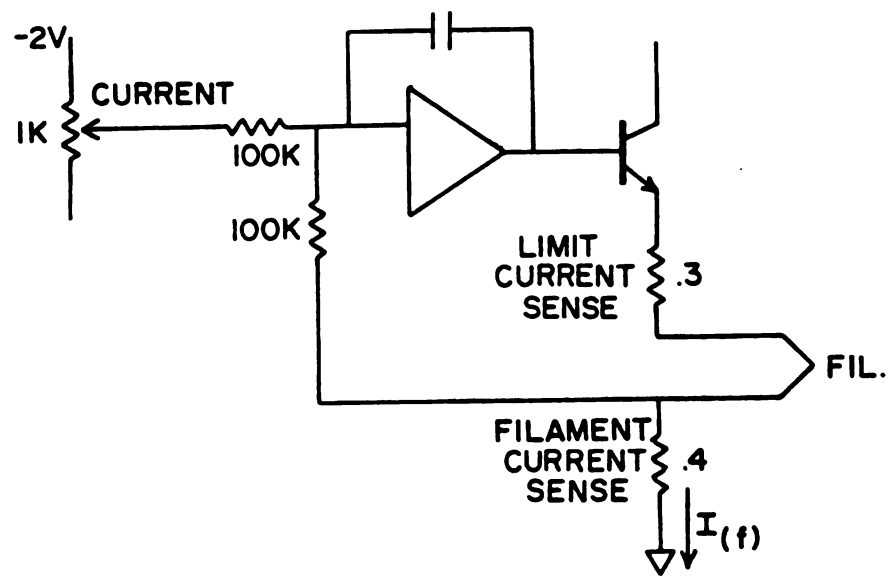

Figure 16. Filament current controller: filament current control mode.

As shown in Figure 17, the emission current control feedback voltage is taken across a 10 Ω resistor in series with the "bias" supply and the ion source "block" through which emission current, I(e), must flow. The instrumentation amplifier gain is set to 100, making its output equal to 1,000 x I(e). This output is used in the metering circuit.

The complete schematic for the filament current controller is shown in Figure 41 of the Appendix. The entire circuit is floated at the 0 to 5 kV ion source "block" potential.

A DM-3104 digital panel meter (Datel-Intersil, Inc.) is used to display either filament or emission current. A divider across the "filament current sense" resistor provides a scaled voltage to the meter representing the value of the filament current such that:

$$\text{meter voltage} = 0.4 \times [4.99 \times 10^3/(4.99 \times 10^3 + 15 \times 10^3)] \times I(f)$$

or

$$\text{meter voltage} = 0.1 \times I(f).$$

The meter decimal point is appropriately placed to read Amperes of filament current or microamperes of emission current.

Also noteworthy are a comparator used to sense an open filament and light an LED, and diodes added to the instrumentation amplifier ("F" in the schematic) circuit for protection from arcing within the ion source.

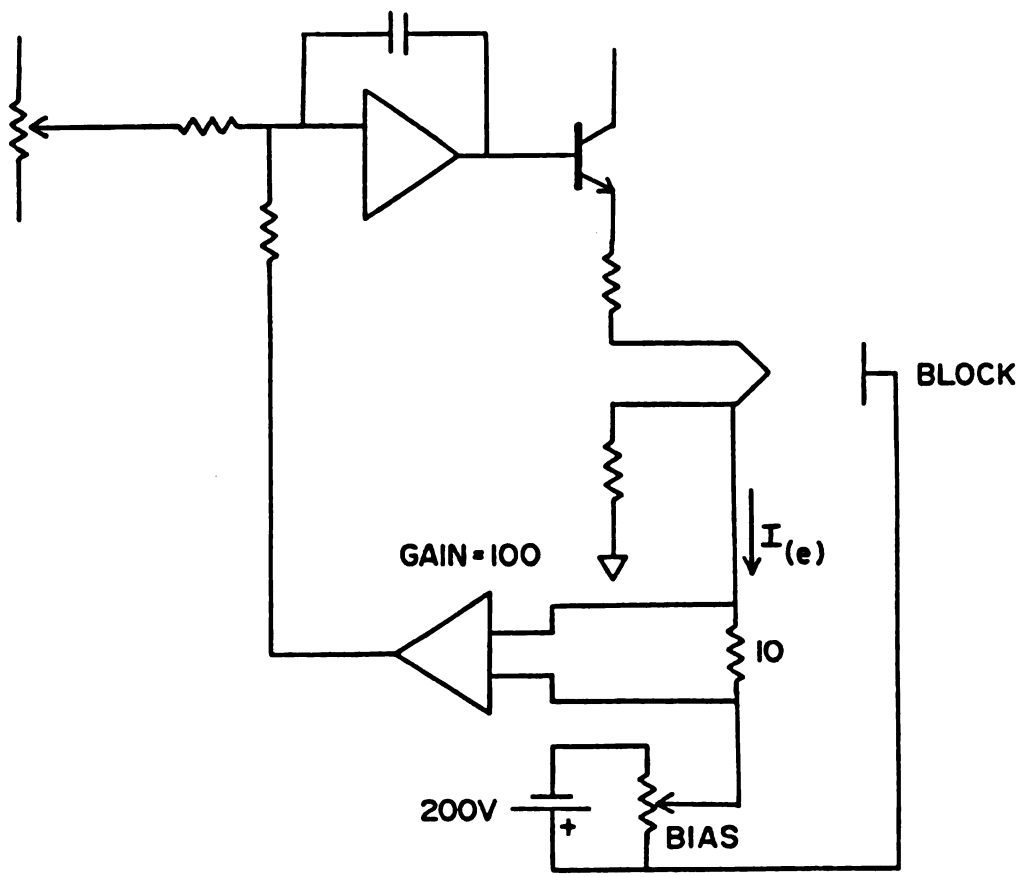

Figure 17. Filament current controller: emission current control mode.

The source high voltage feedthroughs are designed to operate at up to 1,400 V. However, it was desired to operate with accelerating potentials of up to 4,500 V. Arcing between the feedthrough pins and the source housing was observed at voltages above 2,000 V. The base of each feedthrough pin was covered by a short piece of Teflon tubing and an equally short piece of silicon tubing. The source housing closest to the feedthrough pins as well as the base of the pins themselves were then coated with multiple coats of "Red-X TV Corona Dope" (GC Electronics, Rockford, Illinois). No arcing has been observed at repeller voltages up to 4,500 V.

2. The Electrostatic Analyzer:

The electrostatic analyzer is that of the Dupont 21-491B (Figure 5-8 of the Dupont manual). It has a radius of 16.27 cm and a sector angle of 95°. The object slit of the sector is incorporated into the ion source. Two object slit widths are available: 0.076 mm (0.003 in.) and 0.020 mm (0.0008 in.). The image location is very near the electrostatic analyzer exit plate. Using equation (7.24) of reference 85 the separation between the field plates and the image line is 2.6 cm, while the distance from the end of the field plates to the detector side of the exit plate is 3.7 cm. Thus a convenient and reasonable location to place a slit which would limit the range of kinetic energies allowed to pass out of the electrostatic analyzer would be the exit plate. However, the "field plate slit" mounted on the exit plate of the sector (item 6 of Figure 5-8 of the Dupont manual) is wide and is designed to pass a range of kinetic energy values to the mass spectrometer magnet.

To limit the range of kinetic energies allowed to pass out of the electrostatic analyzer, the Dupont exit slit and the beam monitor slit (item 8 of Figure 5-8 of the Dupont manual) were removed and an adjustable image slit was designed as part of the beam deflection assembly. This image slit (see Figure 20) consists of two safety razor blades mounted on an aluminum block which is mounted on the sector exit plate. Adjusting the image slit width is performed by bringing the cutting edges of the razor blades to a snug fit about a spacing shim. The fasteners holding the blades to the aluminum block are then tightened.

The ions passing through the image slit are sampled by a thin wire electrode (diameter of 0.064 cm) connected to the Dupont 21-491B beam monitor. The sampling wire is mounted orthogonal to the ion beam on a separate aluminum plate (see Figure 20).

The electrostatic analyzer power supply was also designed and constructed primarily by Martin Rabb. The design requirements for the electrostatic analyzer power supply were:

1. provide potentials to the electrostatic analyzer plates in three control modes:

    a. in a mode in which the potentials are manually set from front panel controls;

    b. in a fixed ratio to the ion source potentials for normal

operation;

c. in a manner which is decoupled from the ion source potentials and variable from an external control voltage for TRIKES;

2. provide a means to offset the electrostatic analyzer plates voltages with respect to ground.

The electrostatic analyzer power supply, the schematic of which is shown in Figure 42 of the Appendix, is designed to fulfill the requirements listed above. The outputs of the dual tracking supply can be varied between +/-10 V and +/-500 V. The negative output is used to drive the positive section of the supply. The reference for the negative output is the regulated +15 V. Voltage followers drive the dividers in the supply to insure constant impedance as voltage is varied. PNP transistors with sufficiently high voltage ratings could not be found so two transistors are used in series for the negative output. The potentiometer in the base of the upper transistor balances the drop between both transistors in the series pair. In order to use a standard stock transformer, one with a higher voltage rating was chosen and loaded down so as not to exceed the voltage rating of the high voltage transistors.

The three different control mode requirements listed earlier are accomodated as follows:

1. a dual 10 kΩ coarse control potentiometer and a 100 Ω fine control potentiometer are used for "manual" control;

2. a voltage derived from the "block" voltage is used in the "track" control mode (this is the reverse of the commonly employed method in which the "block" voltage tracks the electrostatic analyzer power supply voltages);

3. an external 0 to +5 V source is used to set the outputs between +/-10 V and +/-500 V, respectively, in the "program" control mode.

Both electrostatic analyzer power supply outputs can be offset by +/-15 V using a single front panel control. The offset is accomplished by adding the same voltage at both summing junctions of the operational amplifiers A and B, causing their outputs to shift by equal amounts in the same direction.

3. The Beam Deflection Assembly:

The beam deflection assembly is housed within a stainless steel cross (tubing i.d. is 9.8 cm, o.d. is 10.0 cm) which is equipped with standard Bendix flanges. This is attached to the detector side of the electrostatic analyzer housing using an aluminum mating flange. A note concerning the frame on which the the source, electrostatic analyzer, associated pumping, and the new electronics are mounted is in order. The Bendix flight tube described in a subsequent paragraph is fixed in height so that the Dupont source, electrostatic analyzer, and pumping ride on a table of adjustable height to facilitate the mating (see Figure 14). In addition, this entire frame is mounted on castors so that the BEDER-TOF modification can be rolled away and the conventional Bendix source reinstalled to conduct experiments using the Bendix 12-101.

Of the various waveforms which can be used for beam deflection (78) Bakker has shown that only the square wave introduces no mass discrimination (83). A square wave of period twice as long as the flight time of the largest ion of interest would thus seem to provide an optimum waveform for beam deflection. A burst of ions would be injected into the flight tube on both the rising and falling edges of the square wave. However, only a pulse generator can provide the amplitude and risetime which the theory of beam deflection demands. The use of a pulse generator presents the problem that two overlapping spectra are produced upon each pulse (one on the leading edge and one on the tailing). One of these spectra must be discarded. Bakker has presented

four convenient methods of gating one burst of ions to the flight tube while the other burst is gated away using two pairs of deflection plates (84). Figure 18 presents the four options. The only option used regularly in the BEDER-TOF has been Method I in which the first pair of deflection plates is used to produce the ion bursts and the second pair is used to gate the burst produced on the tailing edge of the pulse away from the flight tube axis. The other options should yield equivalent results but each may exhibit advantages or disadvantages in practice.

The first beam deflection assembly used in the BEDER-TOF was that from a cathode ray tube (CRT). It is represented in Figure 19. The image slit described in a previous paragraph was incorporated in the base which was used to mount the CRT assembly to the exit plate of the electrostatic analyzer. The first element of the lens system was connected to the Dupont beam monitor and intercepted roughly nine tenths of the ions passing through the electrostatic analyzer image slit. Since the deflection plates are not square with respect to the four glass posts which hold the assembly together a He-Ne laser was used to align the assembly in its mounting base.

It was obvious that better sensitivity would be achieved if the lens system of the CRT assembly were not present. Also, greater resolving power was expected from a beam deflection assembly of different design. Equation (12) predicts higher resolution values as the deflection voltage is increased and the accelerating voltage is decreased. However, equation (19) shows that the maximum deflection plate length decreases as the deflection voltage increases and the

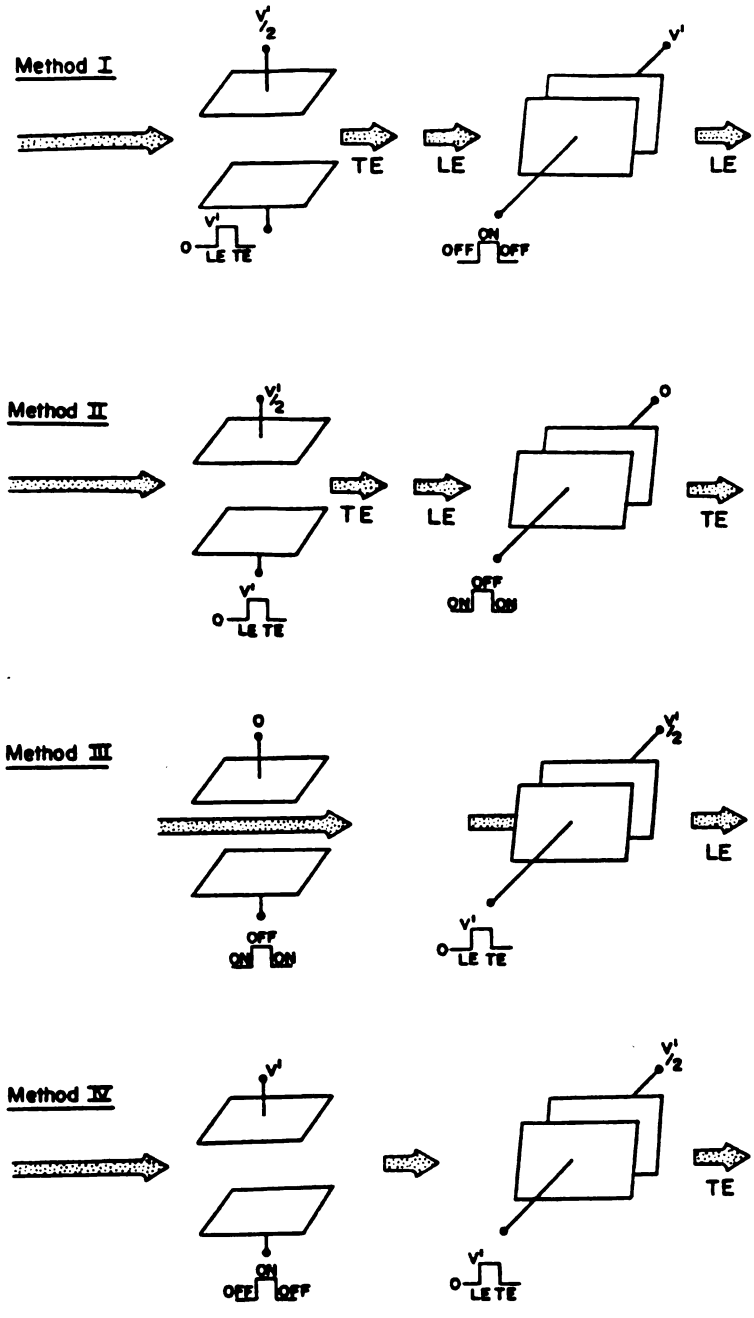

Figure 18. Four proposed methods of pulsing/gating a continuous ion beam with a pulse generator and two pair of deflecting plates. LE = pulse of ions produce upon leading edge field reversal. TE = pulse of ions produced upon trailing edge field reversal.

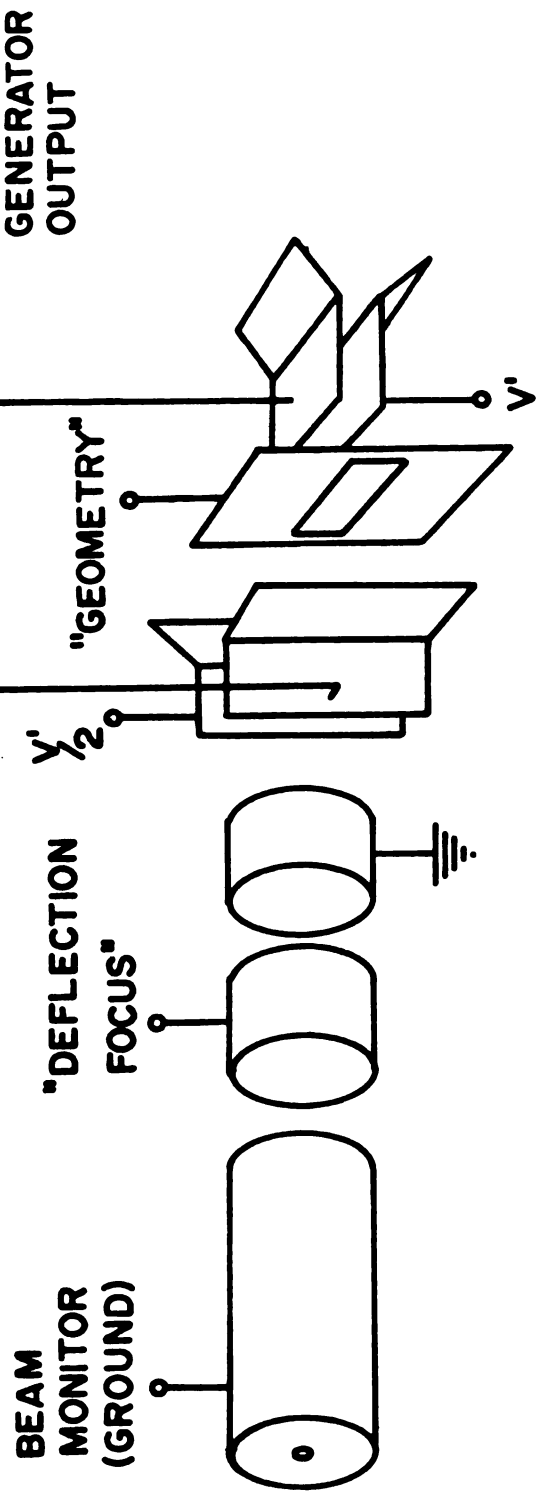

Figure 19. Schematic representation of the CRT beam deflection assembly.

accelerating voltage decreases. The flight time of the fastest ion through the deflection plates is assumed to be long with respect to the rise time of the deflection voltage pulse in the derivation of equation (12). This sets a lower limit on the length of the deflection plates. The "optimized" beam deflection assembly is represented in Figure 20. The length of the pulsing plates was chosen to be 1.4 cm. This is only one (the one most often utilized) of a number of possible configurations of the optimized beam deflection assembly since it is of modular design. The unit can be configured with or without focussing lenses, with or without refractor plates, with or without the geometry electrode, and with both the pulsing and the gating plates in the horizontal direction or with only the former in the horizontal and the latter in the vertical direction.

The only other restrictions on the assembly are: a) the fastest ion from the leading edge burst of ions must not arrive at the gating plates before the gate is fully open, and b) the slowest ion from the leading edge burst of ions must pass through the gating plates before the gate is closed. As the pulsing plates are designed with the assumption that the flight time of the fastest ion must be long with respect to the rise time of the pulse, restriction a) is automatically satisfied, except perhaps for mass 1 at 5,000 V accelerating voltage. Its flight time through one half the length of the pulsing plates is 7 ns while the nominal rise time of the pulse is less than 5 ns (measuring the rise time of the pulse on the deflection plates without affecting the rise time is very difficult - The rise time is observed to be less than 10 ns using the 100 MHz bandpass probe). The maximum pulse width

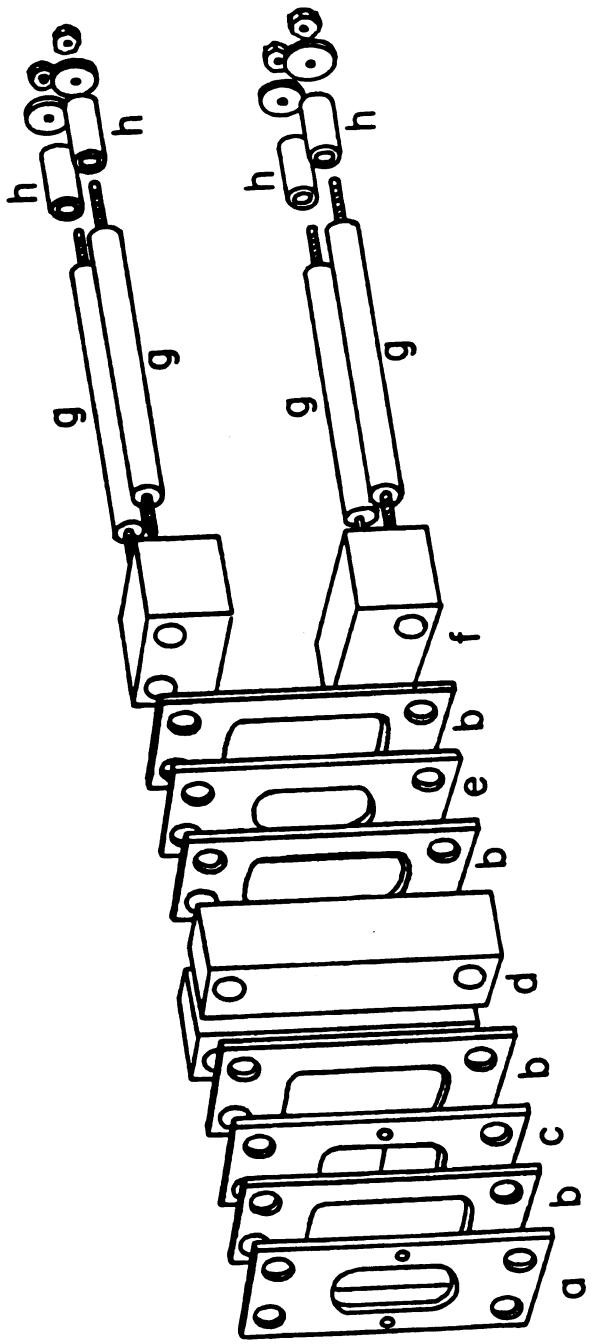

Figure 20. One configuration of the "optimized" beam deflection assembly: a = image slit (see text); b = Teflon insulating sheet (0.8 mm wide); c = beam monitor electrode (see text); d = horizontal deflection plates (height = 6.3 cm, length = 1.4 cm, separation between plates = 0.2 cm) (pulse forming plates); e = geometry electrode; f = vertical deflection plates (gating plates); g = Vespel rods on which elements are mounted; h = Vespel spacers.

of the pulse generator used in these experiments is approximately 2 μs. This, in combination with restriction b), limits the length of the gating pair of plates. The length most commonly used is 1.6 cm. This allows ions of at least mass 1,000 to pass through the gating plates at an accelerating voltage of 700 V (the minimum used) before the gate is closed.

Using equation (12) and the instrumental parameters which were available, the specification requirements of the pulse generator to be used in these experiments were determined to be: a variable pulse amplitude to at least 200 V, a 0 to 10 kHz repetition rate, a variable pulse width to at least 2 μs, and a rise time of less than 5 ns. Dr. Walter Chudobiak of Avtech Electrosystems Ltd. (Ottawa, Ontario, Canada) agreed to build a pulse generator to our specifications. The maximum pulse amplitude of this Model AVR-1-C-MSU1 pulse generator is 200 V and the maximum pulse width is 2 μs. A rear panel output provides a d.c. voltage of the same magnitude as the pulse amplitude. This d.c. output is divided down to furnish potentials to the one d.c. plate of each pair of deflection plates. The voltages for the geometry electrode and deflection focus lens, when incorporated in the beam deflection assembly, are furnished by the dividers shown in Figure 40 of the Appendix. The 0 to 2 kV power supply is a Kepco, Inc. (Flushing, NY) model APH 2000M.

4. The Flight Tube:

The flight tube consists of a 10.0 cm o.d., 9.8 cm i.d. stainless steel tube. Flight tube lengths used in these experiments were 1.1 m and 1.9 m. The tubes were obtained from the Bendix 12-101 and from the remains of a Bendix 14-101 TOF mass spectrometer. The flight tubes are lined with isolated stainless steel tubular mesh. High voltage may be applied to this mesh to post-accelerate the ions (84) but the liner has usually been operated at ground potential. A baffle located between the 12-101 source and flight tube is part of the unmodified flight tube liner. It was removed for the BEDER-TOF experiments. The liner from the 14-101 was rebuilt. Within the mesh are held vertical and horizontal steering plates and an ion lens to direct and focus the ion packets as indicated in Figure 12. The voltages for these steering and focussing elements are supplied by the dividers shown in Figure 40 of the Appendix.

5. The Detector:

The magnetic electron multiplier used in these experiments was also obtained from the Bendix 12-101. The active surface of the multiplier forms the limiting aperture, S (see Figure 9), in these beam deflection experiments. Ions enter the multiplier through an electrode called the "stack". The normal opening in the stack is one inch in diameter. This aperture was modified such that it is variable. The tubular, axial portion of the stack was removed entirely while two holes were drilled on either side of the one inch aperture in the flat portion of the

stack. A razor blade was mounted on either side of the stack using a nut and bolt; the width of the aperture is varied by sliding the razor blades to the desired location and tightening the fasteners. The stack, normally kept at high voltage in the Bendix, was grounded during certain experiments.

The detector signal is amplified using a Comlinear Corp. (Loveland, Colorado) model E220 200 MHz amplifier. The original Bendix high voltage supply and divider is used to power the magnetic electron multiplier. The Comlinear amplifier is powered by a Sola "Solids" +/-15 V supply.

6. The Data Collection System:

Focussing and tuning the instrument are performed by observing the amplified multiplier anode signal with a Tektronix 2235 100 MHz oscilloscope. Data acquisition is performed using a variety of methods. The majority of the data was collected using an EG&G Model 162 boxcar averager with M164 and M165 gated integrator modules. The output of the boxcar was originally recorded using a Varian A-25 strip chart recorder. This was later displaced by the data system based on a Digital Equipment Corp. 11/23+ "front end" processor and a 11/73 "host" processor.

The pulse generator "sync" pulse is used to trigger the boxcar. After a delay, the boxcar time aperture opens and samples the ion current. To collect a mass spectrum, this delay is incremented and the aperture is scanned over the range of flight times corresponding to the ions of interest. An output of the boxcar provides a voltage related to the position of the time aperture along the tof axis. The interface to

the boxcar was designed and constructed by Michael Davenport and John Holland. It consists of a 15 bit tracking analog-to-digital converter which digitizes this boxcar voltage. A Digital Equipment Corp. DRV11-J 16 bit parallel input/output board serves to transfer this digitized value to the 11/23+. A second boxcar output voltage is related to the ion intensity and is first processed by a quad amplifier. Each channel of the amplifier has a successively lower amplification (x64, x16, x4, x1). The channels are multiplexed to a Digital Equipment Corp. AVX11-C 12 bit analog-to-digital converter board in the 11/23+. The DRV11 is also used to monitor the scan status of the boxcar and to control the "reset" function of the boxcar to initiate scans.

Data collection, processing, and display routines were written by Kenneth Hollingshead and proved to be versatile and extremely valuable. The routines are improvements on the familiar MSSIN, MSSOUT, MSSCAL, and MSTEST routines previously described (86). Most of the data for this dissertation were collected using the program MSTEST which simply records the output of the boxcar vs. time. However, the ability to average successive scans of the boxcar acquired using the data system has proven to be invaluable when dealing with low ion currents.

A Tektronix Model 4105 color graphics terminal and a Model 4695 color printer are used to communicate with the data system. Mass storage is provided by a Fujitsu 84 Mbyte M2312K Winchester disk drive and a Kennedy Model 9000 9-track magnetic tape drive. The data system is part of a network and is linked to the primary computer system of the MSU/NIH Mass Spectrometry Facility for data analysis.

In some instances an actual photograph of the scopeface was useful. Excellent results were obtained using the Tektronix C-12 scopeface camera and Type 47 (high contrast, ASA 3000) film.

7. The Vacuum System:

Figure 21 is a schematic diagram of the vacuum system. The instrument is differentially pumped with the only opening between the source and electrostatic analyzer being the object slit. The source side is pumped by a Varian VHS-4 diffusion pump and cryotrap which are backed by an Edwards E2M-18 two-stage rotary vane pump. The cryotrap has rarely been used as the VHS-4 furnishes adequate pumping speed and the Santovac-5 diffusion pump oil provides a relatively clean vacuum, The Edwards mechanical pump is also used to evacuate the inlet system when necessary.

The electrostatic analyzer, deflection plate assembly region, the flight tube, and the detector region are pumped by a Cooke Vacuum Products DPD-4 diffusion pump and water-cooled baffle. The DPD-4 is backed by an Alcatel ZT-2008A rotary vane pump. Both diffusion pumps can be isolated from the mass spectrometer with Vacuum Research Corp. LP-4 pneumatic gate valves. On/off valves for the roughing and backing lines were obtained from Vacoa Co. of Bohemia, N.Y..

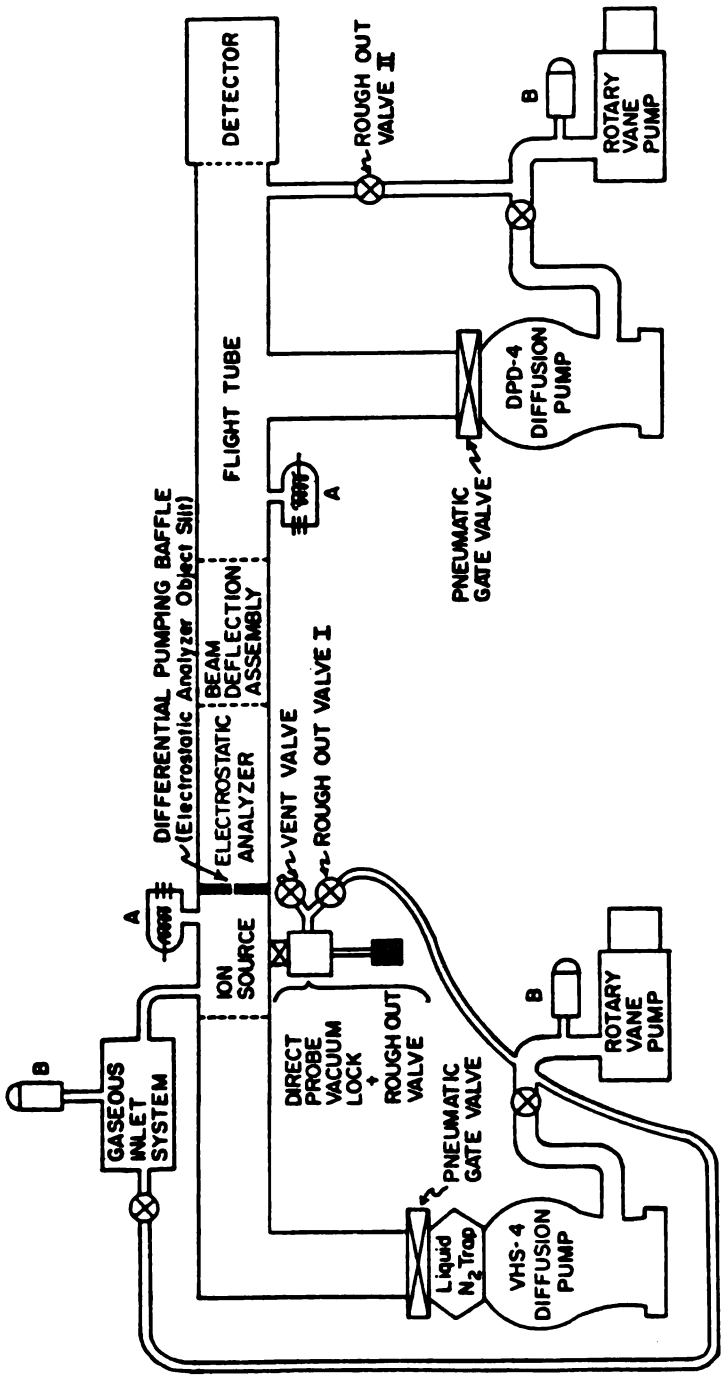

Figure 21. The BEDER-TOF vacuum system: A = ionization gauge tube.
B = thermo-gauge tube.

The pressures above the backing pumps and in the inlet system are monitored by series 260 Granville-Phillips thermo-gauges and controller while the pressures in the source housing and flight tube regions are measured using Bayert-Alpert ion gauge tubes and the series 260 Granville-Phillips controller. A relay in the controller is used to close the two gate valves if the pressure in the instrument increases to the point where the controller turns off the ion gauge tube filament. Heat-actuated relays on each diffusion pump shut off power to the pump heater if the cooling water temperature increases beyond a pre-set point.

C. Experimental Procedures

Studies in resolving power were performed using a relatively low mass inorganic sample, xenon, a low mass organic sample exhibiting a strong metastable decomposition, toluene, and a relatively high mass organic compound, perfluorotributylamine (PFTBA).

To collect a typical spectrum during the course of a resolving power study on the Bendix 12-101, the electronics are turned on and allowed to warm up for at least 30 minutes. The inlet system is evacuated using the mechanical pump and the gas or vapor sample is then allowed to expand into the inlet. Liquid samples are purified by three or more freeze/pump/thaw cycles. The on/off valve to the high vacuum is then carefully opened and the double needle valve is adjusted to bring the pressure to between 1.0×10^{-6} torr and 7.0×10^{-6} torr. Background pressures generally range from 3 to 4×10^{-7} torr measured with the

uncalibrated ion gauge. The Bendix source is only heated by the incandescent source filament. The inlet system is heated to 50-60°C when organic samples are used.

The filament current is then turned on and adjusted to provide between 0.5 and 1.0 μA of trap current (this is an average since the instantaneous values are much higher). The electron beam collimating magnets about the source may be adjusted to maximize the trap current. Observing the multiplier anode current with the Tektronix oscilloscope through a 50 ohm terminator, one may look at the mass spectral peaks of interest using the front panel "variable scope delay" potentiometer. The resolution is then optimized using the "ion focus" control (which controls the amplitude of the ion drawout pulse), the "vertical" and "horizontal deflection" controls (controlling the voltages applied to the flight tube steering plates), and the "ion lens" control. Adjusting the "compensating" magnets located near the ion source on the flight tube may improve the resolution, especially at low mass. The multiplier gain may be adjusted by using the front panel control. The multiplier magnet position should be optimized by slowly rotating the magnet until the maximum signal is observed. The data recording procedures are identical to those described in the BEDER-TOF section which follows.

The gaseous sample introduction procedure for the BEDER-TOF is virtually identical to that used for the Bendix. Since the BEDER-TOF is differentially pumped, the source manifold pressure could be increased to much higher values than that in the Bendix without compromising instrumental performance. In fact, CI spectra have been recorded with the source manifold pressure in the 1.0 to 2.0 x 10^{-4} torr range. The flight tube pressure remains close to two orders-of-magnitude lower than the source manifold pressure in this case. Another major difference is that the BEDER-TOF source is generally heated to approximately 200°C when using organic samples.

Once the BEDER-TOF electronics have warmed up and the sample pressure has stabilized, the filament current may be turned on. With both the "control" and the "meter" switches in the "emission" position, the emission current is slowly brought to a desired value, generally between 50 and 300 μA. Alternatively, a more lengthy filament current regulation procedure may be followed. It is outlined in the BEDER-TOF electronics manual. No particular advantage exists for this alternate procedure. No facilities currently exist for measuring the actual trap current. Using the "rep 1", "rep 2", and "focus" controls and using the appropriate front panel relays to monitor the voltages on the front panel meter, the repeller voltages are set to approximately 1% above the "block" voltage (set with the Bertan power supply) and the focus voltages to 8 to 9% below the block potential. Using the coarse and fine manual controls for the electrostatic analyzer field strength, the sector plates voltages are scanned. The absolute value of the voltages applied to the plates should be scanned over a range which encompasses a

value of 10% of the block voltage. A deflection of the Dupont beam monitor should be noted during the scan. The repeller, focus, and electrostatic analyzer voltages are adjusted to maximize the signal at the beam monitor. Recent entries in the daily operations manual of the BEDER-TOF may be helpful in selecting the optimum voltages. Facilities are provided to connect the beam monitor electrode to a picoammeter if necessary.

For normal operation of the beam deflection assembly the "vert pulse plate d.c." potentiometer should be in full clockwise position. This provides the d.c. voltage necessary for the vertical deflection plates of the beam deflection assembly to act as the gating plates. With the potentiometer in the full clockwise direction the receptacle below the potentiometer gives the Avtech pulse amplitude directly. This amplitude is adjusted on the front panel of the Avtech and should be set at 40 to 60 V when the current configuration of the beam deflection assembly is in use. The "hor pulse plate d.c." potentiometer is generally set at the midpoint of its travel to provide one half the pulse amplitude to the d.c. side of the horizontal pair of plates of the beam deflection assembly. The Avtech is generally operated at its maximum repetition rate of 10 kHz and at its maximum pulse width of approximately 2 μs.

The oscilloscope and the boxcar are triggered from the Avtech "sync" output. Ion peaks should be visible on the oscilloscope, and may be observed with greater detail by using the delayed sweep of the Tektronix oscilloscope. The sensitivity and resolution are optimized by adjusting the repeller voltages, the source focussing voltage, the electrostatic analyzer voltage, the Avtech pulse amplitude, the horizontal and vertical steering plate voltages, the ion lens voltage, and the "deflection focus" and "geometry" voltages if these last two elements are incorporated in the beam deflection assembly. The electrostatic analyzer voltages may be tied to the accelerating voltage by setting the control switch to the "track" position and adjusting the fine and coarse settings located within the electronics cabinet. However, this has normally not been necessary as the electrostatic analyzer and accelerating voltage power supplies demonstrate very little drift once they warm up.

Data collection is accomplished by first bringing the boxcar integrator time aperture to the desired starting position. The "gate out" marks the approximate location of the aperture in time and can be observed relative to the peaks of interest on the oscilloscope. Its position is adjusted by varying the "initial A" or "initial B" (depending on which plug-in module is in use) potentiometers on the M162 front panel with the "hold" and "reset" push buttons depressed. Once the desired location is attained, the hold button is released and the multiplier anode lead is transferred from the oscilloscope to the M164 (or M165) module input. CAUTION: The multiplier high voltage should always be turned off when the signal lead from the E220 amplifier is not

grounded (as during this transfer). This will prevent damage to the amplifier. The output of the boxcar is then zeroed using the appropriate potentiometer on the plug-in module and monitoring the output by running the program MSTEST. MSTEST will also initiate scans, average multiple scans, and store the resulting data when so instructed. Typical M162 settings for a scan encompassing a dozen or so mass units are: function A or B (depending on which plug-in module is in use); aperture delay range of 50 or 100 μs; aperture duration of 5 ns with the M164 module (this is only nominal, actual aperture duration is between 5 and 10 ns) and of 2 ns with the M165 module; time constant of 0.1 ms; and full scan time of 1,000 s with the red decalibrate knob at 10:00 o'clock (turned approximately 90° to the right from the "calibrated" position). Typical M164 settings are: input of 50 ohm; DC coupling; time constant of 10 μs; and exponential averaging mode.

A major goal of early experiments was to determine the influence of the various instrumental parameters on resolving power. Individual voltages are varied while holding all other parameters constant and monitoring the change in resolution for a selected doublet or multiplet on the oscilloscope. Spectra are collected at appropriate intervals for subsequent inspection. Evaluating the influence of other variables on resolving power, such as the boxcar time constant and the use of the Comlinear amplifier, is also relatively simple. In contrast, investigating the influence of certain instrumental parameters, such as object or image slit width, detector aperture width, flight tube length, or the beam deflection assembly configuration, requires that the instrument be vented to atmosphere and that the selected alteration be

made while care is taken not to vary any other instrumental parameter.

The sensitivity studies were performed by placing 50 μl of a 1 μg/μl solution of naphthalene in pentane in a sample vial which was then attached to the inlet system. The solution was held at liquid nitrogen temperatures as the inlet system was evacuated with the roughing pump to minimize loss of naphthalene. The pentane and naphthalene were then introduced to the ion source and the area under the m/z 128 molecular ion peak of naphthalene was monitored on the oscilloscope until it disappeared (often a period of hours). The inlet system and sample vial were heated during the latter part of the run. The oscilloscope peak area was converted to coulombs per second using the equation:

$$\frac{\text{coulombs}}{\text{s}} = \frac{\text{peak area (V x s) x 10,000 pulses per second}}{\text{input resistance (50) x gain of electron multiplier}} \quad (20)$$

Figure 22 represents a typical coulombs/s (amperes) vs. time curve. The current at m/z 128 was then integrated over time and divided by the μg of naphthalene and μA of emission current (or μA of trap current in the case of the Bendix) used. The electron multiplier gain was evaluated by measuring a steady (non-pulsed) beam current at the stainless steel first cathode of the multiplier (lying in a plane perpendicular to the flight tube axis) using a Keithley 610C electrometer with the multiplier voltage turned off. The scope anode current was then measured with the high voltage turned on. The latter value is divided by the former to obtain the gain. The gain was also measured by pulsing the ion beam and monitoring single ion events with a Tektronix 7623A storage oscilloscope. The Comlinear amplifier was not used during sensitivity tests.

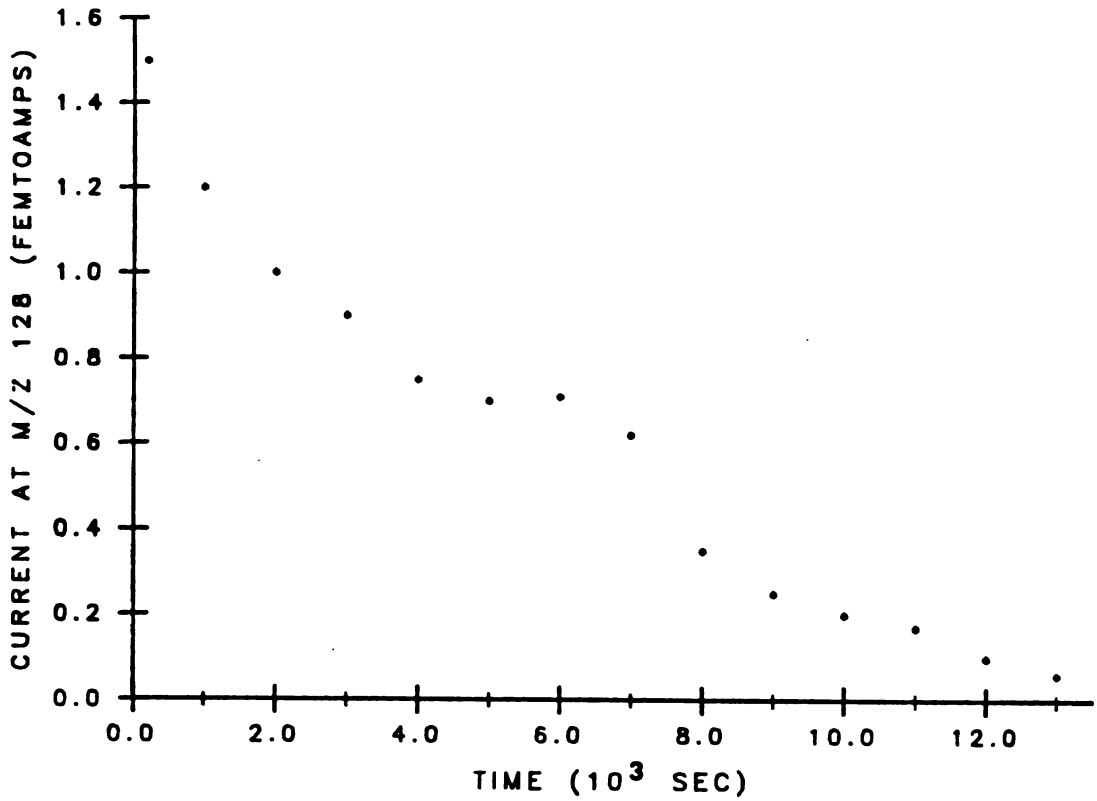

Figure 22. Representation of a typical current vs. time curve collected during sensitivity analyses (simulated). The temperature of the inlet system was increased at approximately 5,000 s in this example.

To obtain CI spectra the Dupont CI source was first installed in the BEDER-TOF. A clean glass probe tip was installed on the Dupont direct probe and the probe was moved into position in the ion source. This simply blocked the direct inlet hole in the ion source block and allowed high pressure to be maintained in the ionization volume. The roughing pump line attached to the inlet system was replaced by a methane line and a vial of acetone was attached to the inlet system. The inlet system was pressurized with methane and the valves to the ion source were carefully opened. The molecular leak inlet of the CI source was not used. The source manifold pressure was regulated to 1.0 to 2.0×10^{-4} torr while the ion source temperature was held at approximately 250°C. For the purposes of this demonstration, no attempt was made to regulate the relative amounts of methane and acetone admitted to the ion source. The EI electron energy was increased from the normal 70 eV to its maximum value of 200 eV. The emission current was regulated at 350 μA.

The Dupont direct probe is a convenient inlet system for solid samples. Initial attempts to measure sensitivity involved the direct probe inlet instead of the gaseous inlet system. Though facilities are provided for heating the sample these were not used since contact with the heated ion source was sufficient to warm the probe tip. To collect a spectrum of a sample introduced by direct probe, the data system was used to initiate repetitive scanning of the boxcar. A M162 full scale scan time of 10 s with the red decalibrate knob in the 8 to 12 o'clock position (turned 30° to 150° to the right from the "calibrated" position) was used. The boxcar time constant was set at its minimum

value. The direct probe inlet region was then evacuated, the vacuum lock valve was opened and the probe was pushed into its receptacle in the ion source block. The filament current was immediately increased to obtain the desired emission current. The remainder of the data collection procedure was identical to that previously described.

CHAPTER 4

RESULTS AND DISCUSSION

In this chapter the best results obtained with the BEDER-TOF will be compared to those obtained with the Bendix and the CVC TOF instruments. The influence of the various instrumental parameters of the BEDER-TOF on mass resolving power will be discussed. The sensitivities of the Bendix and of the BEDER-TOF will then be examined. Finally, the results of other experiments performed on the BEDER-TOF, such as the first CI spectrum collected with reasonable mass resolution using a TOF analyzer, will be presented. The results of the TRIKES experiments will be presented and discussed in the following chapter.

Figure 23 presents a partial spectrum of the isotopes of Xe^+ obtained with the highest resolving power available using the rejuvenated Bendix 12-101. The FWHM resolution at m/z 132 is 359. The xenon pressure was 1.1×10^{-6} torr (background pressure of 4.0×10^{-7} torr) during this analysis while the average trap current was 0.11 μA. Contrary to expectations, the ion lens had a negligible effect on resolving power. It did, however, improve the sensitivity of the Bendix by a factor of at least two while in use. This spectrum was collected with the ion lens at its maximum setting of -1,970 V (the accelerating

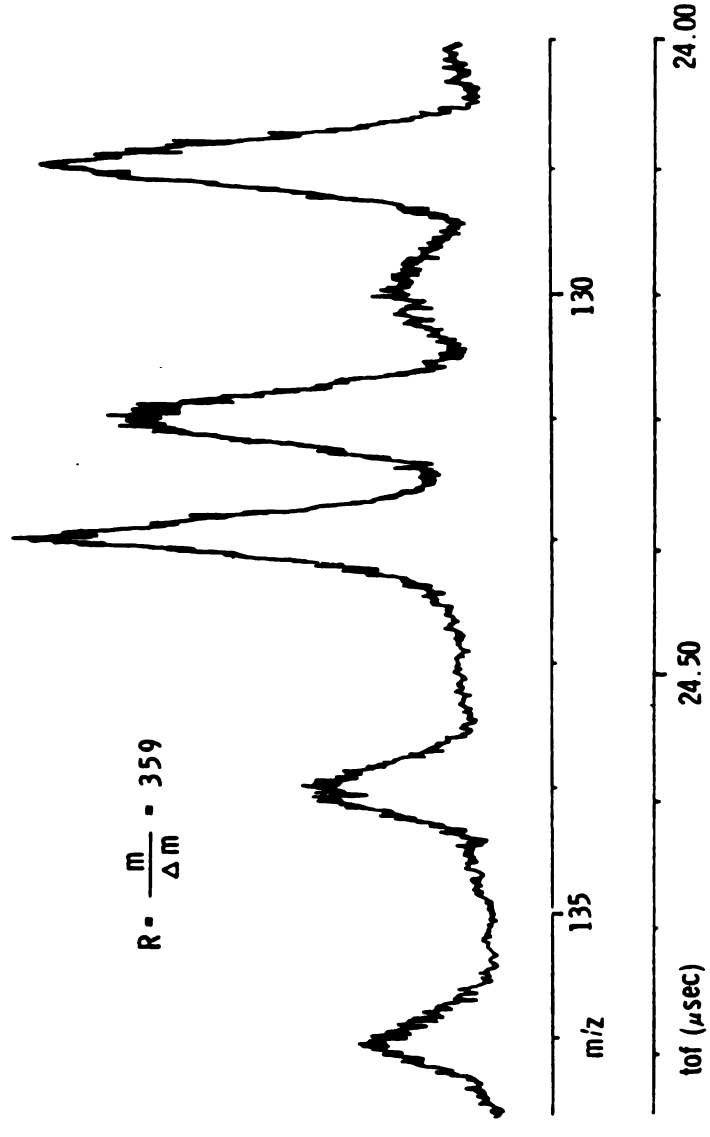

Figure 23. Partial spectrum of the isotopes of xenon collected using the Bendix 12-101. Resolution is FWHM at m/z 132.

voltage was -2,900 V). The detrimental effects of the relatively long rise time of the drawout pulse (roughly 100 ns as measured with the 100 MHz oscilloscope and 10X probe) and of the wide electron beam slits certainly overshadowed the influence of the ion lens on resolving power.

Daughter ions and neutral products of metastable decompositions occurring within the field-free flight tube strike the detector concurrently with the undissociated parent ions. However, kinetic energy release upon such decompositions results in broadening of the tof peak. Thus, lower values for resolution are often obtained in TOF-MS when using samples which are molecular and subject to metastable decomposition. The molecular ion of toluene (at mass 92) is subject to the metastable loss of $H^{\cdot}$ to yield a daughter ion of mass 91. Due to the disparity between the masses of the daughter ion and the neutral product, and due to the conservation of momentum, the change in the velocity of the daughter ion due to kinetic energy release (less than 0.5 eV for this particular decomposition) upon decomposition is rather small (87). No significant broadening of the m/z 92 molecular ion peak was observed as it displayed a resolution of 361. Again, the influence of the kinetic energy release was minor in comparison to that of other factors limiting the resolving power of the Bendix instrument. A slight decrease in resolving power is noted with the BEDER-TOF when toluene is used as a sample in the place of xenon as discussed in a subsequent paragraph.

The high mass ions of PFTBA were not unit-resolved using the Bendix mass spectrometer. This caused difficulties in calculating values for resolution in this mass range since no isotope peaks were visible on the strip chart recording with which to determine the u per cm relationship. However, by assuming that the tof (or cm of stripchart) is directly proportional to the square root of the mass (equation (2) of chapter 1), one may use peaks of known m/z to derive a simple u per cm relationship. The highest FWHM resolution value calculated for mass 502 of PFTBA was 263.

The CVC 2000 demonstrated much higher resolving power than did the Bendix instrument. A resolution of 880 at m/z 132 of xenon was calculated. The slightly lower value of 748 was obtained for the FWHM resolution of the molecular ion peak of toluene at m/z 92. A resolution of 650 was calculated for the m/z 614 molecular ion peak of PFTBA. The contrast between the results obtained from the CVC and those obtained from the Bendix attests to the importance of using an ion drawout pulse with a very short rise time (that of the CVC drawout pulse is less than 20 ns as measured with the 100 MHz oscilloscope and 10X probe). The reduction in the width of the electron beam collimating slits and in the diameter of the ion drawout grids certainly contributes to the improvement in resolving power. Even greater values of resolution can be obtained over a narrow mass range using the time-lag focussing capabilities of the CVC. As discussed in chapter 2, ions of lower mass than those for which the time-lag is optimized will actually be defocussed. The high speed data system (29) being developed in parallel with the BEDER-TOF requires that the entire mass spectrum be in focus.

Time-lag focussing is thus not the optimum choice for improving resolving power when such a high speed data system is used.

Early results obtained using the original CRT beam deflection assembly in the BEDER-TOF are illustrated in Figure 24. The rise in the baseline about the isotopes may be due to scattering of ions from collisions of the pulsed beam with a "geometry" electrode located between the horizontal and vertical deflection plates of the CRT beam deflection assembly (see Figure 19). The FWHM resolution at mass 132 in Figure 24 is 491. The flight tube length in these early studies was 1.1 m. Other relevant instrumental parameters are listed in the figure caption.

Several simple experiments were conducted while using the CRT assembly to determine the effects of various instrumental parameters on resolving power. These results have since been supported by more recent experiments using the optimized beam deflection assembly. For example, the "stack" of the multiplier is normally held at the flight tube liner voltage (i.e., the accelerating voltage) in the Bendix instrument. In contrast, the flight tube liner of the BEDER-TOF is generally at ground. When the Bendix multiplier is used in the BEDER-TOF, how does the accelerating field imposed on the ions at the end of the flight tube affect the resolution of organic ions subject to metastable decomposition? Decelerating fields have previously been used in TOF-MS to determine the percentage of a peak composed of metastable products (88). A strong accelerating or decelerating field would be expected to produce extraneous peaks in the mass spectrum. A less intense field

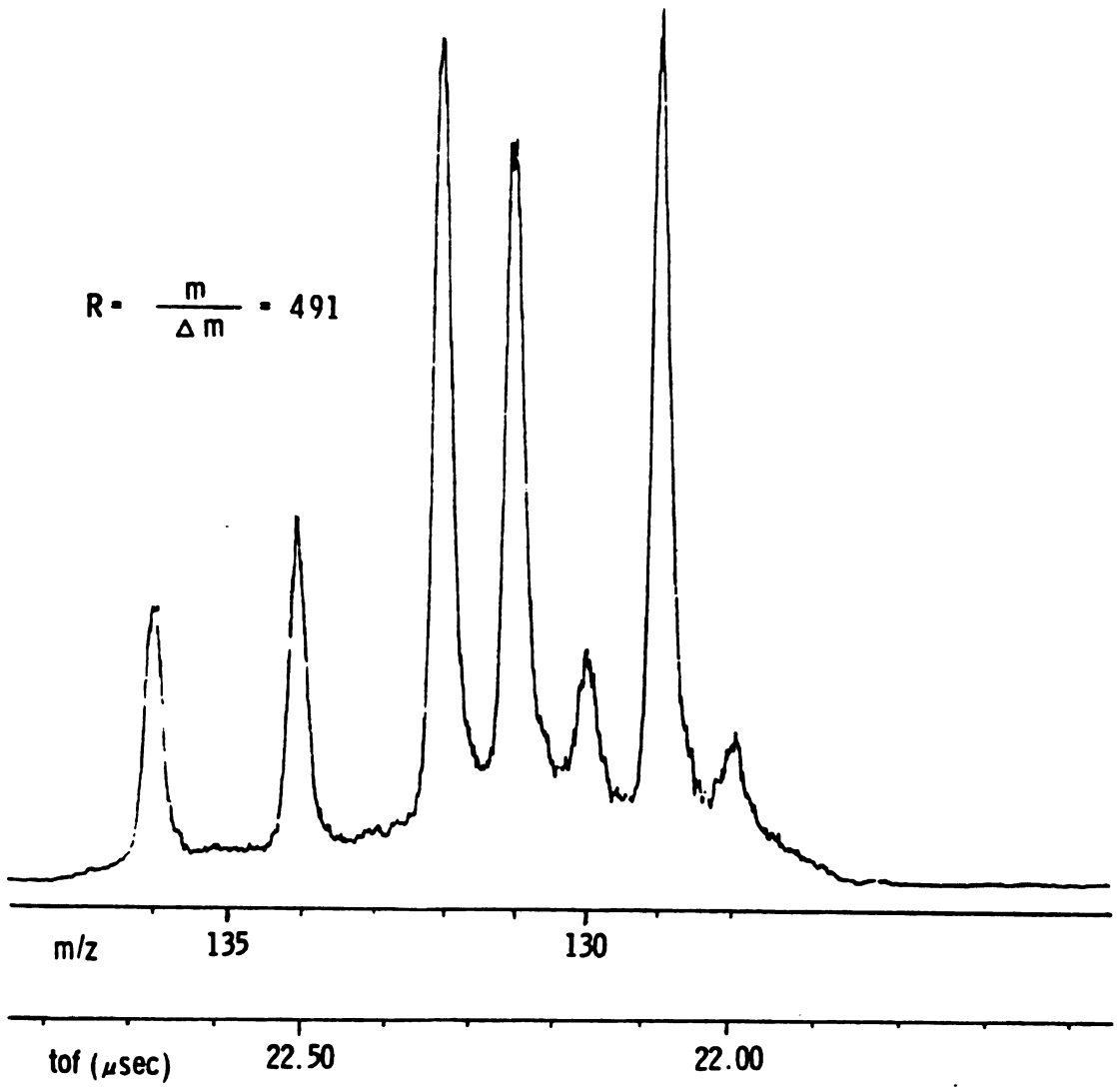

Figure 24. Spectrum of the isotopes of xenon collected using the BEDER-TOF with the CRT beam deflection assembly. Resolution is FWHM at m/z 132. L = 1.1 m, V_o = 1400 V, V' = 30 V, horizontal steering voltage = 83 V.

would simply result in a broadening of the tof peaks as the parent ions, daughter ions, and neutral products begin to separate. The influence of the field was evaluated by collecting spectra of the m/z 91 and 92 doublet of toluene with the stack at high voltage and comparing them with spectra collected with the stack at ground potential. At an accelerating voltage of 1,400 V, the multiplier accelerating field did not significantly affect the resolution of the doublet.

Other significant results of these early experiments are as follows.

1. As expected, the use of the 200 MHz Comlinear amplifier in no way decreases the resolving power as measured with the boxcar integrator.

2. At a boxcar full range scan time setting of 10,000 s (used when scanning over a narrow mass range with the strip chart recorder) an M164 time constant of 100 μs is optimal. A 1 ms time constant significantly degrades resolving power while a 10 μs time constant introduces noise but does not improve the resolving power.

3. The nominal 5 ns aperture duration setting of the boxcar mainframe does not degrade the observed resolution of the Xe^+ isotopes as compared to that obtained using the 2 ns setting of the M165 plug-in module. However, as discussed later, peak widths measured on the oscilloscope were generally narrower than

those calculated from the boxcar output, especially for low mass ions. Resolving power is compromised when using the 50 ns aperture duration setting of the boxcar.

4. As expected, the following parameters have a tremendous effect upon the magnitude of the ion current striking the detector but very little or no effect upon the observed resolving power:

   a. the electrostatic analyzer field strength (when it is varied over a narrow range to admit ions of higher or lower kinetic energy to the beam deflection assembly at constant accelerating voltage)

   b. the emission current

   c. the ion source focus voltages (at a given block voltage)

   d. the ion source repeller voltages (at a given block voltage)

   e. the ion source pressure (so long as the flight tube pressure remains reasonably low)

   f. the field established across the vertical steering plates in the flight tube

Other parameters which do affect resolving power will be discussed in light of the results obtained using the optimized beam deflection

assembly.

Figure 25 represents the best results to date using the optimized beam deflection assembly. The resolution at mass 132 is 982. The flight tube length used when collecting this spectrum was 1.9 m. Other relevant instrumental parameters are listed in the figure caption.

Using similar instrumental conditions, the resolution of 823 calculated for the molecular ion of toluene is lower than that obtained for xenon. One explanation of this observation is that the metastable decomposition to which the molecular ion is subject broadens the peak. Alternatively, the difference can be accounted for by simply considering the resolution vs. mass relationship presented in the following section. A strong metastable daughter of the molecular ion of toluene was observed only at accelerating voltages above roughly 2,000 V using TRIKES. An accelerating voltage of 1,400 V was used in obtaining the spectrum demonstrating a resolution of 823. This lends credence to the latter explanation. Table 1 summarizes the results from the three instruments for xenon and toluene.

In Figure 26 resolution is plotted vs. m/z for the major ions of PFTBA. The resolution ranges from 492 at m/z 69 to 982 at m/z 614. All these ions were in focus simultaneously. This is in contrast to the results obtained using time-lag focussing in conventional TOF instruments where only a narrow mass range is in optimal focus at any one time. An error bar is included for mass 414, one of the ions of lower relative abundance for which resolution was calculated (error bars

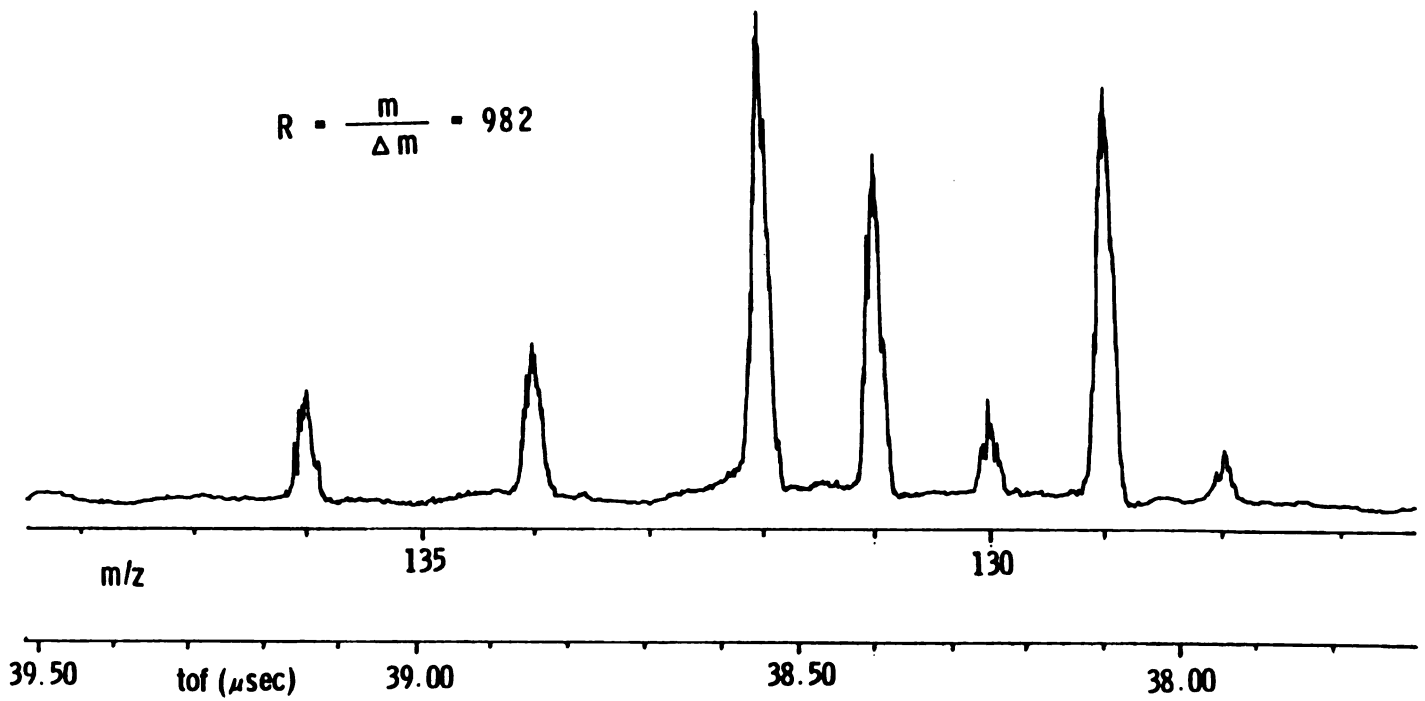

Figure 25. Spectrum of the isotopes of xenon collected using the BEDER-TOF with the optimized beam deflection assembly. Resolution is FWHM at m/z 132. L = 1.9 m, V_o = 1400 V, V' = 60 V, horizontal steering voltage = 38 V.

TABLE 1

COMPARISON OF MASS RESOLVING POWER OBTAINED USING THE BENDIX 12-101, THE CVC 2000, AND THE BEDER-TOF

Instrument	Sample			
	Xenon		Toluene	
	R_{FWHM}[a]	R_{10}[b]	R_{FWHM}[a]	R_{10}[b]
Bendix 12-101	359	177	361	173
CVC 2000[c]	880	497	748	403
BEDER-TOF[d]	982	497	823	407

a. Resolution, R, calculated using the full peak width measured at half maximum (according to equation (4)).

b. Full width of the peak at 10 % peak height used in calculations.

c. Time-lag focussing was not used during these measurements.

d. The "optimized" beam deflection assembly was used for these experiments.

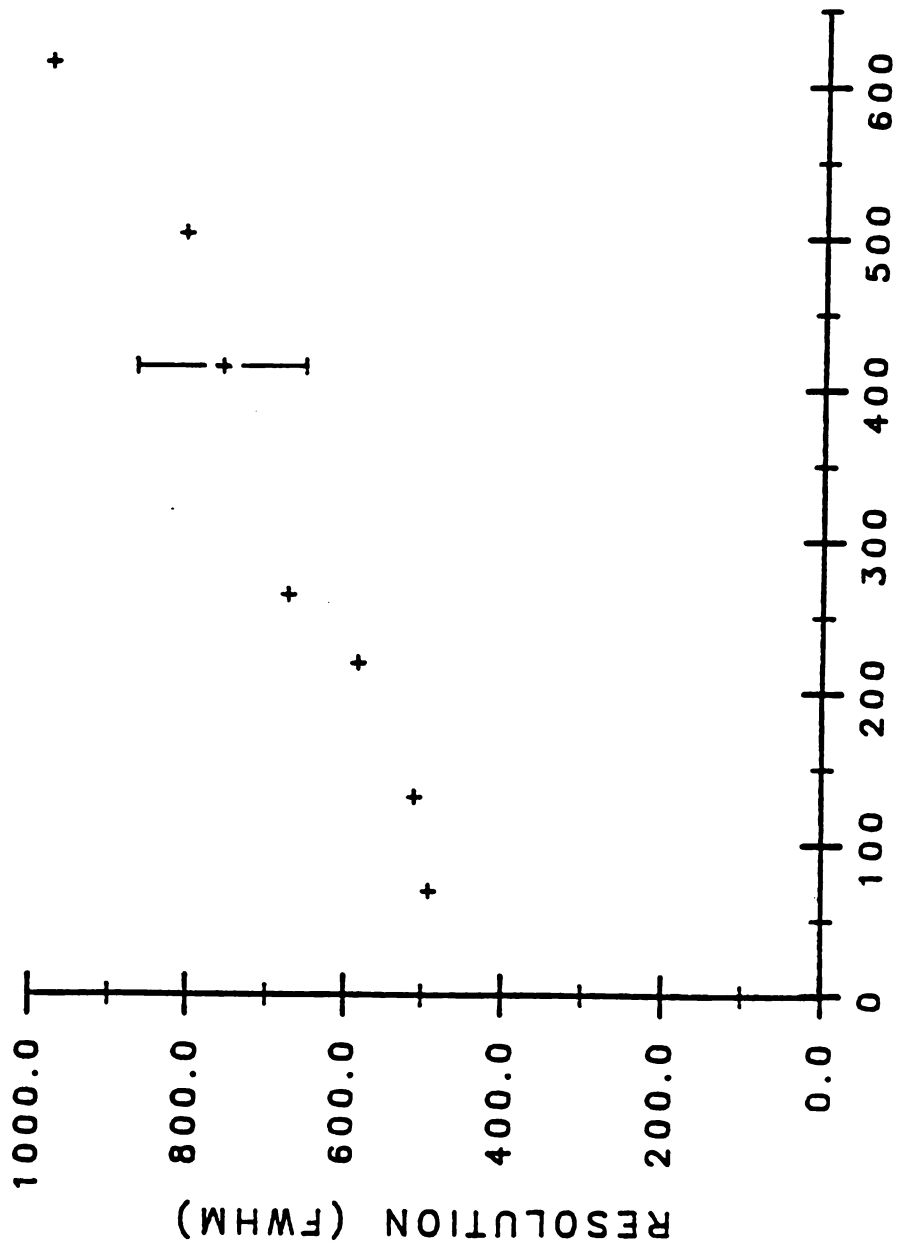

Figure 26. Resolution vs. mass for the major ions of PFTBA.

for the other ions should be no larger than that for mass 414).

Equation (12) does not predict a mass dependence of resolution. At least part of the observed trend in Figure 26 may be due to the data collection procedure. To maintain a constant value for resolution as mass decreases, the width of the peaks must also decrease. However, scanning the 5 to 10 ns boxcar time aperture across the peaks to acquire the spectrum may distort the narrower peaks (just as an optical spectrometer slit limits the minimum width of a spectral line). The calculated peak width of the m/z 69 peak (from the "hard copy" data) in the above experiment is approximately 31 ns. To maintain the resolution of approximately 1,000 obtained at m/z 614 the peak width at m/z 69 would have to be roughly 15 ns. The width of the boxcar aperture is clearly significant in this case. Later investigation revealed that the peak width at half height is no greater than 20 ns as observed on the oscilloscope. At least part of the observed trend toward lower resolution at lower mass is thus due to this artifact of the data collection system. As mentioned earlier, the M165 boxcar plug-in module gave no better resolving power than the M164. These results suggest that the effective aperture width of the M165 (a combination of aperture width and jitter in the delay between the Avtech beam deflection pulse and the opening of the aperture) may be greater than the nominal 2 ns. The discrepancy between the the peak widths as measured on the hard copy output and as estimated on the oscilloscope face did not become apparent until recently. It is probable that higher values of resolution would have been obtained had a recording system with greater time resolution been employed. Measuring the width of the peaks on the oscilloscope

would seem to be a simple solution to this problem. However, the S/N is low at high resolution and measuring the peak widths on the oscilloscope with an absolute error of less than approximately 10 ns would be difficult.

The influence of a number of instrumental parameters on mass resolution in the BEDER-TOF has been determined. In certain cases, attempts have been made to correlate these data with theoretical trends based on equation (12). Figure 27, for example, presents resolving power as a function of image slit width. As expected, resolving power does in fact decrease as the width of the image slit increases and ions of increasingly greater spread in kinetic energy are admitted to the beam deflection region. The experimental and theoretical trends match fairly well at narrow slit widths, but the experimental curve reaches a plateau region while the theoretical curve continues to move to lower resolution values at wider slit widths. This is probably due to the fact that the the theoretical calculations assume that the energy spread of the beam in infinite (i.e., as the slit width is increased, ions of ever increasing kinetic energy spread will be admitted to the beam deflection region). In reality, the energy spread of the beam is finite. Increasing the image slit width beyond the point where the majority of the ions passes through the slit has negligible influence on resolving power.

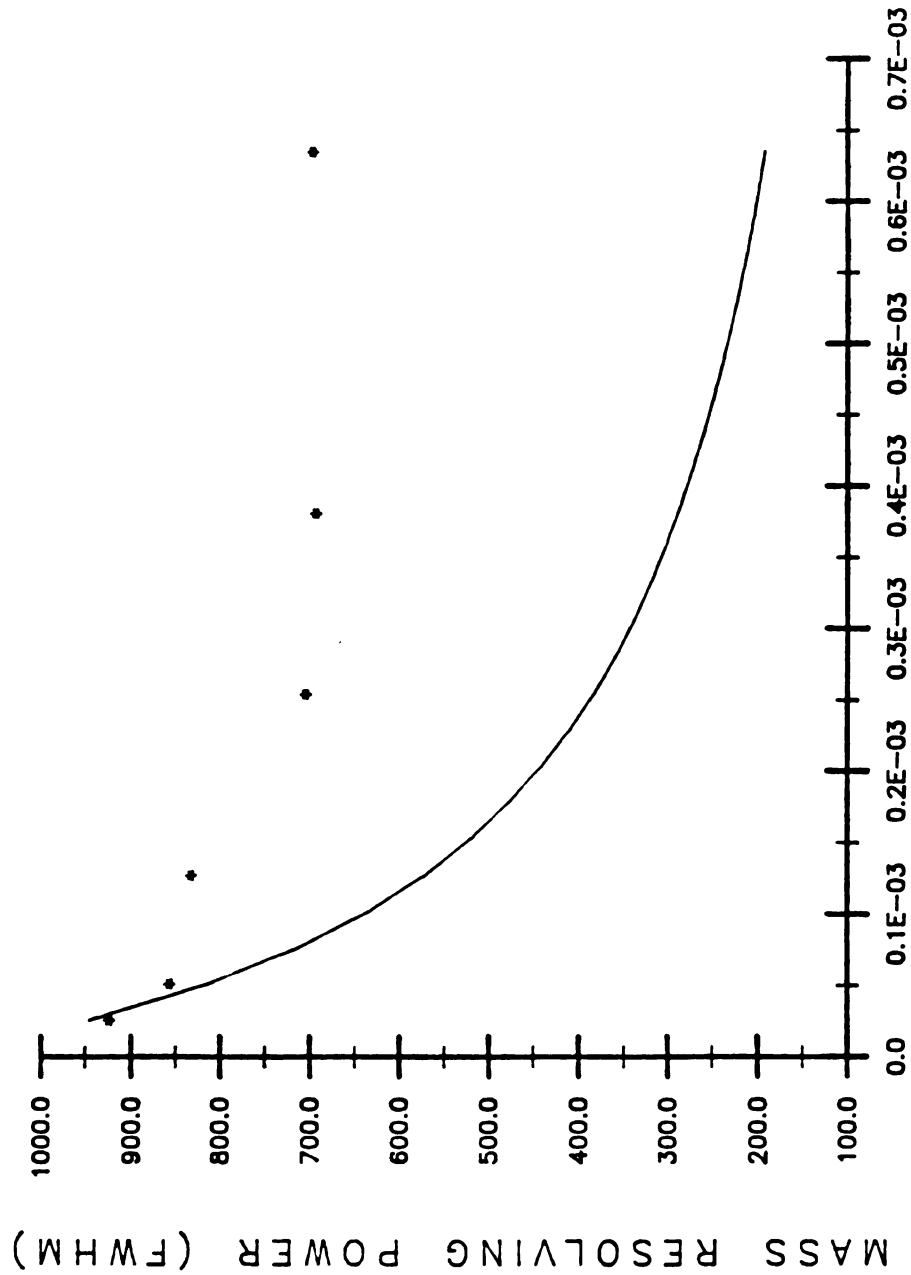

Figure 27. Resolution vs. image slit width. The solid line is calculated from equation (12) while the points are experimental data.

The velocity dispersion of the particular electrostatic analyzer used in the BEDER-TOF is relatively small. This, in combination with the fact that the magnification of this particular sector is 0.80 (from equation (7.27a) of reference 85)(this means that the image of the object slit at the focal plane is actually narrower than the object slit), requires that a very narrow image slit be used to define a beam of quasi-monoenergetic ions. The image slit widths generally used with the 0.076 mm (0.003 in.) object slit are 0.051 mm (0.002 in.) and 0.025 mm (0.001 in.). To obtain still greater resolving power by using the other available object slit of 0.020 mm (0.0008 in.) width one would be required to use still narrower image slits. The present arrangement requires that the image slit width be set with a spacing shim. This design is clearly not practical for image slit widths below 0.001 in.. Using an electrostatic analyzer with a larger radius would be advantageous in this respect.

Holding other conditions constant, a trend toward lower resolving power at higher accelerating voltage is observed (as predicted by equation (12)). For example, in one experiment a resolution of 921 at m/z 132 of xenon was obtained at 2,800 V accelerating voltage while 771 was obtained at 3,500 V. Similarly, the trend toward higher resolving power at higher deflection voltage predicted by equation (12) is observed. For example, a deflection voltage of 39 V gave a resolution of 732 while simply changing the deflection voltage to 60 V increased the resolving power to 857. In the same experiment using a narrower image slit width the results were not quite as dramatic. The resolution increased from 924 to 982. In practice, however, the maximum deflection

voltage that one may use with a particular deflection plate length (see equation (19)) increases with increasing accelerating voltage. Thus, in going to greater accelerating voltage one may increase the deflection voltage and maintain a fairly constant resolution value.

One effect which is not predicted by equation (12) but has been observed in practice is that resolution decreases as the deflection voltage increases beyond a critical value. This critical value is a function of the accelerating voltage. The critical value, for example, lies near 64 V at an accelerating voltage of 1,400 V. As the accelerating voltage is increased, this limiting value also increases. The basis for this effect is not clear. It may be related to the fact that the ions having experienced equal and compensatory forces upon field reversal within the deflection plates (those at and near the midpoint of the length of the deflection plates) emerge from the deflection plates in a plane which is parallel to but displaced from the plane on which they entered the deflection plates (these are planes drawn parallel to those in which the deflection plates lie; see Figure 28). As the field strength within the deflection plates increases or the acceleration voltage decreases, the separation decreases between those ions which emerge from the deflection plates moving parallel to the flight tube axis (ions b_1 in Figure 28) and the deflection plate carrying the higher voltage (V'). Fringing fields, nonhomogeneous fields related to surface imperfections, and diffraction effects exist at the edge and surface of this deflection plate and their strengths increase in magnitude as the deflection voltage increases. As portions of the ion packet pass through different equipotential surfaces of the

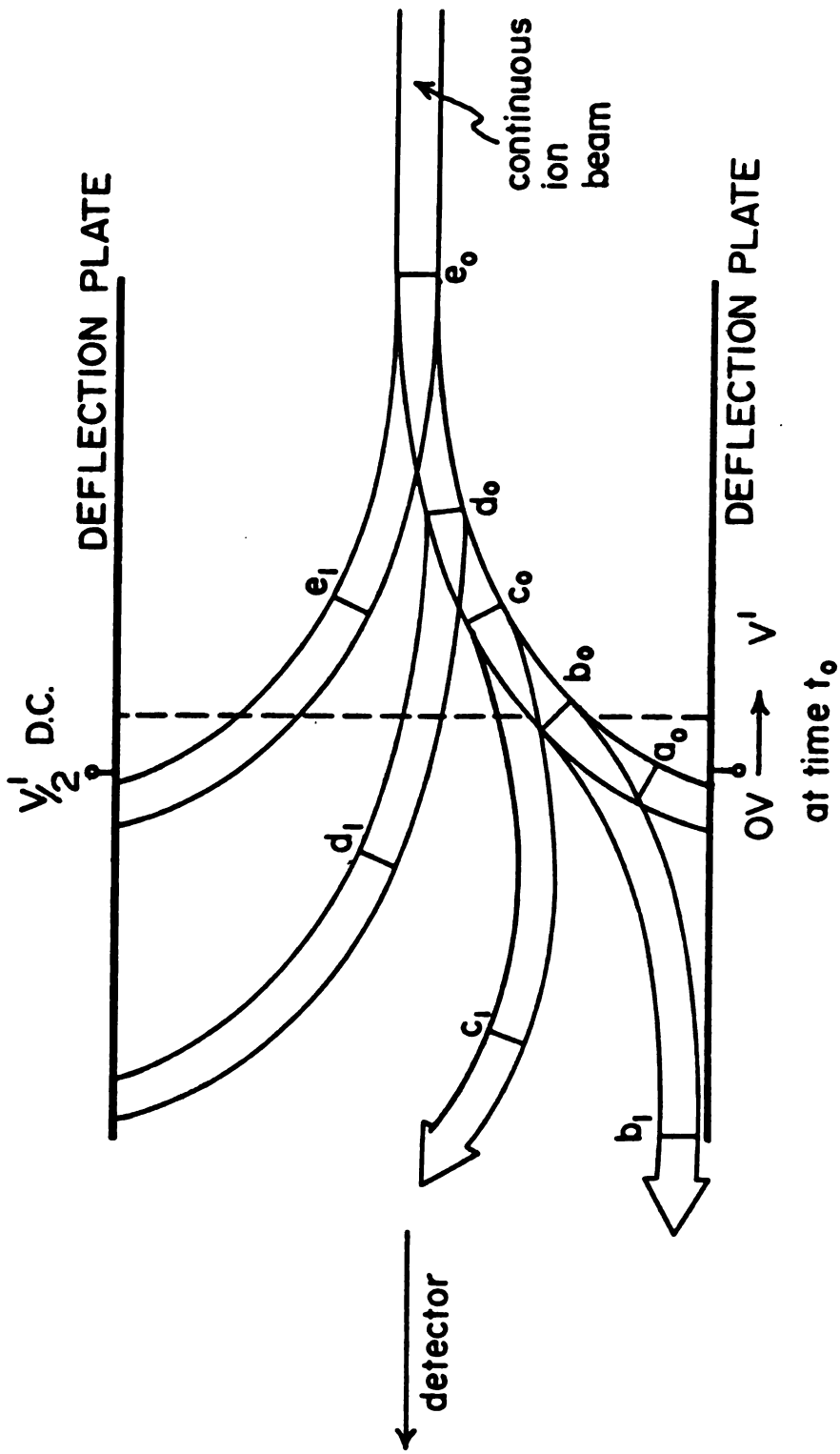

Figure 28. Schematic representation of ion packets between the deflection plates during field reversal. Subscripts refer to consecutive situations (i.e., b_0 is the position of ion packet b at time = 0, while b_1 represents its position at time = $\overline{1}$).

fringing fields, they may acquire differing amounts of kinetic energy. This hypothesis is supported by the fact that the peaks move to shorter flight times, the peak widths increase, and peak heights decrease as the deflection voltage is increased beyond the point where resolution begins to decrease. It appears that for a given ion kinetic energy there exists an optimum combination of deflection voltage and distance between the deflection plates (i.e., an optimum deflection field strength) beyond which these negative effects of increased deflection voltage begin to outweigh the positive effects expected from equation (12).

These observations may help to explain the unexpected influence of the horizontal steering plates on resolving power. (This discussion assumes that the horizontal deflection plates of the beam deflection assembly are used to produce the ion pulses.) These plates, as shown in Figure 12, are situated at roughly half the distance from the beam deflection assembly to the detector. As illustrated in Figure 28, certain ions do not strike deflection plate, neither do they move parallel to the flight tube axis as they emerge from the deflection plates (ions c_1 of Figure 28). These ions are acted on by the force directed away from the deflection plate on which the pulse is applied for a longer time than they are by the force directed toward this plate and thus emerge from the deflection plate region at an angle to the flight tube axis. These ions may be focussed on the detector if a positive voltage is applied to the flight tube horizontal steering plate located on the side of the flight tube opposite the deflection plate on which the pulse is applied. As this positive voltage is increased resolution also increases. During a scan of this horizontal steering

voltage the highest values of resolution have always been observed just before the ion signal disappears. The ions striking the detector at this point would correspond to the ions deflected away from the beam deflection plate with the greatest angle, yet with an angle not so great as to cause the ions to collide with the flight tube before they reach the horizontal steering plates. These ions would also correspond to those with the greatest chance of escaping the deleterious effects of the aforementioned fringing fields. It may be that still greater resolving power may be obtained if the horizontal steering plates are relocated closer to the beam deflection assembly.

Increasing the flight tube length also improves resolving power as one would expect based on equation (12). Using the CRT beam deflection assembly, the resolution at a flight tube length of 1.1 m was 456 at m/z 132 of xenon. The resolution value obtained at a flight tube length of 1.9 m was 778. The factor of 1.7 improvement is far from that of 3 predicted by equation (12a).

The diameter of the detector aperture is among the instrumental parameters which have a dramatic influence on resolving power according to equation (12). Figure 29 illustrates the predicted improvement in resolution as the aperture decreases. The trend toward higher resolution with decreasing aperture width was observed, though on a much less dramatic scale. Figure 30 illustrates the results of two sets of experiments in which the width of the aperture was varied. The first set of six points was collected when the strip-chart recorder was still in use, thus repetitively collected spectra could not be averaged. The

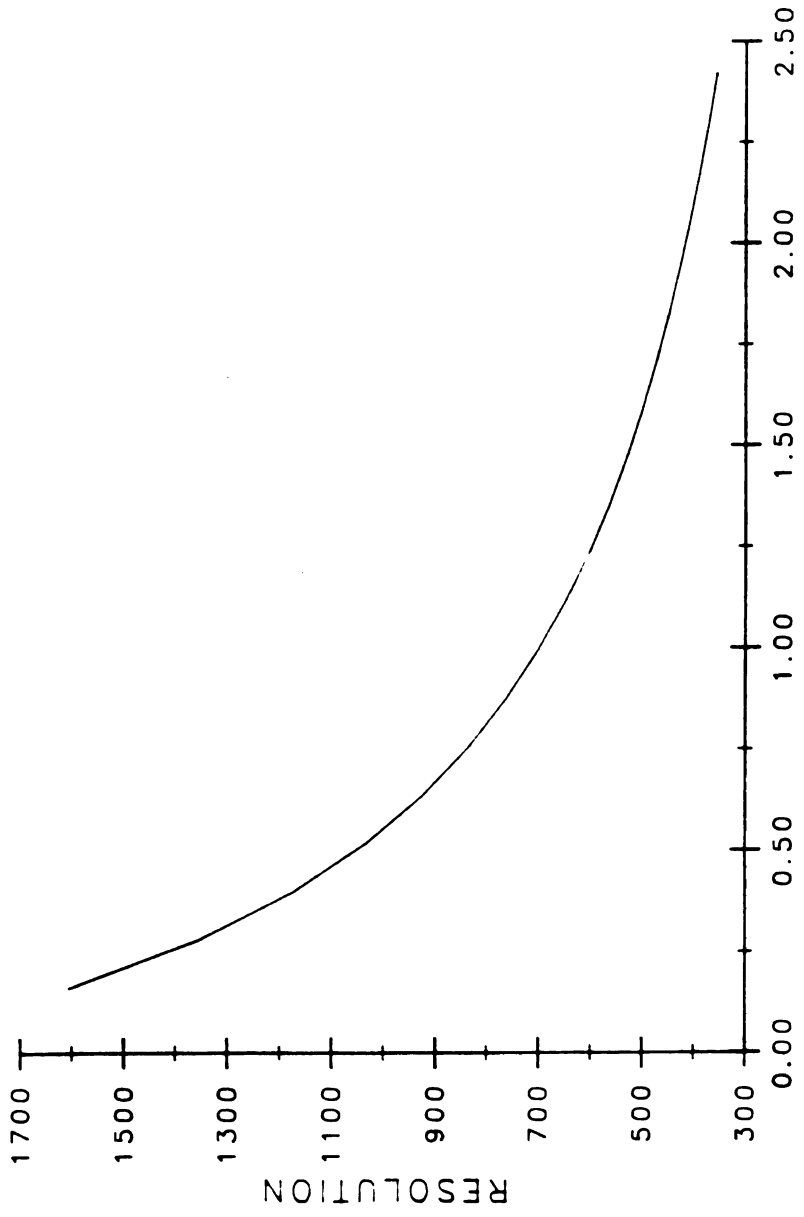

Figure 29. Resolving power as a function of aperture width as calculated according to equation (12).

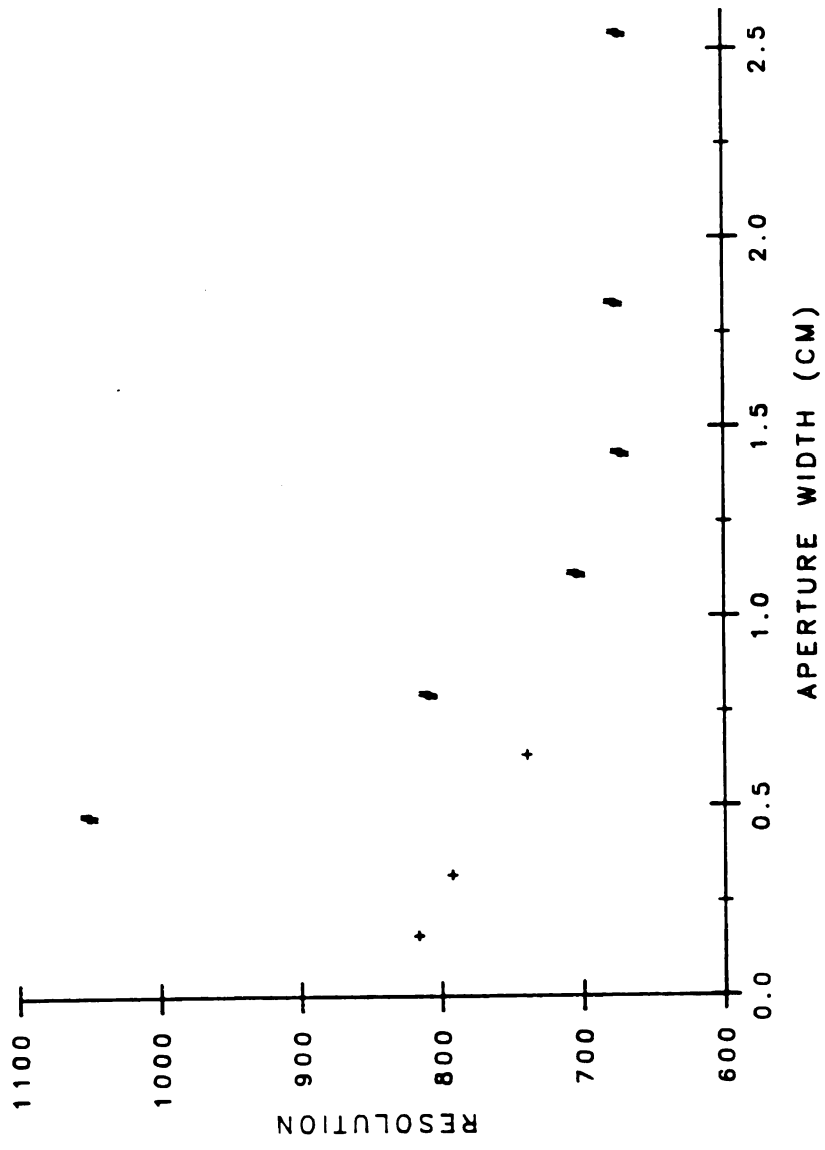

Figure 30. Results of experiments in which resolution for the isotopes of Xe^+ was measured as a function of detector aperture width. The points represented by # are calculated from single scans while those represented by + are calculated from spectra which were averages of 25 scans.

S/N was so low at the aperture width of 0.48 cm that the value of resolution obtained during this run has not been reported as the "highest resolution obtained with the BEDER-TOF". In spite of the low S/N, the trend toward higher resolving power at narrower detector apertures is apparent. The set of three points is calculated from runs during which 25 spectra were averaged with the data system. (Other instrumental parameters differed from those used during the collection of the first six data points.) The S/N in this case was thus much higher.

The efficiency with which secondary electrons are transferred from the first stainless steel cathode of the magnetic electron multiplier to the dynode plate depends on the point of origin of the electrons on the cathode (89). This perhaps explains the fact that no improvement in resolving power was observed until the aperture was restricted beyond approximately 1.25 cm. Ions strike the first cathode in a circle of 2.54 cm in diameter. These results suggest that electrons from the edges of this circle are not transferred to the dynode strip as efficiently as are those from the central portion of the circle.

Other instrumental parameters had little beneficial effect on resolving power and/or sensitivity. A positive voltage applied to the ion lens in the flight tube does produce a slight increase in the magnitude of the ion current striking the detector (an ion lens voltage of approximately 300 V at an accelerating voltage of 1,400 V improved sensitivity by a factor of less than 2 as judged on the oscilloscope). A significant decrease in resolution is noted at ion lens voltages of

this magnitude and beyond. A negative voltage applied to the ion lens of up to 200 V in magnitude has little effect on sensitivity or resolving power. Both positive and negative potentials applied to the flight tube liner (up to $\pm$600 V at an accelerating voltage of 1,400 V) had little beneficial effect on the observed sensitivity or resolving power. The post-acceleration employed by Bakker (90) was done so on a strictly empirical basis. Bakker did report that the post-acceleration improved the resolving power he obtained using beam deflection (84).

The deflection focus electrode of the CRT beam deflection assembly did not favorably influence resolving power. The highest resolution values obtained with the CRT assembly were obtained with this lens at ground. For these reasons the optimized beam deflection assembly has not been operated in a configuration which incorporates the deflection focus lens, though this is a possible configuration. Likewise the geometry electrode of the CRT assembly did not improve resolving power or sensitivity. The optimized assembly has been operated with a geometry electrode as pictured in Figure 20. However, the effect of a positive potential applied to this electrode has been universally negative from the standpoint of resolving power. A voltage on the geometry electrode as small as 3 V can reduce the resolution at m/z 132 of xenon from the high 700's to barely unit resolution.

The sensitivity measured for the optimized deflection plate assembly at maximum resolving power is 4.6×10^{-13} Coulombs at m/z 128 of naphthalene / (μg of naphthalene x μA of emission current). An attempt was made to compare the sensitivity of the BEDER-TOF with that of the Bendix 12-101. The sensitivity of the Bendix is 6.3×10^{-11} Coulombs at m/z 128 of naphthalene / (μg of naphthalene x μA of trap current). Initially, it appears that the BEDER-TOF is two orders-of-magnitude less sensitive than the Bendix. However, the Dupont ion source used in the BEDER-TOF has no electron trap. Thus, the total emission current (which includes both the trap current and the major fraction of electron current which merely strikes the outer surface of the source block and never participates in the ionization process) was used in calculating the sensitivity of the BEDER-TOF. This yields a sensitivity value for the BEDER-TOF which is artificially low with respect to that for the Bendix instrument. The length of the ion source filament used in the BEDER-TOF is over 10 times the diameter of the electron entrance hole in the source block. Based on this geometry it is estimated that the BEDER-TOF is no more than one order-of-magnitude less sensitive than the Bendix 12-101.

This decrease in sensitivity was expected in this experiment since the Bendix uses wide ion apertures (2.54 cm in diameter) while the Dupont source and electric sector of the BEDER-TOF use narrow collimating slits to achieve high kinetic energy resolution. In addition, the Bendix is singly pumped; the flight tube pressure increases simultaneously with ion source pressure. The sensitivity is actually reduced at flight tube pressures above approximately 1×10^{-5}

torr due to collisions of the ions with neutrals and subsequent scattering. In contrast, the BEDER-TOF is differentially pumped. Ion source pressures which would severely limit the sensitivity of the Bendix can be used in the BEDER-TOF. CI spectra have been collected with the BEDER-TOF (see subsequent paragraphs) in which the source manifold pressure was in the 1.0-2.0 x 10^{-4} torr range while the flight tube pressure remained in the low 10^{-6} torr range. Thus, the BEDER-TOF is useful over a much wider range of sample pressures. Because of these different features of each instrument a direct comparison of performance in the realm of sensitivity is difficult. The BEDER-TOF would be advantageous in certain applications while the greater sensitivity of the Bendix 12-101 would be useful in others.

The BEDER-TOF has been developed in parallel with a high speed computer interface (the integrating transient recorder) that will allow for averaging all of the 10,000 spectra which strike the TOF detector each second ("time-array detection") (29). Such a data system requires that the entire mass range be in focus simultaneously; this is accomplished with the BEDER-TOF. Conventional "time-slice detection" TOF data collection methods only detect a narrow portion of each spectrum after each pulse of the ion source and thus discard the majority of the data. These developments in data collection efficiency will offset the lower sensitivity of the BEDER-TOF.

A large level of d.c. background noise is present when using the present configuration of the beam deflection assembly. This, of course, limits the S/N observed on the oscilloscope. The intensity of the background noise increases with increasing acceleration voltage. The great majority of ions emerging from the electrostatic analyzer image slit collide with one of the horizontal deflection plates under the influence of the deflecting field (during the time between field reversals). Reflection of this primary beam and sputtering of the beam deflection plate material is thought to cause the background noise. This implies that the field within the vertical deflection gating plates (see Figure 20) is not sufficient to keep all of these sputtered and reflected ions from striking the multiplier (this is conceivable if scattering in the vertical direction occurs upon reflection or sputtering, or if a large portion of the noise is due to sputtered neutrals). One way to eliminate this problem might be to introduce an angle between the beam deflection plates and the flight tube axis opening toward the electrostatic analyzer. In this way the probability that reflected or sputtered ions and neutrals would eventually strike the detector would be reduced. The beam deflection process would not be disturbed though modeling this process would be more difficult (the field strength between the deflection plates would increase as the ions moved toward the detector along the flight tube axis). A method to reduce sputtering of ions from the electrode material would be to simply manufacture the beam deflection plates from a material with a lower secondary ion yield than aluminum, such as copper (91). Another way to potentially reduce the intensity of the background due to sputtered or reflected ions is to configure the beam deflection assembly with both

the pulsing and the gating pair of plates in the horizontal direction and to use the fourth method of beam deflection/gating shown in Figure 18. The first set of plates acts as the gate and only admits ions to the second pair of plates while the pulse is applied. Ions sputtered or reflected at a variety of angles from one side of the first pair of plates would be subjected to a second strong deflecting field in the horizontal direction within the second pair of plates. These ions would either have to be reflected for a second time or cause sputtering of tertiary ions from the appropriate side of the second pair of plates to contribute to the background noise. Nothing prevents all three proposals from being incorporated in the beam deflection assembly.

Figure 31 is an example of the CI spectra collected with the BEDER-TOF. This work is the first in which CI spectra have been collected with reasonable resolution using a TOF analyzer. The source housing pressure was first increased to 1×10^{-5} torr with acetone (the background pressure was 3×10^{-7} torr). Methane was then used to bring the total pressure to 1.8×10^{-4} torr. The flight tube pressure was roughly 2×10^{-6} torr during the CI experiment. The height of the protonated molecular ion peak at m/z 59 equaled that of the molecular ion peak at m/z 58 at an ion source housing pressure of roughly 1×10^{-4} torr. The peak at m/z 21 is an artifact of the boxcar. The BEDER-TOF was tuned for sensitivity and not for resolution before collecting this spectrum. This spectrum illustrates that the BEDER-TOF is able to use ion sources from which ions cannot be rapidly pulsed, unlike conventional TOF instruments.

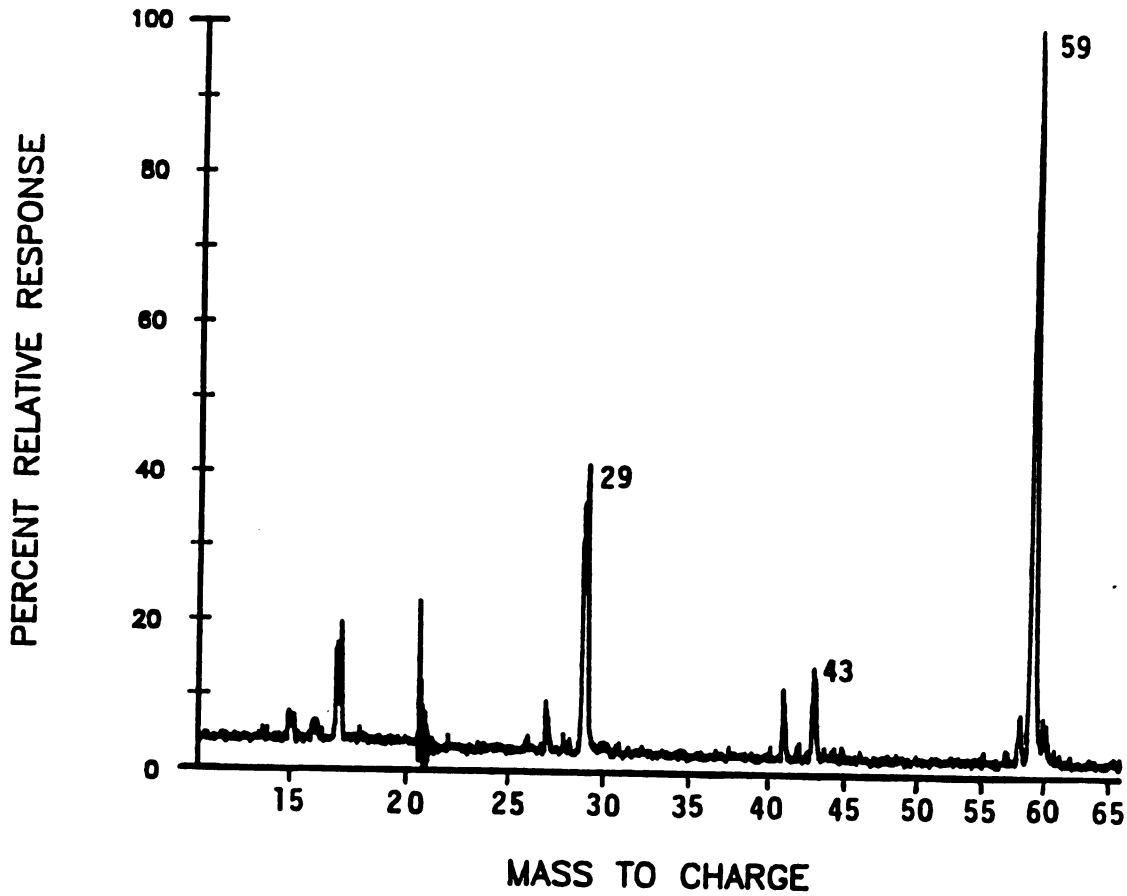

Figure 31. CI TOF analysis of a mixture of methane and acetone. Experimental conditions are listed in the text.

CHAPTER 5

TIME-RESOLVED ION KINETIC ENERGY SPECTROMETRY

A. Introduction

Tandem mass spectrometry (MS/MS) has been shown to be useful in a number of fields. Among these are structure elucidation, fundamental studies of unimolecular decompositions and ion neutral interactions, and complex mixture analysis (92). As the name indicates, "conventional" MS/MS instruments are tandem mass spectrometers (93). Figure 32 is a simplified diagram of the two most common commercially available instruments used for MS/MS. Both instruments use two stages of mass analysis. Ionic products of metastable decompositions or collisionally induced dissociation (CID) occurring within a region located between the two mass dispersive or filtering elements may be analyzed using these instruments.

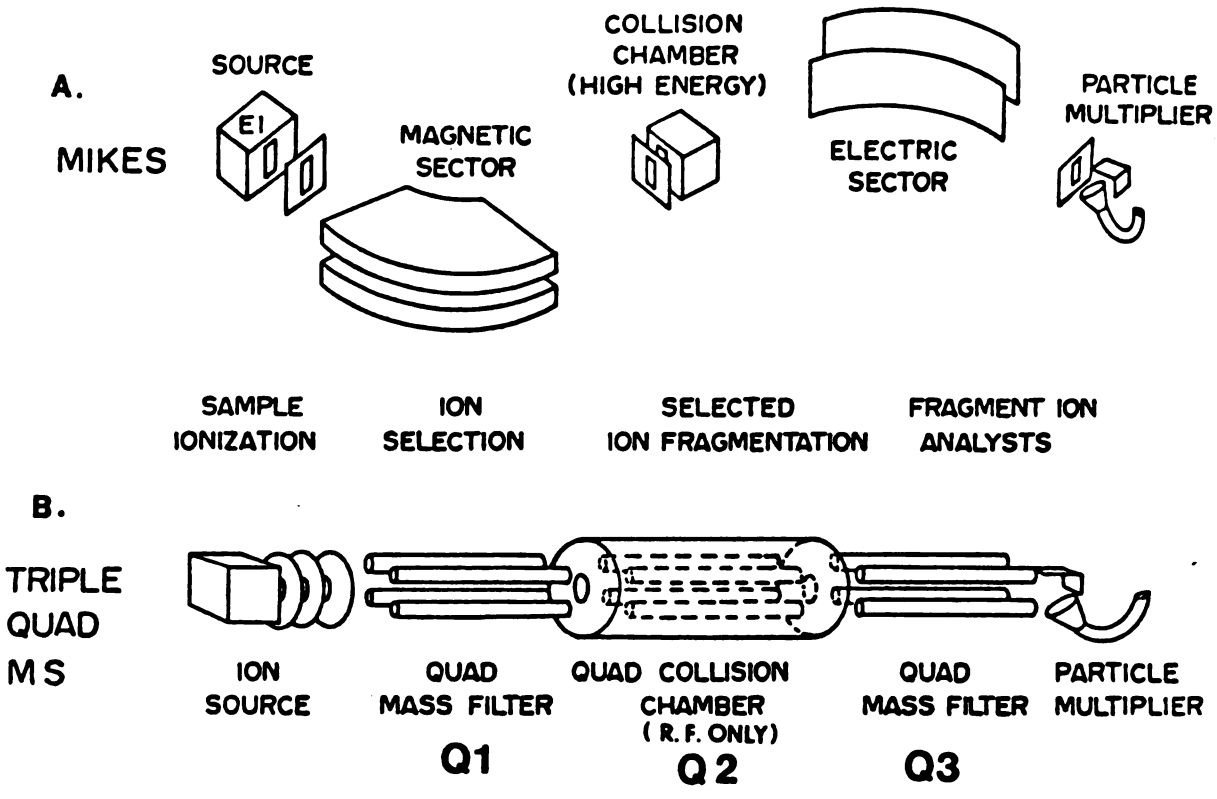

Figure 32. Representation of two of the more common instruments used for MS/MS: a) the MIKES instrument, and b) the instrument for TQMS.

The instrument in Figure 32a is that designed for mass-analyzed ion kinetic energy spectrometry (MIKES) (also called direct analysis of daughter ions (DADI)) (94,95) and consists of a conventional "reverse" geometry double focussing mass spectrometer to which a region for CID has been added. Ions are continuously formed and accelerated from the ion source to constant kinetic energy. A momentum analysis is performed on the ions by the magnetic sector (the first stage of mass analysis) and parent ions of a single momentum (or mass, in this case) are selected for CID within the second field-free region. Daughter ions resulting from CID or metastable decomposition within this second field-free region will have lower kinetic energies than the undissociated parent ions. (Assuming negligible kinetic energy release upon fragmentation, the daughter ion velocity is identical to that of the parent and its mass is necessarily lower than that of the parent; kinetic energy is equal to $1/2mv^2$ where m is mass and v is velocity.) The second stage of mass analysis in the MIKES instrument, the electrostatic analyzer, disperses ions according to their kinetic energies. By scanning the electrostatic analyzer field strength from that necessary to pass the stable ions toward lower field strengths, daughter ions of successively lower mass are brought into focus on the detector.

Three "scan modes" are often used in MS/MS: "daughter" scans, such as that describe in the previous paragraph; "parent" scans, in which the daughter ion mass is held constant while the parent ion mass is varied; and "constant neutral loss" scans in which only daughter ions which result from the loss of a particular neutral fragment mass upon CID of the parent ion are detected.

The MIKES instrument had initial success due to the ease with which daughter scans could be collected (the accelerating voltage, V_o, and the magnetic field strength are held constant while the electrostatic analyzer field strength is scanned). Parent and constant neutral loss scan modes are available for CID occurring between the two sectors of the reverse geometry instrument using a variety of linked scans in which both the electrostatic analyzer field strength and magnetic field strength are scanned simultaneously (96,97). Daughter, parent, and constant neutral loss scans may also be performed to characterize metastable decompositions or CID which occur in the field-free region between the ion source and first sector of both B/E (reverse geometry instruments, such as that used in MIKES, where B stands for the magnetic sector and E represents the electrostatic analyzer) and E/B ("normal" geometry) instruments using linked scans of two of the following variables: magnetic field strength, electrostatic analyzer field strength, and accelerating voltage (98-102). In general parent ion resolution is poor (less than 200) while daughter ion resolution is good (greater than 500-600) when investigating decompositions occurring within the first field-free region. In contrast, daughter ion resolution is generally poor while parent ion resolution is good when

the decompositions being studied occur in the second field-free region.

The instrument illustrated in Figure 32b is that used in triple quadrupole mass spectrometry (TQMS) (103,104). As the name implies, this instrument uses three quadrupole mass filters in tandem. Ions are continuously formed and accelerated out of the ion source. To collect a daughter scan, quadrupole Q1 performs the first stage of mass analysis and transmits parent ions of a single m/z to the second quadrupole, Q2. The parent ions are subjected to CID within Q2. Q2 is operated in a non-mass discriminating ("radio frequency only") mode and has been shown to efficiently contain and transmit stable ions and daughter ions scattered over a wide range of angles (104). These ions are subsequently mass analyzed using the second stage of mass analysis of the TQMS instrument, quadrupole mass filter Q3.

The double focussing instrument and the TQMS instrument are quite different in form and function, each exhibiting its own advantages and disadvantages. A major difference between the two instruments is the collision energy used for CID. The sector instrument uses high collision energy CID (greater than 1 keV, laboratory frame of reference), while the TQMS instrument uses collisions of less than approximately 150 eV (laboratory frame of reference). Though excitation in low and high energy CID is thought to proceed by different mechanisms (105-107), the two techniques often yield similar information. However, the low collision energies of the TQMS instrument offer the possibility of using collisionally induced <u>association</u> (108) for an added dimension of information. On the other hand, processes such as charge stripping,

charge inversion, and ionization of fast neutrals (in "neutralization/reionization" experiments, for example) occur in the high energy collisions of the sector instrument and may be useful for fundamental as well as applied purposes (109).

While ions scattered over a wide range of angles are contained and transmitted by Q2 in the TQMS instrument, only ions scattered over a very narrow range of angles (less than 1°) about the flight tube axis are transmitted to the electrostatic analyzer in the MIKES instrument. An overall transmission efficiency (sum of the ion current passing out of the collision cell over the ion beam current entering the cell) of approximately 50 % has been measured while using a TQMS instrument (110). Transmission efficiencies in sector instruments are generally much lower. McLafferty et al. reported a value of 6 % (111). Instrumental improvements in sector instruments (112) have yielded improved transmission efficiencies. Values as high as 24 % have been reported (113).

The MIKES instrument generally offers unit resolution for the parent ions but less than unit resolution for the daughter ions. As mentioned earlier, parent ion resolution is generally poor when decompositions occurring within the first field-free region are studied using both E/B and B/E instruments. The poor resolving power of one of the two stages of mass analysis is generally considered to be the major disadvantage in using two-sector instruments for MS/MS. In addition, artifact peaks are often observed when using double focussing instruments and linked scans for MS/MS because neither analyzer is a

true "mass" analyzer. In contrast, the mass-to-charge filtering performed by the quadrupole is relatively independent of ion energy (within a relatively low kinetic energy range, as mentioned earlier) and artifact peaks are not observed in TQMS instruments. The quadrupole mass filters of the TQMS instrument are generally operated at unit mass resolution. However, the transmission efficiencies of most TQMS instruments drops dramatically at high mass and this usually limits the practical upper mass limit of these instruments to approximately 1,000 to 2,000 u. This is a disadvantage of the TQMS instrument as compared to the sector instruments.

A number of multi-sector (114,115) and "hybrid" instruments (using both sector and quadrupole analyzers) (116-118) have been built to alleviate the problems discussed above. Most of these use a B/E or E/B combination to perform high resolution analysis of parent ions or of daughter ions. Most of the commercially available hybrid instruments combine a double focussing sector instrument followed by a quadrupole collision cell and a quadrupole mass filter. These instruments have the capability to select parent ions with high mass resolution (greater than 10,000) and to select daughter ions with unit mass resolution. Collision energies ranging up to a few hundred electron volts are available in the region located between the last sector and the final quadrupole mass filter. High energy collisions may be performed within the first two field-free regions. Thus, the multi-sector and hybrid instruments often provide the capability of performing sequential CID's (MS/MS/MS).

The ultimate end of this progression is the four-sector instrument for MS/MS which provides high resolution analysis of both parent and daughter ions (119, 120). The capabilities of such instruments are just now being investigated (121). In addition to the high resolution offered by these instruments, they also eliminate the artifact peaks often observed using two-sector instruments for MS/MS. The greatest disadvantages of the four-sector instruments is their tremendous cost and complexity, and the low level of ion current finally reaching the detector.

Unfortunately, all the instruments discussed above still exhibit a major flaw. The flaw is the same as that discussed in Chapter 1 concerning conventional mass spectrometers. To collect the full MS/MS data field of a compound (the three dimensional data field consisting of the intensities of all the daughter ions of all the parent ions of a particular compound) these instruments must sequentially select a parent ion for CID using the first stage of mass analysis and sequentially detect all the daughter ions using the second stage of mass analysis. Even for compounds with relatively simple mass spectra (few parent ions) and using fast scanning sector analyzers or quadrupole mass filters under computer control, collecting the data field requires on the order of 5 or more seconds.

The added dimension of information offered by MS/MS would be valuable in characterizing samples or events in which the nature of the sample in the ion source changes rapidly (as in capillary GC or pulsed laser desorption). Compromise approaches to this problem include using ionization methods such as CI which produce only a single parent ion from each species of interest (at the expense of the additional structural information offered by the MS/MS data field obtained when all the potential parent ions produced by EI ionization are subjected to CID), and the use of single or multiple reaction monitoring (MRM). The latter approach is similar to selected ion monitoring (SIM) in MS where high sensitivity and selectivity are achieved by only monitoring a few ions related to a particular species of interest. The added selectivity and sensitivity come at the expense of information concerning any additional species which might be present. In MRM only a few selected parent/daughter ion relationships are monitored which correspond to species or compound classes of interest.

The ideal solution, as presented in Chapter 2, is again the use of array detection for additional speed and/or S/N improvement in collecting MS/MS data. Though these improvements would be welcome in many applications where the nature of the ions formed in the ion source changes rapidly, collecting the full MS/MS data field in a repetitive manner during a GC-MS/MS run would soon produce an unmanageable amount of data. Clearly, some discrimination would be required. Two of the three array detection techniques discussed in Chapter 2 have been used in MS/MS: spatial array detection and frequency array detection. Time array detection has yet to be implemented.

The EOID (see Chapter 1) has been used for spatial array detection in MS/MS by Louter *et al.* in a tandem magnetic sector instrument (122,123). The ratio between the highest and lowest mass which may be simultaneously detected using this instrument ranged from 4:1 to 1.06:1. After CID between the two magnetic sectors, the ions were accelerated to 30 keV to reduce the deleterious effects of the kinetic energy spread upon the second stage of mass analysis. The resolution in both stages of analysis was as high as 600. The instrument has more recently been used for fundamental studies in ion/neutral collisions with collision energies ranging from 10 to 6,000 eV (124). The S/N improvement offered by the EOID was an advantage at low collision energies where the signal levels were low. The disadvantages of the EOID are discussed in Chapter 1.

FTMS (see Chapter 1) has also been used for MS/MS (88,125-127). Ions other than the parent ion are ejected from the FTMS cell by broad-band irradiation encompassing all cyclotron frequencies except that of the desired parent ion (using a notch filter). The parent ion is then excited by irradiation at its cyclotron frequency and allowed to undergo CID with either neutral sample molecules (in which case the risk of ion molecule reactions is present (126)) or with a collision gas. The daughter ions are then excited and detected in the usual way (see Chapter 1).

The collision gas may be introduced by using a pulsed valve. In this way one advantage of FTMS for MS/MS, high resolution analysis of the daughter ions, may be obtained without interference from high pressure within the cell during the daughter ion frequency analysis. The first demonstration of this advantage was the simultaneous detection of two different isobaric daughter ions of mass 43 which were products of the CID of different parent ions (128). A daughter ion resolution of 12,000 has since been reported (113). Recently, Marshall has reported better than unit parent ion resolution using a "tailored" frequency-domain excitation pattern (129).

Another advantage of using FTMS for MS/MS is that the parent ion selection, CID, and daughter ion detection all occur in the same cell. These steps are sequential only in time, not in location. This allows for the CID of daughter and granddaughter ions with relative ease (MS/MS/MS/MS...) (22,113). Perhaps the major advantage of FTMS for MS/MS is the speed with which an MS/MS scan sequence can be completed (due to the enhanced S/N and/or speed offered by the simultaneous detection of the daughter ions). The full MS/MS sequence of events (ionization, parent ion selection, pulsing in the collision gas, collision, pumping away the collision gas, excitation of the daughter ions, and detection) for a single parent ion can be completed in 100-200 ms (22). It is concievable that a single (non-averaged) daughter scan of each of 5-10 parent ions of previously determined mass could be collected in one second.

There are limitations in current FTMS technology as it is applied to MS/MS. The greatest limitation is the limit on the total number of ions which can be trapped within the FTMS cell before the MS/MS experiment begins due to space-charge effects. Only the most abundant daughter ions may at times be observed. This limited dynamic range often requires signal averaging and extended analysis time. The fact that the MS/MS sequence of events occurs within the same cell can be a disadvantage, as mentioned earlier, due to the potential for ion molecule reactions with sample molecules, and due to the fact that the collision gas must be pulsed into the cell to achieve CID and pumped away before high resolution daughter ion analysis is possible. In addition, the collision energy resolution for the parent ions in FTMS is not as great as that attainable in conventional tandem instruments.

Time array detection as such has yet to be implemented in TOF-MS and in the application of TOF-MS to MS/MS. Yet the use of TOF instruments to study metastable decompositions and CID is not new. A number of TOF instruments were modified for separation of the undissociated parent ion, daughter ion, and neutral fragment components of TOF peaks which undergo metastable decomposition during their flight from the ion source to the detector (130-133). This was accomplished by applying a retarding electric field at the end of the flight tube either on the multiplier "stack" or on a separate set of grids in front of the multiplier. A further refinement of this design was the inclusion of a pulsed vertical deflection plate in the flight tube which would deflect all of the ions with masses greater than the metastable ion of interest away from the detector (134). In this manner these ions of higher mass

(longer flight time) would not interfere with the detection of the daughter ion peaks. Retarding fields were used in ^{252}Cf fission fragment induced desorption/ionization MS to reveal the proportions of a number of peaks striking the detector at the end of a 3 m long flight tube which are due to metastable products (135). Ninety-six percent of the molecular ion peak (and $M+H^+$ adduct) of chlorophyll *a* was revealed to be composed of daughter ions and neutral products of metastable decompositions. This application of a retarding field at the end of the flight tube is essentially a kinetic energy analysis of the undissociated parent ions and daughter ions.

A two dimensional array detector has been proposed for the study of daughter ions from metastable decompositions or CID (120). It appears that this proposal is similar to that of Bakker (136), in which an impulse is imposed on ions traveling between a pair of deflection plates. If the voltage pulse is of short enough duration, the velocity imposed on the ions perpendicular to their original flight axis is inversely proportional to their mass. Bakker's proposal was based on Fowler and Good's "impulse sweeping" (78) method of beam deflection. By applying the voltage pulse at the proper time to one side of a pair of deflection plates located in a region of the flight tube where the ions have already separated into isobaric packets, one may choose to look at the daughter ions of a single parent ion.

Many other TOF instruments have been designed to study ion neutral and ion photon interactions. Among these are a tandem quadrupole/TOF mass spectrometer (137), and an interesting magnetic sector/TOF instrument which uses a solid surface as the CID target (138). A reflectron TOF mass spectrometer (see Chapter 2) has been used to study the photodissociation of selected ions (139). The laser pulse is used to photodissociate the ions in an isobaric packet at the end of the first field-free region. The daughter ions have lower energies than the undissociated parent ions, spend less time in the reflecting field, and have shorter total flight times to the detector than the undissociated parent ions. The reflecting field performs an energy analysis on the undissociated parent and daughter ions.

During the meetings of the discussion group referred to in Chapter 1, the idea of combining velocity analysis with momentum analysis of stable and daughter ions which are products of parent ion decompositions occurring within the first-field free region of a single focussing magnetic mass spectrometer was proposed. Assuming that the kinetic energy release upon decomposition is negligible, a daughter ion would have the same velocity as its parent ion. The flight times of the daughter ion and of a stable ion having the mass of the parent to the detector would also be assumed to be identical. The flight times of the ions would thus establish parent ion-daughter ion relationships. The daughter ion momentum would necessarily be lower than that of the parent ion and thus daughter ions could be separated from stable ions and from other daughter ions by momentum dispersion in a magnetic field. The mass of any ion, whether daughter or stable, is unambiguously determined

by the measurement of both velocity and momentum.

This proposal is the basis of the current research in time-resolved ion momentum spectrometry (TRIMS) (31,32,140-143). Unlike conventional MS/MS instruments in which the stages of mass analysis are performed sequentially in space and/or time, the momentum and tof analyses are performed simultaneously in TRIMS. Parent ion-daughter ion relationships are established by inspection of the data after data collection is completed.

The idea of combining velocity (tof) analysis with simultaneous kinetic energy analysis of stable and daughter ions arose at a later date during the aforementioned discussions. As in TRIMS, parent ion-daughter ion relationships are established by virtue of the fact that parent ions and daughter ions have nearly identical velocities. In an instrument using constant energy acceleration (see Chapter 1) all of the stable ions would exhibit the same kinetic energy. The kinetic energies of daughter ions are necessarily lower than those of their parent ions. A kinetic energy filter such as an electrostatic analyzer could be used to separate stable ions from daughter ions which are products of decompositions occurring between the acceleration stage and the kinetic energy analysis. The mass of any ion would be determined by the measurement of its velocity and kinetic energy.

The BEDER-TOF is suitable for a preliminary investigation of this MS/MS technique, hereafter called time-resolved ion kinetic energy spectrometry (TRIKES) (144,145). Conducting this preliminary investigation became a third goal of this research in TOF-MS.

Once the integrating transient recorder for time array detection (29) is combined with the TRIMS or TRIKES instruments, collection of the full MS/MS data field may be possible with one scan of the magnetic or electrostatic field. This would enable the collection of the MS/MS data field on the time frame of the elution of a chromatographic peak and would provide the full power of MS/MS in chromatographic detection.

B. Theory

The equations governing TRIKES are presented in this section.

If a parent ion of mass m_p undergoes CID or metastable decomposition after acceleration from the source, producing a daughter ion of mass m_d, and the kinetic energy release upon fragmentation is negligible, then the velocities of the daughter and of the parent are assumed to be identical:

$$v_d = v_p \qquad (21).$$

Therefore, their flight times are also assumed to be identical:

$$(tof)_d = (tof)_p \qquad (22)$$

(where the subscripts d and p designate daughter ion and parent ion values, respectively).

In the current BEDER-TOF instrument only metastable decompositions occurring within the first field-free region between the source and electrostatic analyzer are observed using TRIKES. Since the mass of the daughter ion is necessarily smaller than that of the parent ion, the daughter ion kinetic energy will be smaller than that of the parent. Only ions of a particular kinetic energy are allowed to pass through an electrostatic analyzer of field strength $\underline{E}$, following equation (23):

$$m\ v^2/a = z\ e\ E \qquad (23).$$

Rearranging equation (2) of Chapter 1 yields an expression for velocity:

$$v = \sqrt{2\ z\ e\ V_o\ /\ m} \qquad (2c).$$

Substituting equation (2c) into equation (23) and rearranging, one obtains a relationship between the mass-to-charge ratio of any ion (parent or daughter), its tof, and the electrostatic analyzer field strength necessary to pass the ion:

$$m/z = e\ a\ E\ (tof)^2\ /\ L^2 \qquad (24).$$

Since E is related to the kinetic energy of the ion and tof is related to the velocity of the ion, equation (24) indicates that the m/z of any ion can be unambiguously determined in TRIKES irrespective of the velocity distribution of that ion. Using equations (22) and (24), a simple relationship is established between the masses of the parent and the daughter ions and the field strengths necessary to pass the two:

$$\frac{m_d}{m_p} = \frac{E_d}{E_p} \qquad (25).$$

In MS/MS analyses, a variety of scan modes are useful (92). Figure 33 is a plot of flight times vs. electrostatic analyzer field strength for the stable and daughter ions of n-decane. The stable ions are represented by the bar graph spectrum lying on a line of constant field strength (this assumes constant energy acceleration from the ion source). Examples of the various scan modes are represented by the appropriate E vs. tof curves shown in Figure 33. The equations governing these scan modes are presented below.

In a daughter scan one simply detects all the daughter ions of a particular parent ion. This is the simplest of scan modes in TRIKES and is described by equation (25a):

$$m_d = \frac{E_d}{E_p} m_p \qquad (25a).$$

One simply holds the tof constant, thus monitoring only ions with the same tof as the parent ion. E_p and m_p are constants in a daughter scan while E_d is decreased to observe ions of lower kinetic energy and mass, m_d. This is illustrated by the lines labelled "d" in Figure 33.

In a parent scan one detects all the parent ions of a particular daughter ion. Equation (25b) describes the parent scan:

$$m_p = \frac{E_p}{E_d} m_d \qquad (25b).$$

Both E_p and m_d are constants. As E_d is scanned to vary the parent ion mass, m_p, tof_p is also scanned such that the product of E_d and $(tof_p)^2$ remains constant to satisfy equation (24a):

$$m_d = z\ e\ a\ E_d\ (tof_p)^2 / L^2 \qquad (24a).$$

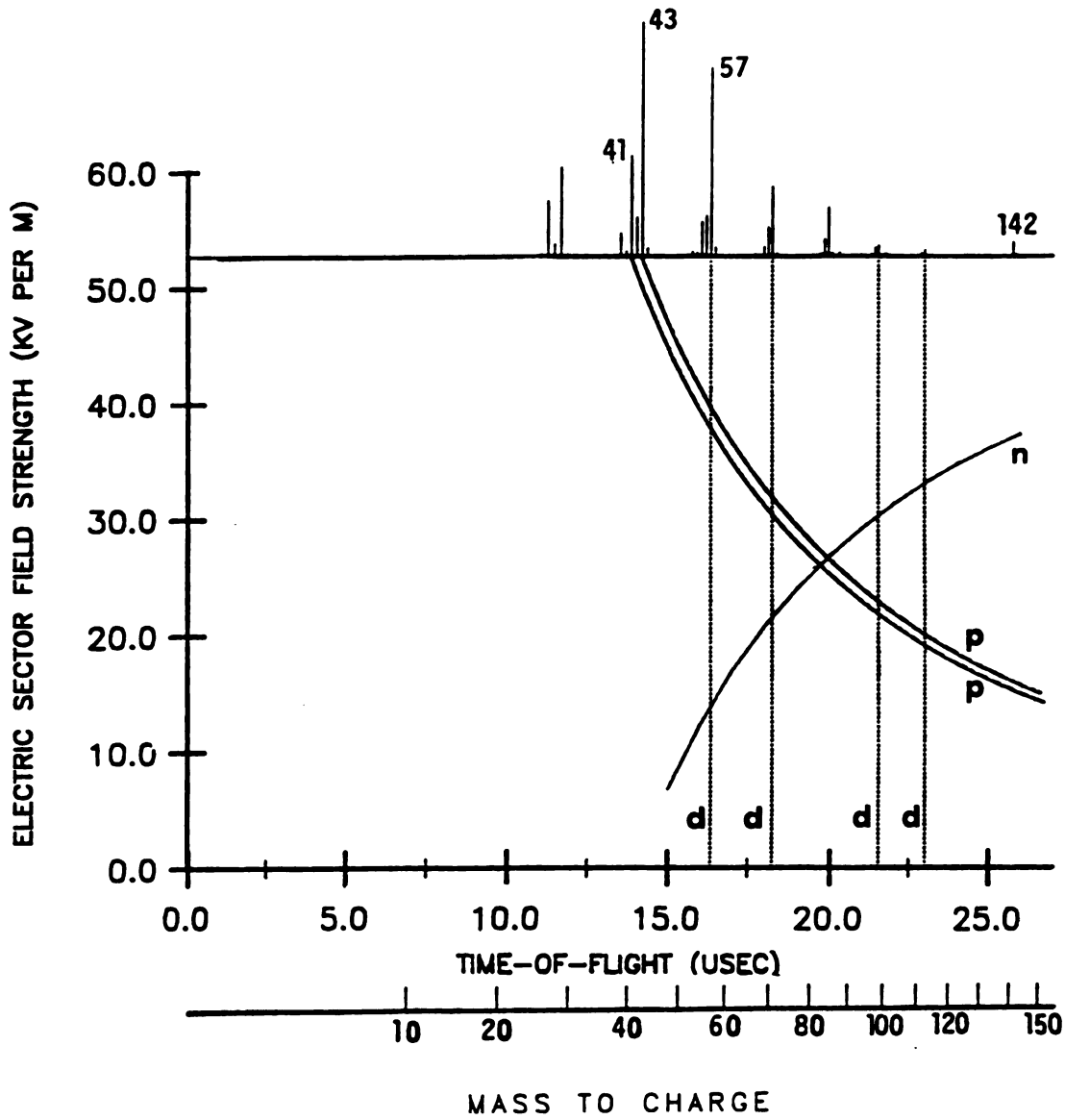

Figure 33. MS/MS data field (E vs. tof) for n-decane (simulated). The stable ions lie along a line of constant E. Daughter scans of parents of mass 57, 71, 99, and 113 are labelled "d". Parent scans of daughters of mass 41 and 43 are labelled "p". Constant neutral loss scan of neutral loss 42 is labelled "n".

This scan mode is illustrated by the line labelled "p" in Figure 33. All daughters of a particular mass lie along such parabolas. Daughter ions are spread over a wider range of flight times and electrostatic analyzer field strengths than are stable ions due to kinetic energy release upon metastable decomposition. This is illustrated in Figure 34. The width of the distribution is related to the kinetic energy bandpass of the electrostatic analyzer and the resolution of the TOF analysis while the length of the distribution is related to the magnitude of the kinetic energy release.

In a constant neutral loss scan one detects only daughter ions separated from their parents by a particular neutral loss, m_n. This type of scan is often useful in screening for particular classes of compounds. To perform a neutral loss scan in TRIKES, both tof and E are scanned such that [$(tof)^2 (2 V_o - a E)$] is constant, to satisfy equation (26):

$$m_n = (2 V_o - a E) z e (tof)^2 / L^2 \qquad (26).$$

This is illustrated by the line labelled "n" in Figure 33.

C. Experimental Section

The BEDER-TOF, as described in Chapter 3, has been used for the studies in TRIKES.

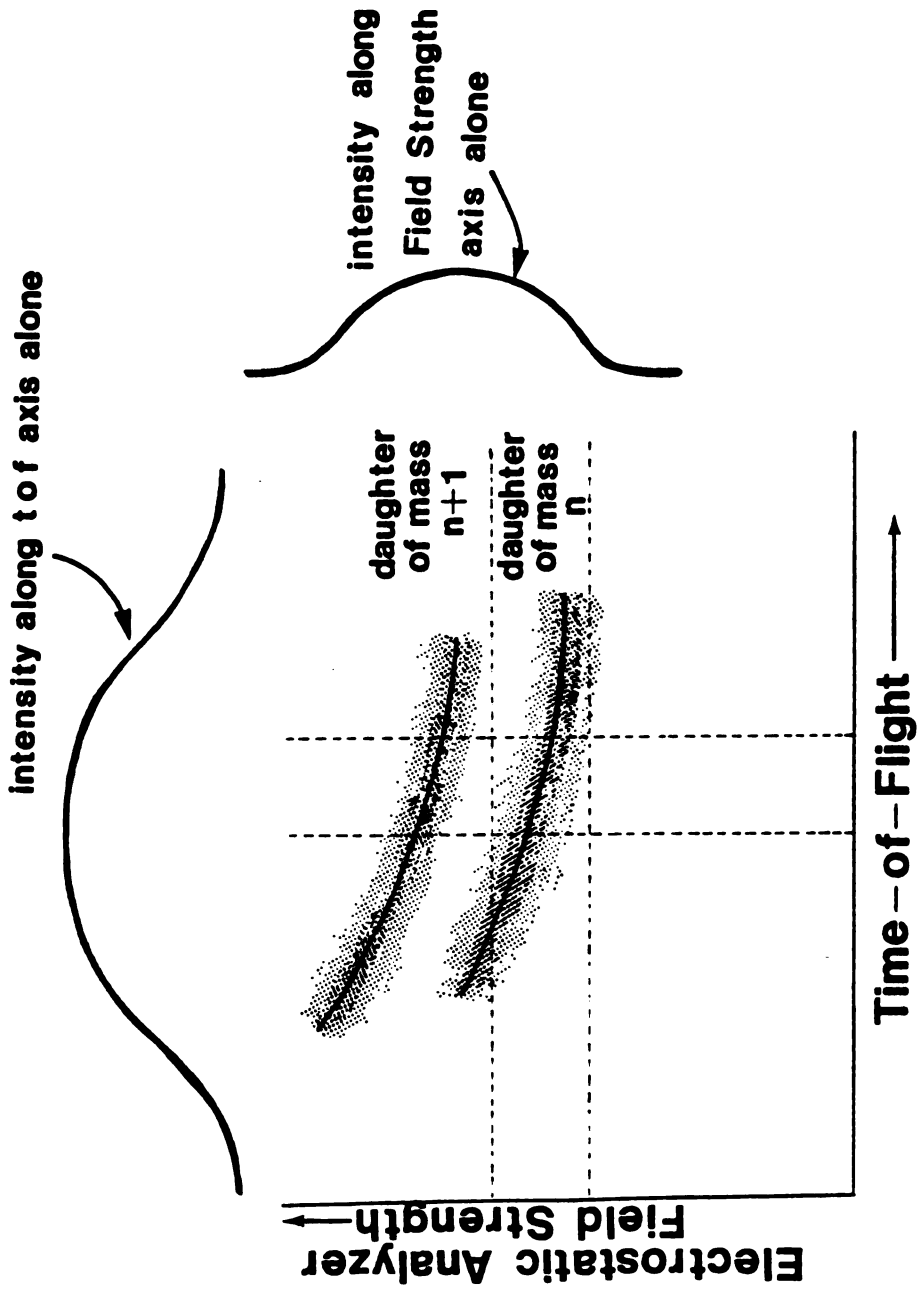

Figure 34. Enlarged portion of the E-tof plane showing two daughter ions lying on parabolas of constant mass (determined by E x $(tof)^2$ product). The combination of E and tof measurements yields higher daughter ion resolution than do either E or tof measurements alone.

Parent and constant neutral loss scans would be most easily performed by using a computer to control the position of the time aperture of the boxcar along the tof axis or the electric sector field strength (or both) to perform the appropriate linked scan (see section B of this Chapter). The software and hardware to accomplish this task has not yet been written and/or purchased. In contrast, daughter scans are relatively easy to implement, since the boxcar time aperture position is held constant at the arrival time of the stable ion having the mass of the parent ion while the electrostatic analyzer is scanned. All the scans performed during this preliminary investigation of TRIKES have thus been daughter scans.

To perform a daughter scan, the stable ion having the mass of the parent ion of interest is brought into view on the oscilloscope as described in Chapter 3. The electrostatic analyzer voltages yielding the greatest peak intensity are recorded. The signal cable from the E220 amplifier is then disconnected from the oscilloscope and connected to the boxcar averager. Using the MSTEST program, the boxcar is zeroed and the boxcar time aperture (aperture widths of 5 ns and 50 ns have been employed) is scanned across the peak of interest (the red "scan select halt" button on the M162 must be depressed to scan the aperture) using either the "initial B" or "initial A" control potentiometer depending on which M164 plug-in module is used to collect the data. The aperture is centered on the tof of the ion of interest.

To scan the electrostatic analyzer field strength, the front panel "electric sector" control is switched to the "program" position. For convenience, the 0 to +5 V "scan out" signal from the boxcar plug-in module not being used to collect data is used to control the electrostatic analyzer voltages power supply. To do so it must be connected to the "program" input cable. If the boxcar plug-in module A is used to control the electrostatic analyzer scan and plug-in module B is used to collect the data, for example, the boxcar "scan select A" button would be depressed while the M162 "function" switch would be at position "B". Using equation (25a), one may calculate the approximate electrostatic analyzer voltages corresponding to the daughter ions of interest. The power supply voltages are then set lower than those calculated (to encompass the daughter ions during the electrostatic analyzer scan) with the "initial A" potentiometer (the "scan select halt" button must be depressed to set this potentiometer and then released). Using MSTEST to initiate and average scans, the maximum electrostatic analyzer field strength attained during a scan is determined by the number of data points collected during a scan and the delay time between data points. Both of these parameters must be set in MSTEST before scanning may be initiated.

Most of the TRIKES studies have been performed using n-decane as sample. The metastable decompositions of this compound have been well characterized (146-148). The initial experiments were performed using toluene and n-butyl benzene as samples. The sample pressure was generally set between 6.0×10^{-6} torr and 1.2×10^{-5} torr (the background pressure was usually below 3×10^{-7} torr).

Once the conditions necessary for the observation of daughter ions using the BEDER-TOF for TRIKES were achieved, the influence of a number of instrumental parameters on resolution and sensitivity was investigated. Among these parameters were the ion lens voltage, the horizontal and vertical steering plates voltages, the Avtech beam deflection voltage, the high voltage on the multiplier stack, the boxcar aperture duration, the boxcar time constant, the ion source repeller voltages, and the accelerating voltage.

D. Results and Discussion

The first observation of what was later shown to be daughter ions using the BEDER-TOF was inadvertently made during a normal resolution study in which the sample was toluene. As the electrostatic analyzer was manually scanned from high to low field through the field strength necessary to pass stable ions, the peak intensities at and near the arrival times of masses 91 and 92 increased to a maximum and then decreased. However, the peak intensity at mass 92 did not decrease to background as soon as that at mass 91. In fact, it appeared that the peak intensity at mass 92 went through a second much less intense maximum after the peak at mass 91 had disappeared. A few of the spectra collected during this "defocussing" of the electrostatic analyzer are presented in Figure 35.

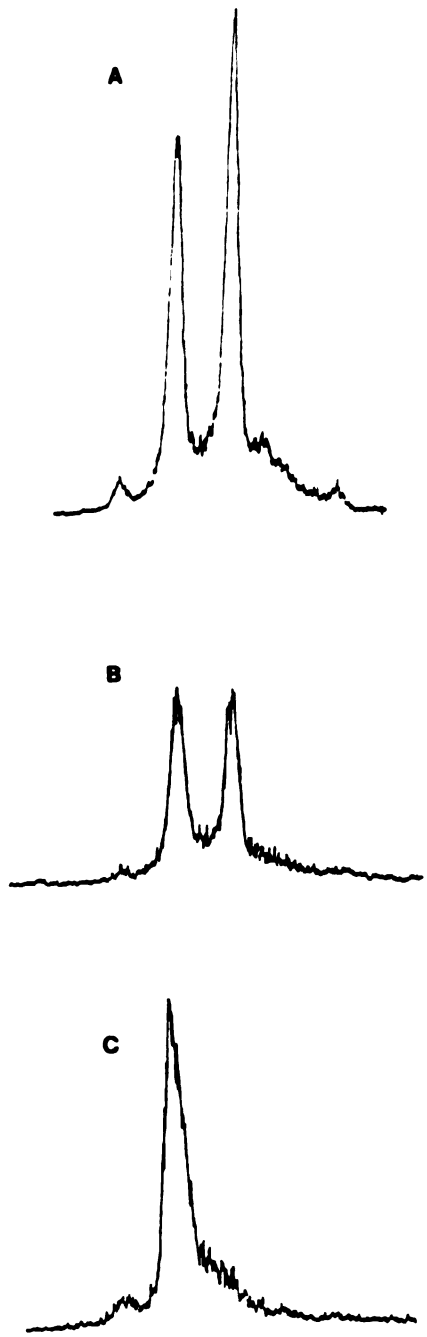

Figure 35. Selected spectra collected during "defocussing" of the electrostatic analyzer. The peaks are those of the $M^{+\cdot}$ and M - 1 ions of toluene. (a): Electrostatic analyzer field strength is that necessary to pass the stable ions, E_o; (b): E is 0.9947 E_o; (c): E is 0.9876 E_o. The chart sensitivity in (b) and (c) is approximately six times that in (a).

This phenomenon was later shown to be due to the aforementioned metastable decomposition of the molecular ion of toluene to form an ion of mass 91 through loss of H•. Figure 36 shows one of the first succesful TRIKES spectra obtained in the manner outlined in the preceding section. The metastable decomposition studied was again the loss of H• from the molecular ion of toluene. These early results were quite encouraging as the ratio of the field strengths at the peak maxima agreed with the ratio of the masses to within 0.06 %. Equation (25) is thus shown to hold under the conditions of this test.

A subsequent series of experiments with n-butyl benzene and n-decane were disappointing as no daughter ions could be observed using the procedure outlined above. The initial success with toluene was in part due to the intensity of the metastable decomposition which was studied. The BEDER-TOF does not currently have a collision cell for CID and only daughter ions which are products of metastable decompositions occurring within the 7.4 cm long field-free region between the ion source and electrostatic analyzer are observed by TRIKES. However, a number of other factors which contributed to the lack of success in these early trials are discussed in the following paragraphs.

The accelerating voltages used in these first runs were 700 V and 1,400 V. The repeller voltages were generally only slightly greater than the accelerating voltage. After arcing problems at the ion source high voltage feedthroughs were corrected (as described in Chapter 3) higher accelerating voltages and higher repeller voltages (relative to the accelerating voltage) were used (up to 4,300 V accelerating voltage

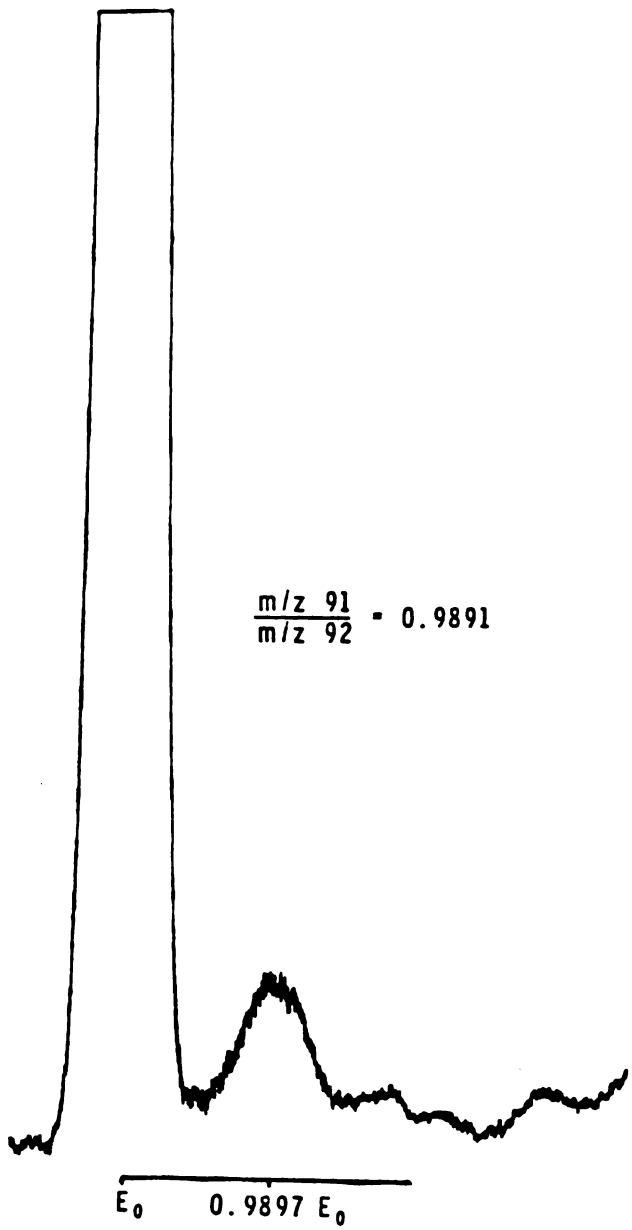

Figure 36. Initial TRIKES daughter scan collected using the BEDER-TOF. The stable ion is the molecular ion of toluene. The daughter ion peak at lower field strength is that of m/z 91 resulting from loss of H· from metastable molecular ions. Notable instrumental conditions were: L = 1.1 m, V_o = 1,400 V, repellers = 1,425 V, horizontal steering plate = 82 V, V' = 32 V, image slit width = 0.64 mm (0.025 in.), boxcar time aperture = 500 ns.

and 4,500 V repeller voltage). Much better results were obtained under these conditions. This is probably due to at least two factors:

a. at low repeller voltages the kinetics of the decompositions may allow the majority of the decompositions to occur before the parent ions reach the region between the ion source and the electrostatic analyzer; and

b. the gain of the electron multiplier increases with increasing accelerating voltage; this latter point is especially important as the kinetic energies and momenta of the daughter ions are even lower than that of the stable ions.

In addition, the beam deflection plates are in essence small electrostatic analyzers. For a given deflection plate length there exists a deflection field strength (deflection voltage/distance between the deflection plates) beyond which no ions are allowed to pass into the flight tube, as indicated by equation (19) of Chapter 2. As the kinetic energy of the ions decreases, this critical field strength also decreases. The TRIKES results have thus been obtained using the lowest deflection voltage which still yields reasonable tof resolution for the stable ions. An attempt has not been made to determine the critical deflection voltage for particular daughter ions.

The same holds true for the horizontal and vertical steering plates located within the flight tube. As mentioned in Chapter 4, the horizontal steering plates' potentials had a tremendous effect on resolution in normal TOF studies. The first TRIKES scans were also attempted with a potential field applied across the horizontal steering plates for improved tof resolution for the stable ions. It soon became obvious that this did not improve TRIKES spectra. The steering plates have been at the flight tube potential (ground) in all subsequent TRIKES scans.

The stack of the multiplier was at high voltage during the early runs. This shifted the flight times of the daughter ions away from that of the stable ions of parent ion mass (to shorter flight times). The daughter ions which struck the detector at the average stable ion flight time were those entering the electrostatic analyzer with lower than average kinetic energies. The detected daughter ion peak was thus shifted to slightly lower mass as calculated according to equation (25a) (this shift was generally less than 0.5 u). As illustrated in the results which follow, much better calculated values of daughter ion mass have been obtained since the detector stack was grounded during TRIKES studies.

A note is in order concerning another effect of the magnetic electron multiplier on daughter ions. Previous investigators (89) have shown that stable ions are deflected away from the flight tube axis as they enter the magnetic field of the multiplier. The relative deflection depends on the momentum of the ions and is thus more pronounced at low mass. Fortunately, this effect was shown to have little influence on the relative abundances of the stable ions at normal TOF accelerating voltages (2,800 V and above). This momentum analysis of the daughter ions, however, was shown to be a severe hindrance in the analysis of low mass daughter ions formed upon metastable decompositions of parent ions within the flight tube. The effect was more pronounced as the difference between the daughter ion and parent ion masses (momenta) increased. From this standpoint, a channel electron multiplier array (CEMA) would be a desirable replacement for the magnetic electron multiplier.

A daughter scan is shown in Figure 37. The parent ion is the molecular ion of n-decane at mass 142. Metastable ions at mass 84, 85, 98, 99, 112, and 113 are visible. Table 2 compares the known masses of the daughters to those calculated according to equation (25a). The average relative deviation is 0.20 %. A slight negative systematic error is apparent. This systematic error may be due to the short accelerating region between the stack and the first cathode of the electron multiplier. As mentioned earlier, the S/N level is very low when using the current configuration of the BEDER-TOF for TRIKES. THe spectrum shown in Figure 37 is an average of 100 consecutively obtained spectra and required 11 hours to collect.

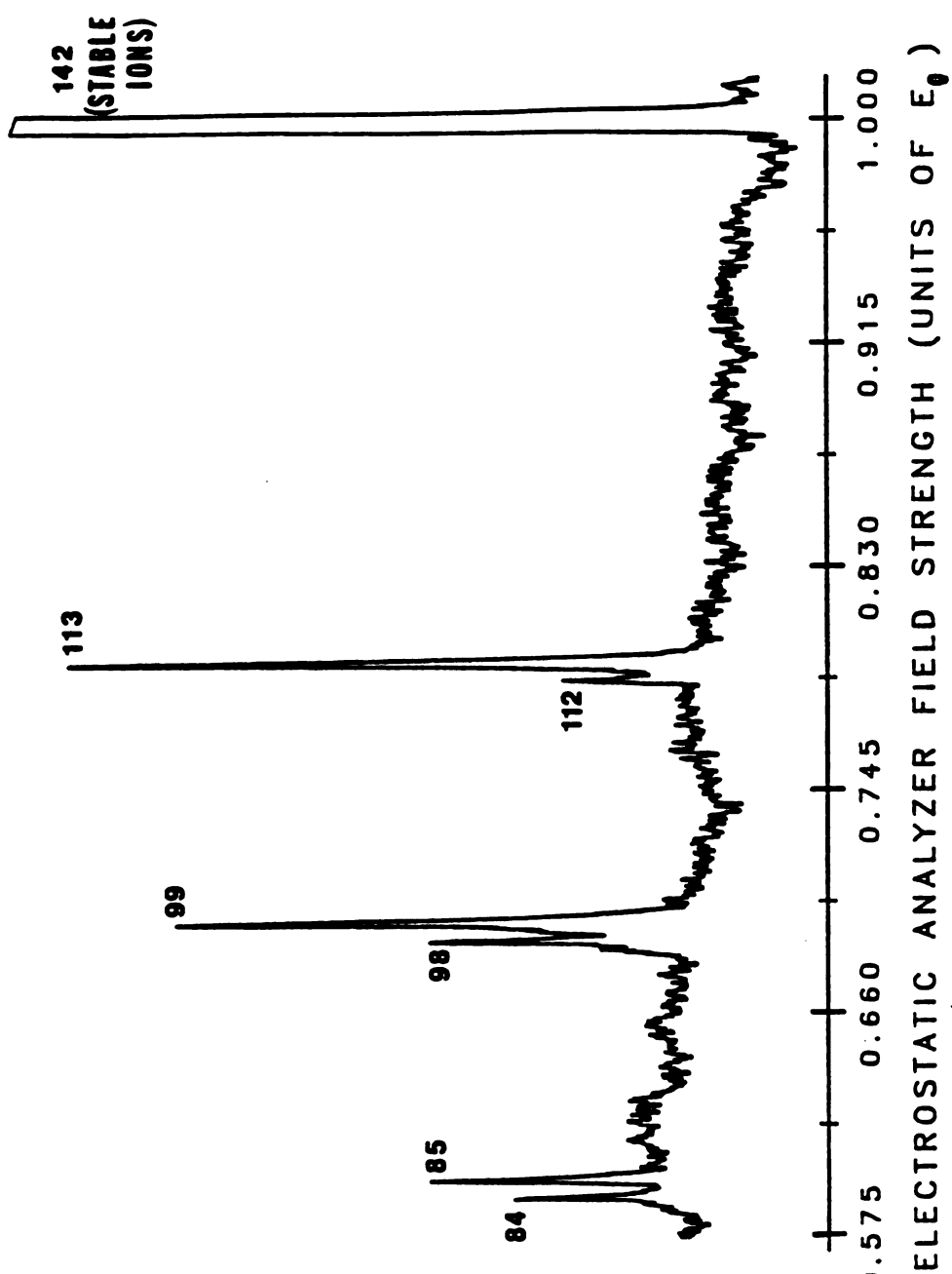

Figure 37. Daughter scan of the molecular ion of n-decane (mass 142). The height of the m/z 113 daughter ion peak is approximately 3 % of that of the undissociated molecular ion. This is an average of 100 consecutively collected spectra. L = 1.9 m, V_o = 4,300 V, repellers = 4,450 V, horizontal steering plate = 0 V, V' = 55 V, image slit width = 0.025 mm (0.001 in.), boxcar time aperture = 5 ns.

TABLE 2

COMPARISON OF CALCULATED VS. KNOWN MASSES FOR THE DAUGHTER IONS OF THE MOLECULAR ION OF N-DECANE[a]

Empirical Formula of the Daughter Ion	Mass of the Daughter Ion (u)		Relative Deviation (%)
	Known	Calculated[b]	
$C_8H_{17}^{+\cdot}$	113.13	112.93	0.18
$C_8H_{16}^{+}$	112.12	111.94	0.16
$C_7H_{15}^{+\cdot}$	99.12	98.88	0.24
$C_7H_{14}^{+}$	98.11	97.88	0.23
$C_6H_{13}^{+\cdot}$	85.10	84.92	0.21
$C_6H_{12}^{+}$	84.09	83.93	0.19

a) Data is from the constant parent scan shown in Figure 37.

b) according to equation (25a).

At least unit resolution for the daughter ions has been observed in all the daughter scans collected to date. The three doublets of daughter ions in the daughter scan of m/z 142 of n-decane were often used to study daughter ion resolution. Figure 38 is an averaged daughter scan about the daughters of masses 113 and 112. This spectrum required two and a half hours to collect and is an average of 400 scans. A daughter ion resolution of 475 is calculated from this doublet. The accelerating voltage used when collecting this spectrum was 4,300 V. Lower accelerating voltages yield somewhat lower daughter ion resolution. A resolution of 391 was calculated from this same doublet at an accelerating voltage of 3,000 V. The boxcar averager aperture duration was 5 ns (nominal) while collecting the spectra illustrated in Figures 37 and 38. As expected, longer aperture durations gave lower daughter ion resolution. The 112/113 doublet resolution was 206 using a 50 ns aperture and a 3,000 V accelerating voltage. A positive voltage was applied to the ion lens since this increased the magnitude of the daughter ion current striking the detector. The influence on the flight times was minimal.

A comparison of the results of a typical MIKES scan to those obtained in this preliminary study of TRIKES shows that the combination of kinetic energy and velocity analysis offers much better resolution for the daughter ions than does the kinetic energy analysis alone. Daughter ion resolution is generally limited to values under approximately 200 in MIKES (113).

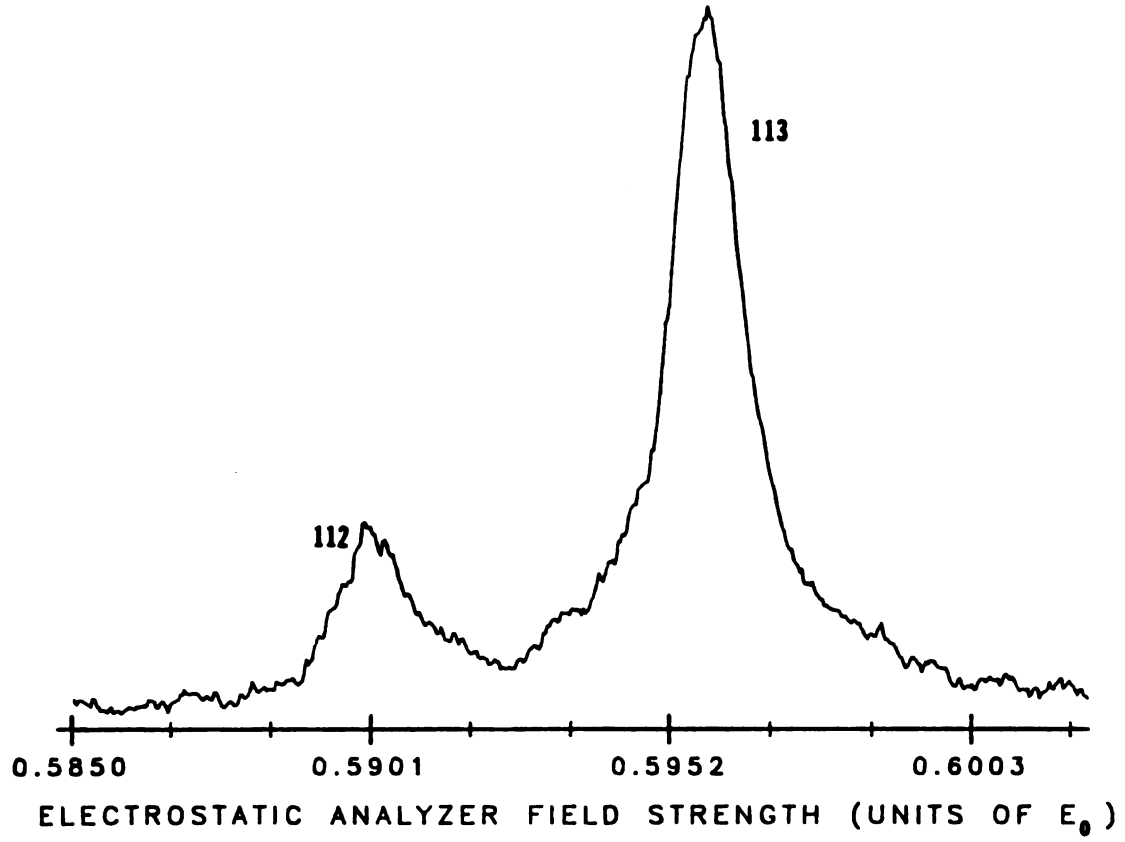

Figure 38. Average of 400 consecutively collected daughter scans of the molecular ion of n-decane about the daughter ions of mass 112 and 113. Instrumental conditions are identical to those listed in Figure 31 except that the repeller voltages are 4,500 V.

Though parent scans have not yet been implemented in TRIKES, parent ion resolution is expected to be lower than daughter ion resolution due to the kinetic energy (velocity) distribution of the daughter ions as illustrated in Figure 34. This is analogous to the situation in TRIMS (32). Though the mass of the daughter ion is unambiguously determined (irrespective of the ion's velocity), centroiding techniques may be necessary to determine the proper parent ion.

CHAPTER 6

CONCLUSIONS

The goals of this research in TOF-MS were to achieve at least unit mass resolution over a 1-800 u mass range, to allow for the use of ion sources in TOF-MS which are not suitable for pulsed operation on the time scale necessary for conventional TOF analysis, and to conduct a preliminary investigation of TRIKES. These goals have been achieved. Consideration of the results and discussion presented in this dissertation suggests a number of instrumental modifications which may improve the operating characteristics of the BEDER-TOF. The mechanisms by which a number of instrumental parameters influence resolution are still not fully understood. Though the influences of all the instrumental parameters on resolution follow the general trends set forth in Chapter 2, a better understanding of the mechanisms by which these parameters influence the operating characteristics of the BEDER-TOF will surely suggest additional instrumental improvements. For example, the original "optimized" deflection plates were separated by 2 mm. An experiment is currently underway in which these plates will be replaced by plates separated by 10 mm in an attempt to perhaps reduce the large level of background noise, to make the full range of deflection voltages offered by the Avtech pulse generator useful, and to

hopefully gain a better understanding of the beam deflection process.

The lowest accelerating voltage generally employed in the BEDER-TOF is 700 V. The maximum mass which may pass through the gating deflection plates of the current version of the BEDER-TOF at this accelerating voltage is approximately 1,000 u. This is frustrating to an investigator working in TOF-MS since the mass range of TOF instruments is often said to be "infinite". (So long as an ion survives the mass analysis period (i.e., the acceleration from the ion source), and so long as the particles striking the detector located at the end of the flight tube produce a signal, a peak will be produced at the mass of the original ion.) A number of strategies might be employed to increase or eliminate this high mass limit of the BEDER-TOF.

One solution might be to use beam deflection/gating methods II or III in Figure 14 of Chapter 3. A disadvantage of method II is that high mass ions from the leading edge pulse might still be between the two pairs of deflection plates when the gate is opened, allowing the low mass ions of the trailing edge pulse to pass through the gate. These high mass ions would overlap with the trailing edge spectrum. The high mass ions of the trailing edge spectrum, however, would never overtake those of the leading edge spectrum (since their velocities would be identical). Thus, TOF analysis of the trailing edge high mass ions would be possible. A similar problem might be present when using method III. High mass ions might still be within the pulse generating pair of deflection plates (the second pair in this method) when the trailing edge of the pulse occurs. These ions might overlap with the low mass

ions of the following spectrum. But they would not interfere with the analysis of the high mass ions which entered the flight tube upon the leading edge of the pulse.

When using methods II and III, only one deflecting field is available to keep the d.c. ion beam from penetrating into the flight tube. Thus, any ions which are sputtered or reflected from the pulsing deflection plate between field reversals would have a greater chance of striking the detector than if methods I or IV were in use. This would produce more background noise (unless the majority of the noise is due to fast neutral species).

Another obvious solution, which would simply extend the mass range (and retain some high mass limit), would be to obtain a pulse generator capable of producing pulses of longer duration (hopefully with a similar risetime and maximum amplitude) and continue to use method I of Figure 14. In this manner the gate could be held "open" longer, allowing higher mass ions to enter the flight tube. Since tof is proportional to the square root of the mass, a small increase in the "open" time entails a relatively large increase in the high mass limit.

The natural extension of this solution would be to use a square wave generator for beam deflection in the place of the pulse generator. The period of the square wave would have to be twice the flight time of the highest mass ion in the spectrum. The gating set of deflection plates would not be needed in this case and the high mass limit would no longer exist. The risetime and the maximum amplitude provided by a

square wave generator would probably not be as desirable as those provided by a pulse generator and resolution might suffer.

Finally, a solution which is attractive is the use of a pulse generator with a pulse width on the order of a few nanoseconds or less. If the rising and falling edges of the pulse were close enough in time, the two ion packets produced would overlap and appear as one. This would also eliminate the need for the gating plates (and thus remove the high mass limit) and increase the sensitivity by a factor of two. However, finding or building such a pulse generator may be difficult.

Two simple modifications may both improve mass resolving power and verify the theory of the beam deflection process presented in this dissertation. Resolving power decreases as the deflection voltage is increased beyond a point which is a function of the accelerating voltage as described in Chapter 4. This effect is presumed to be due to ions reaching the detector which come too close to the deflection plate on which the Avtech pulse is applied. Dr. J. F. Holland has suggested that simply moving the image slit of the electrostatic analyzer away from this plate (in a direction perpendicular to the flight tube axis) might allow the use of higher deflection voltages without the deleterious effects observed when the slit is centered between the deflection plates.

Secondly, as illustrated in Figure 28 of Chapter 4, the ions which reach the detector do not lie on a plane which is perpendicular to the flight tube axis. These ions lie on a plane which is at a slight angle to this perpendicular. Setting the first cathode of the electron multiplier at this angle should improve mass resolving power without modifying the gain of the multiplier.

Another modification which would be relatively easy to implement and which might produce great improvements in mass resolution would be the incorporation of Muga's velocity compaction design (71,72) in either the BEDER-TOF or the CVC TOF mass spectrometer. As described in Chapter 2, no report of the use of this technique with organic samples has appeared. Daughter ions which are products of metastable decompositions occurring within the first field-free region would produce extraneous peaks in the mass spectrum. However, this might be used as a means to study these metastable decompositions.

TRIKES studies are limited by the low S/N available using the current version of the BEDER-TOF. A region containing a collision gas for CID between the ion source and the electrostatic analyzer should greatly increase the utility of this new technique in both applied and fundamental studies of ion neutral interactions.

The BEDER-TOF should be useful in TRIKES studies of the kinetic energy releases involved in metastable decompositions and CID. This feature of TRIMS has already been discussed (139). The study of the kinetics of metastable decompositions may also be possible in TRIKES. Rate constants might be estimated by studying the changes in the stable and daughter ion abundances as the accelerating voltage is varied but the potential difference between the ion source block and the repeller plates is held constant (so that the ions spend approximately the same amount of time in the ion source but spend a variable amount of time between the ion source and the electrostatic analyzer). Holding the ion source block constant and varying the repeller voltages would vary the time spent by the ions in the ion source after their formation and might yield complementary information.

The improvements in S/N and/or data collection rate promised by time array detection should greatly extend the utility of the BEDER-TOF in applications where the signal levels are inherently low (as is currently the case in TRIKES) or in applications where the nature of the ions produced in the ion source is changing rapidly (as in capillary GC-MS or desorption/ionization experiments).

Finally, a personal note is in order. Designing, constructing, and using the BEDER-TOF has been one of the most rewarding, yet one of the most frustrating, experiences of my life. Many a day were spent searching for the source of the latest problem in a string of disappointing failures. In contrast, I learned what "dancing with joy" really meant when I saw the first faint peaks produced by the BEDER-TOF.

APPENDIX

APPENDIX

SCHEMATIC DIAGRAMS OF ELECTRONIC CIRCUITS

Presented here are the schematic diagrams of the electronic circuits designed to power the BEDER-TOF. All capacitance values are in microfarads while all values of resistance are in ohms. All resistors have power ratings of 1/4 watt unless otherwise stated. All potentiometers power ratings are 1 watt with the exception of that of the "Ion Lens" potentiometer which is 5 watts. The operational amplifiers in the schematic diagrams are identified as: A, B, C, D = TL084; E = LM356; F = INA101; G = LM311.

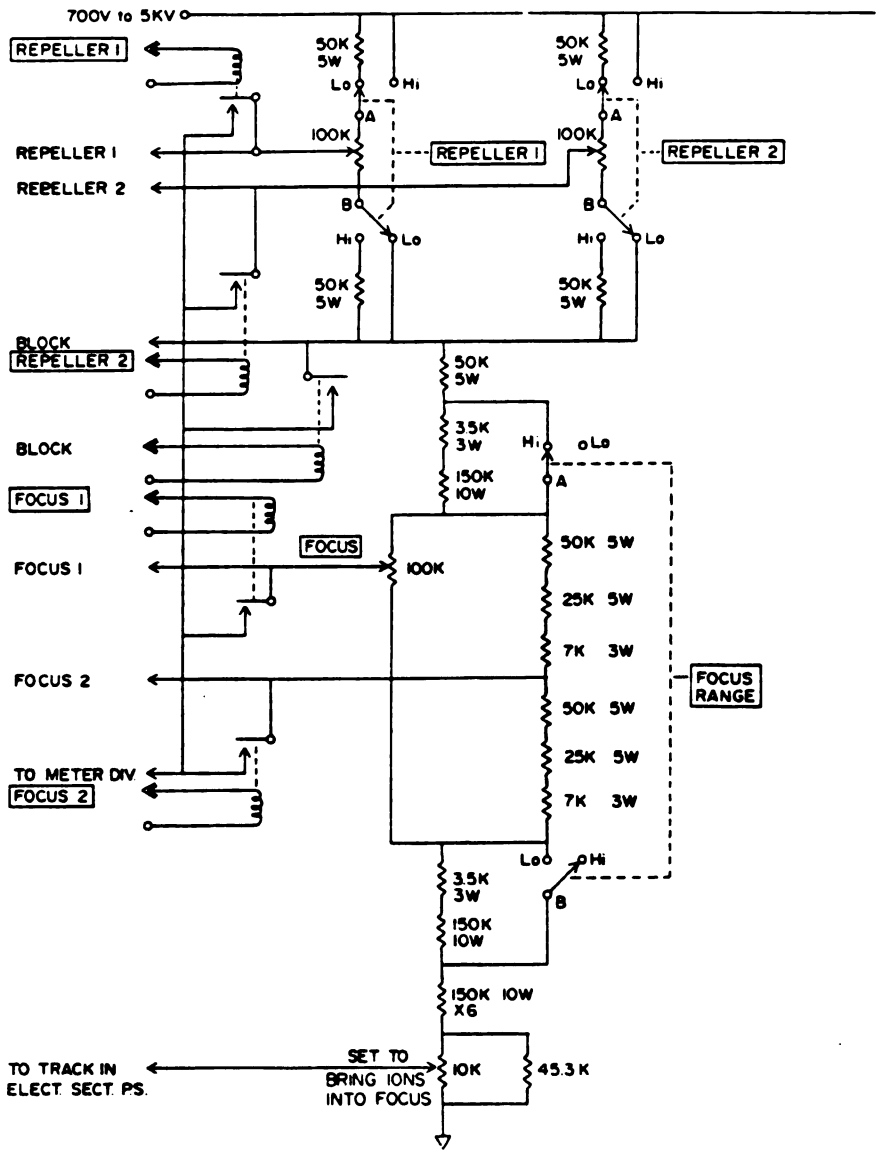

Figure 39. Schematic representation of voltage dividers supplying ion source high voltages.

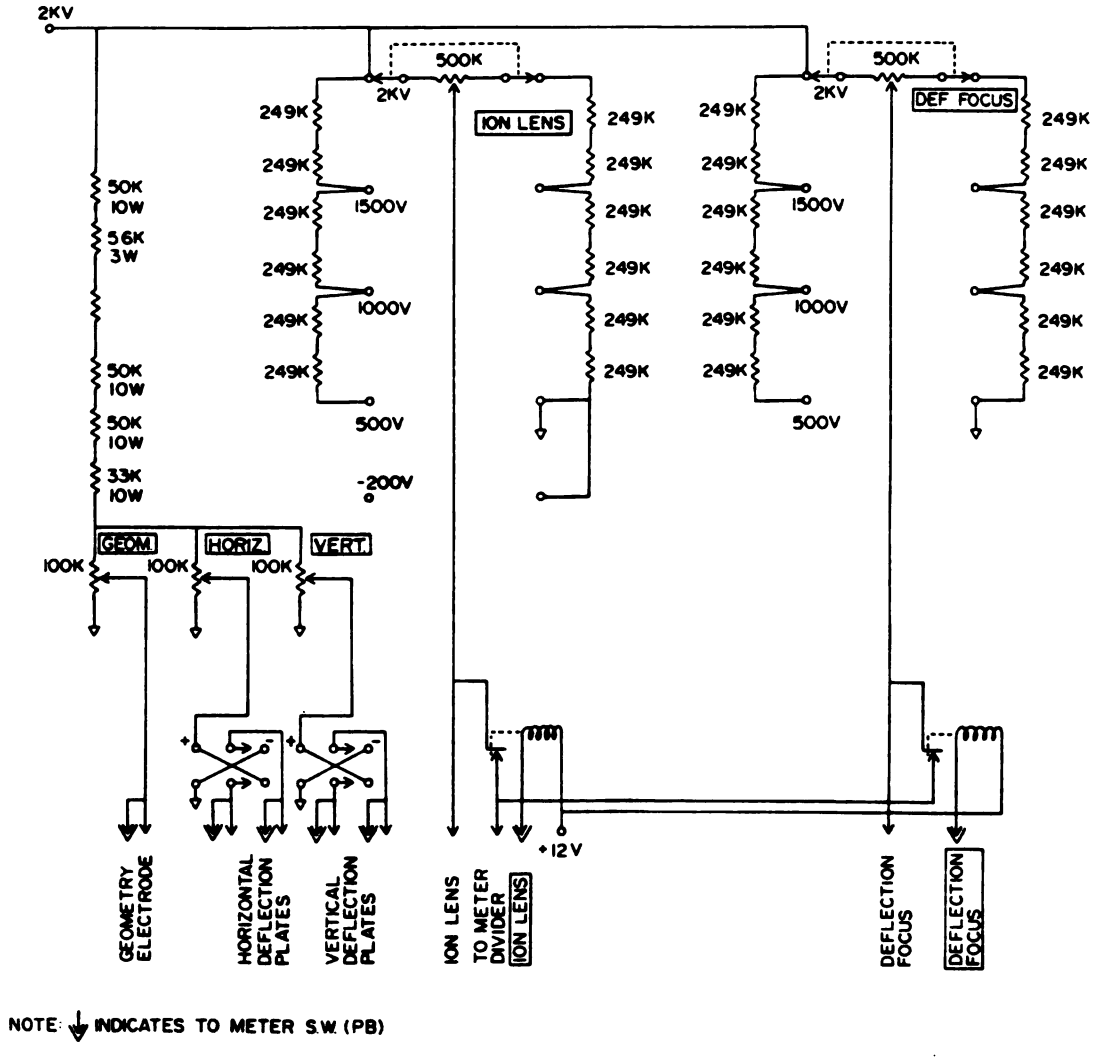

Figure 40. Schematic representation of voltage dividers supplying flight tube focussing and steering elements voltages.

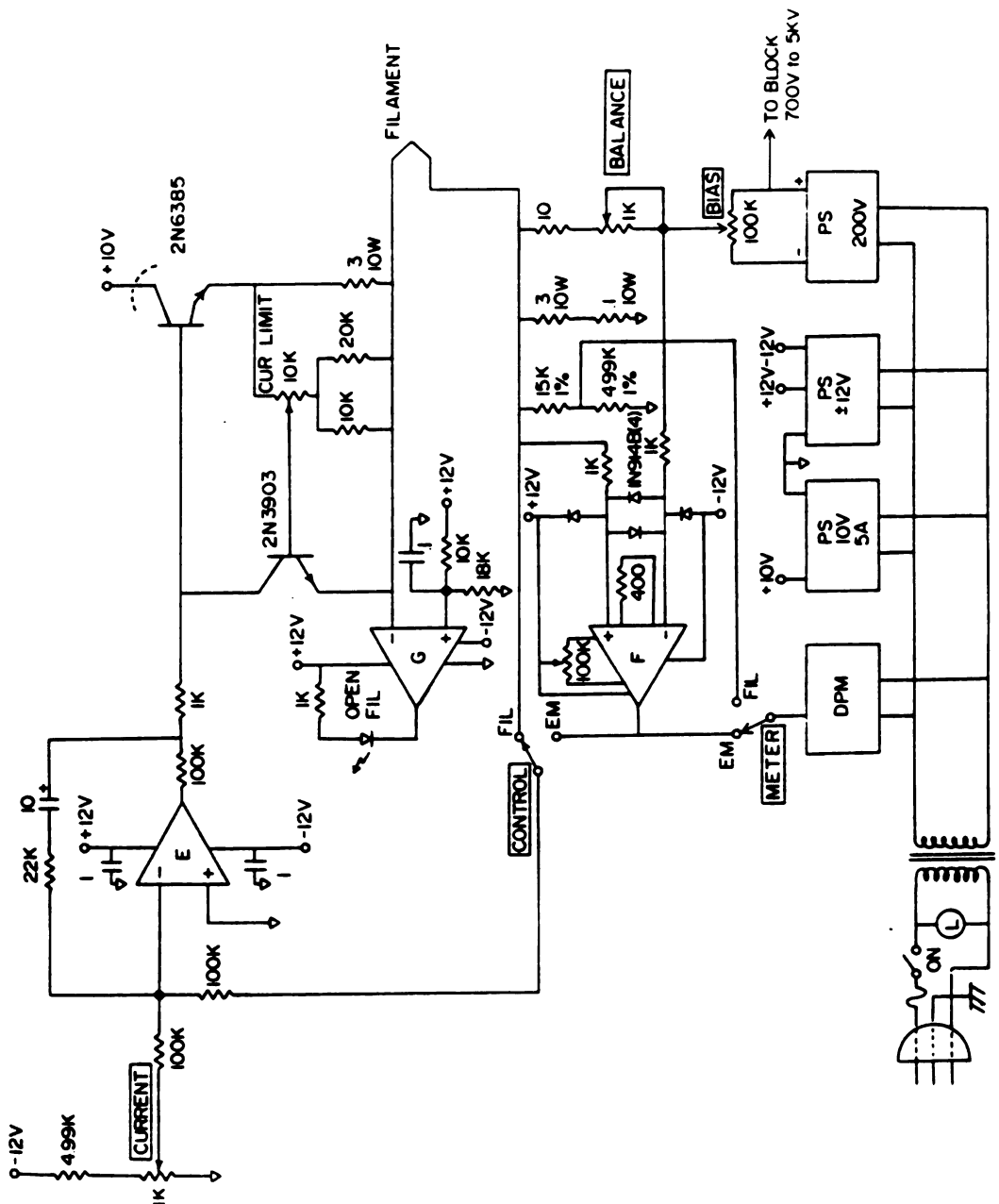

Figure 41. Schematic representation of the filament current controller.

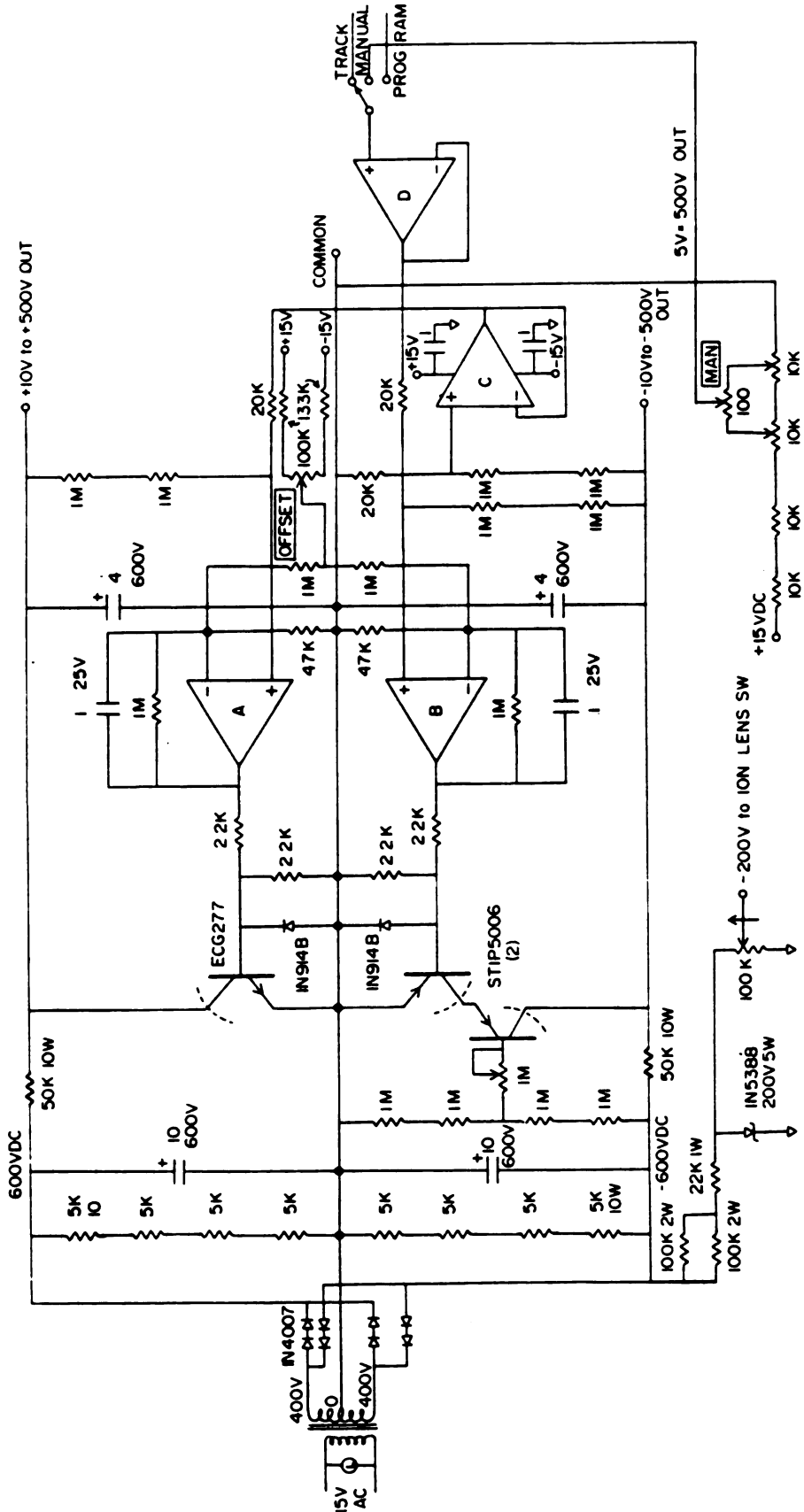

Figure 42. Schematic representation of the electrostatic analyzer power supply.

REFERENCES

REFERENCES

1. J. J. Vrbanac, C. C. Sweeley, J. D. Pinkston, Biomed. Mass Spectrom. 1983, 10, 155.

2. C. E. Giffin, H. G. Boettger, D. D. Norris, Int. J. Mass Spectrom. Ion Phys. 1974, 15, 437.

3. H. H. Tuithof, A. J. H. Boerboom, Int. J. Mass Spectrom. Ion Phys. 1974, 15, 105.

4. H. H. Tuithof, A. J. H. Boerboom, H. L. C. Meuzelaar, Int. J. Mass Spectrom. Ion Phys. 1975, 17, 299.

5. J. H. Beynon, D. O. Jones, R. G. Cooks, Anal. Chem. 1975, 47, 1734.

6. H. H. Tuithof, A. J. H. Boerboom, Int. J. Mass Spectrom. Ion Phys. 1976, 20, 107.

7. H. G. Boettger, C. E. Giffin, D. D. Norris, in "Multichannel Image Detectors, American Chemical Society Symposium Series - 102", Y. Talmi, Ed., American Chemical Society: Washington, D.C., 1979; p. 291.

8. G. J. Louter, A. J. H. Boerboom, P. F. M. Stalmeier, H. H. Tuithof, J. Kistemaker, Int. J. Mass Spectrom. Ion Phys. 1980, 33, 335.

9. B. Hedfjall, R. Ryhage, Anal. Chem. 1979, 51, 1687.

10. B. Hedfjall, R. Ryhage, Anal. Chem. 1981, 53, 1641.

11. M. B. Comisarow, A. G. Marshall, Chem. Phys. Let. 1974, 25, 282.

12. M. B. Comisarow, A. G. Marshall, Can. J. Chem. 1974, 52, 1997.

13. C. L. Wilkins, Anal. Chem. 1978, 50, 493A.

14. M. Comisarow, Adv. Mass Spectrom. 1978, 7B, 1042.

15. R. T. McIver, Jr., Amer. Lab. 1980, November, 18.

16. E. B. Ledford, Jr., Sahba Ghaderi, D. L. Wilkins, M. L. Gross, Adv. Mass Spectrom. 1980, 8B, 1707.

17. M. B. Comisarow, Adv. Mass Spectrom. 1980, 8B, 1698.

18. C. L. Wilkins, M. L. Gross, Anal. Chem. 1981, 53, 1661a.

19. resolution of over a million shown in Spectrospin sales brochure.

20. P. Fellgett, Le Journal de Physique et le Radium 1958, 19, 187.

21. R. L. White, E. C. Onyiriuka, C. L. Wilkins, Anal Chem. 1983, 55, 339.

22. R. T. McIver, Jr., W. D. Bowers, in "Tandem Mass Spectrometry (MS/MS)", F. W. McLafferty, ed., Wiley: New York, 1983.

23. R. B. Cody, R. C. Burnier, B. S. Freiser, Anal. Chem. 1982, 54, 96.

24. E. B. Ledford, Jr., R. L. White, Sahba Ghaderi, C. L. Wilkins, M. L. Gross, Anal. Chem. 1980, 52, 2450.

25. J. Kinsinger, S. Ghaderi, R. Hein, A. Hanna, J. Marra, Presented at the 30th Annual Conference on Mass Spectrometry and Allied Topics, June 6-11, 1982, Honolulu, Hawaii; book of abstracts p. 280.

26. S. Ghaderi, D. P. Littlejohn, Presented at the 33rd Annual Conference on Mass Spectrometry and Allied Topics, May 26-31, 1985, San Diego, California; paper ROC12.

27. R. T. McIver, Jr., R. L. Hunter, W. D. Bowers, Int. J. Mass Spectrom. Ion Proces. 1985, 64, 67.

28. W. E. Stephens, Bull. Amer. Phys. Soc. 1946, 21, 22.

29. J. F. Holland, C. G. Enke, J. Allison, J. T. Stults, J. D. Pinkston, B. Newcome, J. T. Watson, Anal. Chem. 1983, 55, 997A.

30. R. J. Cotter, Anal. Chem. 1981, 53, 719.

31. C. G. Enke, J. T. Stults, J. F. Holland, J. D. Pinkston, J. Allison, J. T. Watson, Int. J. Mass Spectrom. Ion Phys. 1983, 46, 229.

32. J. T. Stults, C. G. Enke, J. F. Holland, Anal. Chem. 1983, 55, 1323.

33. W. C. Wiley, I. H. McLaren, Rev. Sci. Instrum. 1955, 26, 1150.

34. M. H. Studier, Rev. Sci. Instrum. 1963, 34, 1367.

35. F. A. Baker, J. B. Hasted, Phil. Trans. Roy. Soc. (London) 1966, 261, 33.

36. R. Stein, Int. J. Mass Spectrom. Ion Phys. 1974, 14, 205.

37. C. W. Polley, Jr., A. J. Illies, G. G. Meisels, Anal. Chem. 1980, 52, 1797.

38. B. T. Chait, K. G. Standing, Int. J. Mass Spectrom. Ion Phys. 1981, 40, 185.

39. A. E. Cameron, D. F. Eggers, Jr., Rev. Sci. Instrum. 1948, 19, 605.

40. R. Keller, Helv. Phys. Acta 1949, 22, 386.

41. H. Takekoshi, K. Turuoka, S. Shimizu, Bulletin of the Institute for Chemical Research, Kyoto University 1951, 27, 52.

42. M. M. Wolff, W. E. Stephens, Rev. Sci. Instrum. 1953, 24, 616.

43. W. Fishwick, L'Onde Electrique 1954, 34, 110.

44. H. S. Katzenstein, S. S. Friedland, Rev. Sci. Instrum. 1955, 26, 324.

45. V. I. Karataev, B. A. Mamyrin, D. V. Shmikk, Sov. Phys. Tech. Phys. 1972, 16, 1177; translated from Zhurnal Tekhnicheskoi Fiziki 1971, 41, 1498.

46. B. A. Mamyrin, V. I. Karataev, D. V. Smikk, V. A. Zagulin, Sov. Phys. - JETP 1973, 37, 45; translated from Zh. Eksp. Teor. Fiz. 1973, 64, 82.

47. B. A. Mamyrin, D. V. Shmikk, Sov. Phys. - JETP 1979, 49, 762; translated from Zh. Eksp. Teor. Fiz 1979, 76, 1500.

48. G. S. Janes, U.S. Patent No. 3727047, filed on July 22, 1971, appl. no. 165067, granted Apr. 10, 1973, 10 pp.

49. T. Dingle, B. W. Griffiths, J. C. Ruckman, Vacuum 1981, 31, 571.

50. D. M. Hercules, R. J. Day, K. Balasanmugam, T. A. Dang, C. P. Li, Anal. Chem. 1982, 54, 280A.

51. U. Boesl, H. J. Neusser, R. Weinkauf, E. W. Schlag, J. Phys. Chem. 1982, 86, 4857.

52. E. W. Schlag, H. J. Neusser, Acc. Chem. Res. 1983, 16, 355.

53. R. W. Odom, S. E. Buttrill, Jr., R. H. Fleming, M. Rossi, L. N. Goeller, W. Gohl, Int. J. Mass Spectrom. Ion Phys. 1983, 49, 319.

54. M. A. Johnson, M. L. Alexander, W. C. Lineberger, Presented at the 33rd Annual Conference on Mass Spectrometry and Allied Topics, May 26-31, 1985, San Diego, California; paper TOD1

55. W. Gohl, R. Kutscher, H. J. Laue, H. Wollnik, Int. J. Mass Spectrom. Ion Phys. 1983, 48, 411.

56. C. J. Moorman, R. W. Bonham, Proceedings of the 15th Annual Meeting of the ASTM Committee E-14, 1967; p.457.

57. C. J. Moorman, J. Q. Parmater, U.S. Patent No. 3576992, filed Sept. 13, 1968.

58. W. P. Poschenrieder, Int. J. Mass Spectrom. Ion Phys. 1971, 6, 413.

59. W. P. Poschenrieder, G. -H. Oetjen, J. Vac. Sci. Technol. 1972, 9, 212.

60. W. P. Poschenrieder, Int. J. Mass Spectrom. Ion Phys. 1972, 9, 357.

61. E. W. Mueller, S. V. Krishnaswamy, Rev. Sci. Instrum. 1974, 45, 1053.

62. O. Nishikawa, K. Kurihara, M. Nachi, M. Konishi, M. Wada, Rev. Sci. Instrum. 1981, 52, 810.

63. T. Sakurai, T. Matsuo, H. Matsuda, Int. J. Mass Spectrom. Ion Phys. 1985, 63, 273.

64. J. M. B. Bakker, Advances in Mass Spectrometry 1971, 5, 278.

65. J. M. B. Bakker, Int. J. Mass Spectrom. Ion Phys. 1971, 6, 291.

66. J. M. B. Bakker, Dyn. Mass Spectrom. 1975, 4, 25.

67. J. M. B. Bakker, D. A. Freer, J. F. J. Todd, Dyn. Mass Spectrom. 1981, 6, 91.

68. V. V. Zashkvara, A. M. II'in, B. U. Ashimbaeva, Sov. Phys. Tech Phys. 1980, 25, 848; translated from Zh. Tekh. Fiz. 1980, 50, 1464.

69. C. Berger, J. Appl. Phys. 1983, 54, 3699.

70. C. S. Su, Nucl. Instrum. Methods Phys. Res. 1984, 220, 431.

71. N. L. Marable, G. Sanzone, Int. J. Mass Spectrom. Ion Phys. 1974, 13, 185.

72. J. A. Browder, R. L. Miller, W. A. Thomas, G. Sanzone, Int. J. Mass Spectrom. Ion Phys. 1981, 37, 99.

73. M. H. Studier, Rev. Sci. Instrum. 1963, 34, 1367.

74. M. L. Muga, International Patent Classification H01J 49/40, application no. PCT/US82/00676, 17 May 1982.

75. M. L. Muga, Presented at the 32nd Annual Conference on Mass Spectrometry and Allied Topics, May 27-June 1, 1984, San Antonio, Texas; p. 241.

76. R. Paquin, M. Baril, Can. J. Phys. 1976, 54, 1833.

77. personal communication

78. T. K. Fowler, W. M. Good, Nucl. Instrum. Meth. 1960, 7, 245.

79. C. M. Turner, S. D. Bloom, Rev. Sci. Instrum. 1958, 29, 480.

80. J. H. Anderson, D. Swann, Nucl. Instrum. Meth. 1964, 30, 1.

81. P. W. Chudleigh, Rev. Sci. Instrum. 1968, 39, 356.

82. J. M. B. Bakker, J. Phys. E: Sci. Instrum. 1973, 6, 457.

83. J. M. B. Bakker, J. Phys. E: Sci. Instrum. 1973, 6, 785.

84. J. M. B. Bakker, J. Phys. E: Sci. Instrum. 1974, 7, 364.

85. H. E. Duckworth, S. N. Ghoshal, in "Mass Spectrometry", C. A. McDowell, ed., McGraw Hill: New York, 1963; Chapter 7.

86. F. E. Martin, J. F. Holland, C. C. Sweeley, in "Biomedical Applications of Mass Spectrometry", first supplementary volume, G. R. Weller, O. C. Dermer, eds., John Wiley: New York, 1980; pp. 51-55.

87. R. G. Cooks, J. H. Beynon, R. M. Caprioli, G. R. Lester, "Metastable Ions", Elsevier: Amsterdam, 1973; pp. 57-70.

88. W. W. Hunt, Jr., R. E. Huffman, K. E. McGee, Rev. Sci. Instrum. 1964, 35, 82.

89. W. W. Hunt, Jr., K. E. McGee, J. K. Streeter, S. E. Maughan, Rev. Sci. Instrum. 1968, 39, 1793.

90. personal communication

91. D. M. Hercules, S. H. Hercules, J. Chem. Ed. 1984, 61, 592.

92. F. W. McLafferty, ed., "Tandem Mass Spectrometry (MS/MS)", Wiley: New York, 1983.

93. R. A. Yost, D. D. Fetterolf, Mass Spectrom. Rev. 1983, 2, 1.

94. K. H. Maurer, C. Brunee, G. Kappur, D. Habfast, U. Schroder, P. Shulze, Presented at the 19th Annual Conference on Mass Spectrometry and Allied Topics, Atlanta, GA, May 1971.

95. J. H. Beynon, R. G. Cooks, Res./Dev. 1971, 22, No. 11, 26.

96. R. K. Boyd, C. J. Porter, J. H. Beynon, Org. Mass Spectrom. 1981, 16, 490.

97. D. Zakett, A. E. Schoen, R. W. Kondret, R. G. Cooks, J. Am. Chem. Soc. 1979, 101, 6781.

98. D. S. Millington, J. A. Smith, Org. Mass Spectrom. 1977, 12, 264.

99. W. F. Haddon, Org. Mass Spectrom. 1980, 15, 539.

100. M. Barber, R. M. Elliott, Presented at the ASTM Committee E-14 Conference on Mass Spectrometry, Montreal, June 1964.

101. S. Evans, R. Graham, Adv. Mass Spectrom. 1974, 6, 429.

102. R. K. Boyd, J. H. Beynon, Org. Mass Spectrom. 1977, 12, 163.

103. R. A. Yost, C. G. Enke, J. Am. Chem. Soc. 1978, 100, 2274.

104. P. H. Dawson, J. Fulford, Int. J. Mass Spectrom. Ion Phys. 1982, 42, 195.

105. R. G. Cooks, in "Collision Spectroscopy", R. G. Cooks, Ed., Plenum Press: New York, 1978; p. 357.

106. R. A. Yost, C. G. Enke, E. McGilvery, D. Smith, J. D. Morrison, Int. J. Mass Spectrom. Ion Phys. 1979, 30, 127.

107. D. J. Douglas, J. Phys. Chem. 1982, 86, 185.

108. D. D. Fetterolf, R. A. Yost, J. R. Eyler, Org. Mass Spectrom. 1984, 19, 104.

109. P. O. Danis, C. Wesdemiotis, F. W. McLafferty, J. Am. Chem. Soc. 1983, 105, 7454.

110. R. A. Yost, C. G. Enke, Anal. Chem. 1979, 51, 1251A.

111. F. W. McLafferty, P. J. Todd, O. C. McGilvery, M. A. Baldwin, J. Am. Chem. Soc. 1980, 102, 3360.

112. M. L. Gross, E. K. Chess, P. A. Lyon, F. W. Crow, S. Evans, H. Tudge, Int. J. Mass Spectrom. Ion Phys. 1982, 42, 243.

113. F. W. Crow, K. B. Tomer, M. L. Gross, Mass Spectrom. Rev. 1983, 2, 47.

114. A. Maquestiau, Y. Van Haverbeke, R. Flammang, M. Abrassant, D. Finet, Bull. Soc. Chim. Belg. 1978, 87, 765.

115. D. H. Russell, E. H. McBay, T. R. Mueller, Am. Lab. 1980, Sept., 50.

116. U. von Zahn, H. Tatarczyk, Phys. Lett. 1964, 12, 190.

117. G. L. Glish, S. A. McLuckey, T. Y. Ridley, R. G. Cooks, Int. J. Mass Spectrom. Ion Phys. 1982, 41, 157.

118. J. H. Beynon, F. M. Harris, B. N. Green, R. H. Bateman, Org. Mass Spectrom. 1982, 17, 55.

119. J. H. Futrell, C. D. Miller, Rev. Sci. Instrum. 1966, 37, 1521.

120. F. W. McLafferty, Science 1981, 214, 280.

121. J. R. Hass, B. N. Green, R. H. Bateman, P. A. Bott, Presented at the 32nd Annual Conference on Mass Spectrometry and Allied Topics, May 27-June 1, 1984, San Antonio, Texas; book of abstracts p. 380.

122. C. J. Louter, A. J. H. Boerboom, P. F. M. Stalmeier, H. H. Tuithof, J. Kistemaker, Int. J. Mass Spectrom. Ion Phys. 1980, 33, 335.

123. A. J. H. Boerboom, in "Tandem Mass Spectrometry (MS/MS)", F.W. McLafferty, ed., Wiley: New York, 1983; Chapter 11.

124. S. A. McLuckey, C. E. D. Ouwerkerk, A. J. H. Boerboom, P. G. Kistemaker, Int. J. Mass Spectrom. Ion Proc. 1984, 59, 85.

125. R. T. McIver, Jr., Presented at the 29th Annual Conference on Mass Spectrometry and Allied Topics, Minneapolis, MN, June 1981.

126. R. B. Cody, B. S. Freiser, Int. J. Mass Spectrom. Ion Phys. 1982, 41, 199.

127. R. B. Cody, R. C. Burnier, B. S. Freiser, Anal. Chem. 1982, 54, 96.

128. R. B. Cody, B. S. Freiser, Anal. Chem. 1982, 54, 1431.

129. A. G. Marshall, T. L. Wang, T. L. Ricca, Presented at the 33rd Annual Conference on Mass Spectrometry and Allied Topics, May 26-31, 1985, San Diego, California; paper ROC6.

130. R. E. Ferguson, K. E. McCulloh, H. M. Rosenstock, Presented at the 10th Annual Meeting of the ASTM Committee E-14 on Mass Spectrometry, New Orleans, June 1962.

131. W. W. Hunt, Jr., R. E. Huffman, J. Saari, G. Wassel, J. F. Betts, E. H. Paufve, W. Wyess, R. A. Fluegge, Rev. Sci. Instrum. 1964, 35, 88.

132. R. E. Ferguson, K. E. McCulloh, H. M. Rosenstock, J. Chem. Phys. 1965, 42, 100.

133. D. L. Dugger, R. W. Kiser, J. Chem. Phys. 1967, 47, 5054.

134. W. F. Haddon, F. W. McLafferty, Anal. Chem. 1969, 41, 31.

135. B. T. Chait, F. H. Field, Int. J. Mass Spectrom. Ion Phys. 1981, 41, 17.

136. J. M. B. Bakker, Int. J. Mass Spectrom. Ion Phys. 1973, 11, 305.

137. G. L. Glish, D. E. Goeringer, Anal. Chem. 1984, 56, 2291.

138. R. M. Gandy, R. Ampulski, J. Prusaczyk, R. H. Johnsen, Int. J. Mass Spectrom. Ion Phys. 1977, 24, 363.

139. M. A. Johnson, M. L. Alexander, W. C. Lineberger, Presented at the 33rd Annual Conference on Mass Spectrometry and Allied Topics, May 26-31, 1985, San Diego, California; paper TOD 1.

140. J. T. Stults, C. G. Enke, J. F. Holland, Presented at the 32nd Annual Conference on Mass Spectrometry and Allied Topics, May 27-June 1, 1984, San Antonio, Texas; p. 519 of the book of abstracts.

141. C. Lifshitz, S. Gefen, R. Arakawa, Presented at the 32nd Annual Conference on Mass Spectrometry and Allied Topics, May 27-June 1, 1984, San Antonio, Texas; p. 162 of the book of abstracts.

142. H. Zeininger, J. D. Fassett, L. J. Moore, Presented at the 33rd Annual Conference on Mass Spectrometry and Allied Topics, May 26-31, 1985, San Diego, California; poster RPE4.

143. J. T. Stults, Ph.D. Dissertation, Michigan State University, East Lansing, Michigan, 1985.

144. J. D. Pinkston, Presented at the 33rd Annual Conference on Mass Spectrometry and Allied Topics, May 26-31, 1985, San Diego, California; paper ROC 8.

145. J. D. Pinkston, M. Rabb, J. T. Watson, J. Allison, manuscript in preparation for the Review of Scientific Instruments.

146. T. W. Shannon, T. E. Mead, C. G. Warner, F. W. McLafferty, Anal. Chem. 1967, 39, 1748.

147. J. E. Coutant, F. W. McLafferty, Int. J. Mass Spectrom. Ion Phys. 1972, 8, 323.

148. C. Hwang, R. W. Kiser, Int. J. Mass Spectrom. Ion Phys. 1978, 27, 209.